# THE HYPOTHESIS OF INCREMENTAL COMPLEMENTARY ENERGY EQUIVALENCE FOR DAMAGE MODELING IN CONTINUUM DAMAGE MECHANICS

BY

YANGHU MOU

A Thesis

Submitted to the Faculty of Graduate Studies

in Partial Fulfillment of the Requirements

for the Degree of

**DOCTOR OF PHILOSOPHY**

Department of Mechanical and Industrial Engineering

University of Manitoba

Winnipeg, Manitoba, Canada

@ June 1995

National Library
of Canada

Acquisitions and
Bibliographic Services Branch

395 Wellington Street
Ottawa, Ontario
K1A 0N4

Bibliothèque nationale
du Canada

Direction des acquisitions et
des services bibliographiques

395, rue Wellington
Ottawa (Ontario)
K1A 0N4

*Your file Votre référence*

*Our file Notre référence*

**The author has granted an irrevocable non-exclusive licence allowing the National Library of Canada to reproduce, loan, distribute or sell copies of his/her thesis by any means and in any form or format, making this thesis available to interested persons.**

**L'auteur a accordé une licence irrévocable et non exclusive permettant à la Bibliothèque nationale du Canada de reproduire, prêter, distribuer ou vendre des copies de sa thèse de quelque manière et sous quelque forme que ce soit pour mettre des exemplaires de cette thèse à la disposition des personnes intéressées.**

**The author retains ownership of the copyright in his/her thesis. Neither the thesis nor substantial extracts from it may be printed or otherwise reproduced without his/her permission.**

**L'auteur conserve la propriété du droit d'auteur qui protège sa thèse. Ni la thèse ni des extraits substantiels de celle-ci ne doivent être imprimés ou autrement reproduits sans son autorisation.**

ISBN 0-612-13385-0

Canada

Name _____

*Dissertation Abstracts International* is arranged by broad, general subject categories. Please select the one subject which most nearly describes the content of your dissertation. Enter the corresponding four-digit code in the spaces provided.

Applied Mechanics
SUBJECT TERM

0346
SUBJECT CODE

U·M·I

## Subject Categories

# THE HUMANITIES AND SOCIAL SCIENCES

### COMMUNICATIONS AND THE ARTS
- Architecture ..... 0729
- Art History ..... 0377
- Cinema ..... 0900
- Dance ..... 0378
- Fine Arts ..... 0357
- Information Science ..... 0723
- Journalism ..... 0391
- Library Science ..... 0399
- Mass Communications ..... 0708
- Music ..... 0413
- Speech Communication ..... 0459
- Theater ..... 0465

### EDUCATION
- General ..... 0515
- Administration ..... 0514
- Adult and Continuing ..... 0516
- Agricultural ..... 0517
- Art ..... 0273
- Bilingual and Multicultural ..... 0282
- Business ..... 0688
- Community College ..... 0275
- Curriculum and Instruction ..... 0727
- Early Childhood ..... 0518
- Elementary ..... 0524
- Finance ..... 0277
- Guidance and Counseling ..... 0519
- Health ..... 0680
- Higher ..... 0745
- History of ..... 0520
- Home Economics ..... 0278
- Industrial ..... 0521
- Language and Literature ..... 0279
- Mathematics ..... 0280
- Music ..... 0522
- Philosophy of ..... 0998
- Physical ..... 0523
- Psychology ..... 0525
- Reading ..... 0535
- Religious ..... 0527
- Sciences ..... 0714
- Secondary ..... 0533
- Social Sciences ..... 0534
- Sociology of ..... 0340
- Special ..... 0529
- Teacher Training ..... 0530
- Technology ..... 0710
- Tests and Measurements ..... 0288
- Vocational ..... 0747

### LANGUAGE, LITERATURE AND LINGUISTICS
- Language
  - General ..... 0679
  - Ancient ..... 0289
  - Linguistics ..... 0290
  - Modern ..... 0291
- Literature
  - General ..... 0401
  - Classical ..... 0294
  - Comparative ..... 0295
  - Medieval ..... 0297
  - Modern ..... 0298
  - African ..... 0316
  - American ..... 0591
  - Asian ..... 0305
  - Canadian (English) ..... 0352
  - Canadian (French) ..... 0355
  - English ..... 0593
  - Germanic ..... 0311
  - Latin American ..... 0312
  - Middle Eastern ..... 0315
  - Romance ..... 0313
  - Slavic and East European ..... 0314

### PHILOSOPHY, RELIGION AND THEOLOGY
- Philosophy ..... 0422
- Religion
  - General ..... 0318
  - Biblical Studies ..... 0321
  - Clergy ..... 0319
  - History of ..... 0320
  - Philosophy of ..... 0322
- Theology ..... 0469

### SOCIAL SCIENCES
- American Studies ..... 0323
- Anthropology
  - Archaeology ..... 0324
  - Cultural ..... 0326
  - Physical ..... 0327
- Business Administration
  - General ..... 0310
  - Accounting ..... 0272
  - Banking ..... 0770
  - Management ..... 0454
  - Marketing ..... 0338
- Canadian Studies ..... 0385
- Economics
  - General ..... 0501
  - Agricultural ..... 0503
  - Commerce-Business ..... 0505
  - Finance ..... 0508
  - History ..... 0509
  - Labor ..... 0510
  - Theory ..... 0511
- Folklore ..... 0358
- Geography ..... 0366
- Gerontology ..... 0351
- History
  - General ..... 0578
  - Ancient ..... 0579
  - Medieval ..... 0581
  - Modern ..... 0582
  - Black ..... 0328
  - African ..... 0331
  - Asia, Australia and Oceania ..... 0332
  - Canadian ..... 0334
  - European ..... 0335
  - Latin American ..... 0336
  - Middle Eastern ..... 0333
  - United States ..... 0337
- History of Science ..... 0585
- Law ..... 0398
- Political Science
  - General ..... 0615
  - International Law and Relations ..... 0616
  - Public Administration ..... 0617
- Recreation ..... 0814
- Social Work ..... 0452
- Sociology
  - General ..... 0626
  - Criminology and Penology ..... 0627
  - Demography ..... 0938
  - Ethnic and Racial Studies ..... 0631
  - Individual and Family Studies ..... 0628
  - Industrial and Labor Relations ..... 0629
  - Public and Social Welfare ..... 0630
  - Social Structure and Development ..... 0700
  - Theory and Methods ..... 0344
- Transportation ..... 0709
- Urban and Regional Planning ..... 0999
- Women's Studies ..... 0453

# THE SCIENCES AND ENGINEERING

### BIOLOGICAL SCIENCES
- Agriculture
  - General ..... 0473
  - Agronomy ..... 0285
  - Animal Culture and Nutrition ..... 0475
  - Animal Pathology ..... 0476
  - Food Science and Technology ..... 0359
  - Forestry and Wildlife ..... 0478
  - Plant Culture ..... 0479
  - Plant Pathology ..... 0480
  - Plant Physiology ..... 0817
  - Range Management ..... 0777
  - Wood Technology ..... 0746
- Biology
  - General ..... 0306
  - Anatomy ..... 0287
  - Biostatistics ..... 0308
  - Botany ..... 0309
  - Cell ..... 0379
  - Ecology ..... 0329
  - Entomology ..... 0353
  - Genetics ..... 0369
  - Limnology ..... 0793
  - Microbiology ..... 0410
  - Molecular ..... 0307
  - Neuroscience ..... 0317
  - Oceanography ..... 0416
  - Physiology ..... 0433
  - Radiation ..... 0821
  - Veterinary Science ..... 0778
  - Zoology ..... 0472
- Biophysics
  - General ..... 0786
  - Medical ..... 0760

### EARTH SCIENCES
- Biogeochemistry ..... 0425
- Geochemistry ..... 0996
- Geodesy ..... 0370
- Geology ..... 0372
- Geophysics ..... 0373
- Hydrology ..... 0388
- Mineralogy ..... 0411
- Paleobotany ..... 0345
- Paleoecology ..... 0426
- Paleontology ..... 0418
- Paleozoology ..... 0985
- Palynology ..... 0427
- Physical Geography ..... 0368
- Physical Oceanography ..... 0415

### HEALTH AND ENVIRONMENTAL SCIENCES
- Environmental Sciences ..... 0768
- Health Sciences
  - General ..... 0566
  - Audiology ..... 0300
  - Chemotherapy ..... 0992
  - Dentistry ..... 0567
  - Education ..... 0350
  - Hospital Management ..... 0769
  - Human Development ..... 0758
  - Immunology ..... 0982
  - Medicine and Surgery ..... 0564
  - Mental Health ..... 0347
  - Nursing ..... 0569
  - Nutrition ..... 0570
  - Obstetrics and Gynecology ..... 0380
  - Occupational Health and Therapy ..... 0354
  - Ophthalmology ..... 0381
  - Pathology ..... 0571
  - Pharmacology ..... 0419
  - Pharmacy ..... 0572
  - Physical Therapy ..... 0382
  - Public Health ..... 0573
  - Radiology ..... 0574
  - Recreation ..... 0575
  - Speech Pathology ..... 0460
  - Toxicology ..... 0383
- Home Economics ..... 0386

### PHYSICAL SCIENCES
#### Pure Sciences
- Chemistry
  - General ..... 0485
  - Agricultural ..... 0749
  - Analytical ..... 0486
  - Biochemistry ..... 0487
  - Inorganic ..... 0488
  - Nuclear ..... 0738
  - Organic ..... 0490
  - Pharmaceutical ..... 0491
  - Physical ..... 0494
  - Polymer ..... 0495
  - Radiation ..... 0754
- Mathematics ..... 0405
- Physics
  - General ..... 0605
  - Acoustics ..... 0986
  - Astronomy and Astrophysics ..... 0606
  - Atmospheric Science ..... 0608
  - Atomic ..... 0748
  - Electronics and Electricity ..... 0607
  - Elementary Particles and High Energy ..... 0798
  - Fluid and Plasma ..... 0759
  - Molecular ..... 0609
  - Nuclear ..... 0610
  - Optics ..... 0752
  - Radiation ..... 0756
  - Solid State ..... 0611
- Statistics ..... 0463

#### Applied Sciences
- Applied Mechanics ..... 0346
- Computer Science ..... 0984
- Engineering
  - General ..... 0537
  - Aerospace ..... 0538
  - Agricultural ..... 0539
  - Automotive ..... 0540
  - Biomedical ..... 0541
  - Chemical ..... 0542
  - Civil ..... 0543
  - Electronics and Electrical ..... 0544
  - Heat and Thermodynamics ..... 0348
  - Hydraulic ..... 0545
  - Industrial ..... 0546
  - Marine ..... 0547
  - Materials Science ..... 0794
  - Mechanical ..... 0548
  - Metallurgy ..... 0743
  - Mining ..... 0551
  - Nuclear ..... 0552
  - Packaging ..... 0549
  - Petroleum ..... 0765
  - Sanitary and Municipal ..... 0554
  - System Science ..... 0790
- Geotechnology ..... 0428
- Operations Research ..... 0796
- Plastics Technology ..... 0795
- Textile Technology ..... 0994

### PSYCHOLOGY
- General ..... 0621
- Behavioral ..... 0384
- Clinical ..... 0622
- Developmental ..... 0620
- Experimental ..... 0623
- Industrial ..... 0624
- Personality ..... 0625
- Physiological ..... 0989
- Psychobiology ..... 0349
- Psychometrics ..... 0632
- Social ..... 0451

Nom _____

*Dissertation Abstracts International* est organisé en catégories de sujets. Veuillez s.v.p. choisir le sujet qui décrit le mieux votre thèse et inscrivez le code numérique approprié dans l'espace réservé ci-dessous.

_____ ☐☐☐ U·M·I

SUJET — CODE DE SUJET

## Catégories par sujets

# HUMANITÉS ET SCIENCES SOCIALES

### COMMUNICATIONS ET LES ARTS
Architecture ..... 0729
Beaux-arts ..... 0357
Bibliothéconomie ..... 0399
Cinéma ..... 0900
Communication verbale ..... 0459
Communications ..... 0708
Danse ..... 0378
Histoire de l'art ..... 0377
Journalisme ..... 0391
Musique ..... 0413
Sciences de l'information ..... 0723
Théâtre ..... 0465

### ÉDUCATION
Généralités ..... 515
Administration ..... 0514
Art ..... 0273
Collèges communautaires ..... 0275
Commerce ..... 0688
Économie domestique ..... 0278
Éducation permanente ..... 0516
Éducation préscolaire ..... 0518
Éducation sanitaire ..... 0680
Enseignement agricole ..... 0517
Enseignement bilingue et multiculturel ..... 0282
Enseignement industriel ..... 0521
Enseignement primaire. ..... 0524
Enseignement professionnel ..... 0747
Enseignement religieux ..... 0527
Enseignement secondaire ..... 0533
Enseignement spécial ..... 0529
Enseignement supérieur ..... 0745
Évaluation ..... 0288
Finances ..... 0277
Formation des enseignants ..... 0530
Histoire de l'éducation ..... 0520
Langues et littérature ..... 0279
Lecture ..... 0535
Mathématiques ..... 0280
Musique ..... 0522
Orientation et consultation ..... 0519
Philosophie de l'éducation ..... 0998
Physique ..... 0523
Programmes d'études et enseignement ..... 0727
Psychologie ..... 0525
Sciences ..... 0714
Sciences sociales ..... 0534
Sociologie de l'éducation ..... 0340
Technologie ..... 0710

### LANGUE, LITTÉRATURE ET LINGUISTIQUE
Langues
- Généralités ..... 0679
- Anciennes ..... 0289
- Linguistique ..... 0290
- Modernes ..... 0291

Littérature
- Généralités ..... 0401
- Anciennes ..... 0294
- Comparée ..... 0295
- Médiévale ..... 0297
- Moderne ..... 0298
- Africaine ..... 0316
- Américaine ..... 0591
- Anglaise ..... 0593
- Asiatique ..... 0305
- Canadienne (Anglaise) ..... 0352
- Canadienne (Française) ..... 0355
- Germanique ..... 0311
- Latino-américaine ..... 0312
- Moyen-orientale ..... 0315
- Romane ..... 0313
- Slave et est-européenne ..... 0314

### PHILOSOPHIE, RELIGION ET THÉOLOGIE
Philosophie ..... 0422
Religion
- Généralités ..... 0318
- Clergé ..... 0319
- Études bibliques ..... 0321
- Histoire des religions ..... 0320
- Philosophie de la religion ..... 0322

Théologie ..... 0469

### SCIENCES SOCIALES
Anthropologie
- Archéologie ..... 0324
- Culturelle ..... 0326
- Physique ..... 0327

Droit ..... 0398
Économie
- Généralités ..... 0501
- Commerce-Affaires ..... 0505
- Économie agricole ..... 0503
- Économie du travail ..... 0510
- Finances ..... 0508
- Histoire ..... 0509
- Théorie ..... 0511

Études américaines ..... 0323
Études canadiennes ..... 0385
Études féministes ..... 0453
Folklore ..... 0358
Géographie ..... 0366
Gérontologie ..... 0351
Gestion des affaires
- Généralités ..... 0310
- Administration ..... 0454
- Banques ..... 0770
- Comptabilité ..... 0272
- Marketing ..... 0338

Histoire
- Histoire générale ..... 0578
- Ancienne ..... 0579
- Médiévale ..... 0581
- Moderne ..... 0582
- Histoire des noirs ..... 0328
- Africaine ..... 0331
- Canadienne ..... 0334
- États-Unis ..... 0337
- Européenne ..... 0335
- Moyen-orientale ..... 0333
- Latino-américaine ..... 0336
- Asie, Australie et Océanie ..... 0332

Histoire des sciences ..... 0585
Loisirs ..... 0814
Planification urbaine et régionale ..... 0999
Science politique
- Généralités ..... 0615
- Administration publique ..... 0617
- Droit et relations internationales ..... 0616

Sociologie
- Généralités ..... 0626
- Aide et bien-être social ..... 0630
- Criminologie et établissements pénitentiaires ..... 0627
- Démographie ..... 0938
- Études de l' individu et de la famille ..... 0628
- Études des relations interethniques et des relations raciales ..... 0631
- Structure et développement social ..... 0700
- Théorie et méthodes. ..... 0344
- Travail et relations industrielles ..... 0629

Transports ..... 0709
Travail social ..... 0452

# SCIENCES ET INGÉNIERIE

### SCIENCES BIOLOGIQUES
Agriculture
- Généralités ..... 0473
- Agronomie. ..... 0285
- Alimentation et technologie alimentaire ..... 0359
- Culture ..... 0479
- Élevage et alimentation ..... 0475
- Exploitation des pâturages ..... 0777
- Pathologie animale ..... 0476
- Pathologie végétale ..... 0480
- Physiologie végétale ..... 0817
- Sylviculture et faune ..... 0478
- Technologie du bois ..... 0746

Biologie
- Généralités ..... 0306
- Anatomie ..... 0287
- Biologie (Statistiques) ..... 0308
- Biologie moléculaire ..... 0307
- Botanique ..... 0309
- Cellule ..... 0379
- Écologie ..... 0329
- Entomologie ..... 0353
- Génétique ..... 0369
- Limnologie ..... 0793
- Microbiologie ..... 0410
- Neurologie ..... 0317
- Océanographie ..... 0416
- Physiologie ..... 0433
- Radiation ..... 0821
- Science vétérinaire ..... 0778
- Zoologie ..... 0472

Biophysique
- Généralités ..... 0786
- Medicale ..... 0760

### SCIENCES DE LA TERRE
Biogéochimie ..... 0425
Géochimie ..... 0996
Géodésie ..... 0370
Géographie physique ..... 0368
Géologie ..... 0372
Géophysique ..... 0373
Hydrologie ..... 0388
Minéralogie ..... 0411
Océanographie physique ..... 0415
Paléobotanique ..... 0345
Paléoécologie ..... 0426
Paléontologie ..... 0418
Paléozoologie ..... 0985
Palynologie ..... 0427

### SCIENCES DE LA SANTÉ ET DE L'ENVIRONNEMENT
Économie domestique ..... 0386
Sciences de l'environnement ..... 0768
Sciences de la santé
- Généralités ..... 0566
- Administration des hôpitaux ..... 0769
- Alimentation et nutrition ..... 0570
- Audiologie ..... 0300
- Chimiothérapie ..... 0992
- Dentisterie ..... 0567
- Développement humain ..... 0758
- Enseignement ..... 0350
- Immunologie ..... 0982
- Loisirs ..... 0575
- Médecine du travail et thérapie ..... 0354
- Médecine et chirurgie ..... 0564
- Obstétrique et gynécologie ..... 0380
- Ophtalmologie ..... 0381
- Orthophonie ..... 0460
- Pathologie ..... 0571
- Pharmacie ..... 0572
- Pharmacologie ..... 0419
- Physiothérapie ..... 0382
- Radiologie ..... 0574
- Santé mentale ..... 0347
- Santé publique ..... 0573
- Soins infirmiers ..... 0569
- Toxicologie ..... 0383

### SCIENCES PHYSIQUES
#### Sciences Pures
Chimie
- Généralités ..... 0485
- Biochimie ..... 487
- Chimie agricole ..... 0749
- Chimie analytique ..... 0486
- Chimie minérale ..... 0488
- Chimie nucléaire ..... 0738
- Chimie organique ..... 0490
- Chimie pharmaceutique ..... 0491
- Physique ..... 0494
- PolymÈres ..... 0495
- Radiation ..... 0754

Mathématiques ..... 0405
Physique
- Généralités ..... 0605
- Acoustique ..... 0986
- Astronomie et astrophysique ..... 0606
- Électronique et électricité ..... 0607
- Fluides et plasma ..... 0759
- Météorologie ..... 0608
- Optique ..... 0752
- Particules (Physique nucléaire) ..... 0798
- Physique atomique ..... 0748
- Physique de l'état solide ..... 0611
- Physique moléculaire ..... 0609
- Physique nucléaire ..... 0610
- Radiation ..... 0756

Statistiques ..... 0463

#### Sciences Appliqués Et Technologie
Informatique ..... 0984
Ingénierie
- Généralités ..... 0537
- Agricole ..... 0539
- Automobile ..... 0540
- Biomédicale ..... 0541
- Chaleur et thermodynamique ..... 0348
- Conditionnement (Emballage) ..... 0549
- Génie aérospatial ..... 0538
- Génie chimique ..... 0542
- Génie civil ..... 0543
- Génie électronique et électrique ..... 0544
- Génie industriel ..... 0546
- Génie mécanique ..... 0548
- Génie nucléaire ..... 0552
- Ingénierie des systèmes ..... 0790
- Mécanique navale ..... 0547
- Métallurgie ..... 0743
- Science des matériaux ..... 0794
- Technique du pétrole ..... 0765
- Technique minière ..... 0551
- Techniques sanitaires et municipales ..... 0554
- Technologie hydraulique ..... 0545

Mécanique appliquée ..... 0346
Géotechnologie ..... 0428
Matières plastiques (Technologie) ..... 0795
Recherche opérationnelle ..... 0796
Textiles et tissus (Technologie) ..... 0794

### PSYCHOLOGIE
Généralités ..... 0621
Personnalité ..... 0625
Psychobiologie ..... 0349
Psychologie clinique ..... 0622
Psychologie du comportement ..... 0384
Psychologie du développement ..... 0620
Psychologie expérimentale ..... 0623
Psychologie industrielle ..... 0624
Psychologie physiologique ..... 0989
Psychologie sociale ..... 0451
Psychométrie ..... 0632

# THE HYPOTHESIS OF INCREMENTAL COMPLEMENTARY ENERGY EQUIVALENCE FOR DAMAGE MODELING IN CONTINUUM DAMAGE MECHANICS

BY

YANGHU MOU

A Thesis submitted to the Faculty of Graduate Studies of the University of Manitoba in partial fulfillment of the requirements of the degree of

DOCTOR OF PHILOSOPHY

© 1995

Permission has been granted to the LIBRARY OF THE UNIVERSITY OF MANITOBA to lend or sell copies of this thesis, to the NATIONAL LIBRARY OF CANADA to microfilm this thesis and to lend or sell copies of the film, and LIBRARY MICROFILMS to publish an abstract of this thesis.

The author reserves other publication rights, and neither the thesis nor extensive extracts from it may be printed or other-wise reproduced without the author's written permission.

# ABSTRACT

Continuum damage mechanics uses damage variables as internal state variables of a material to describe material deterioration under unfavorable conditions. In deriving the constitutive equations for damaged materials, the hypothesis of *incremental complementary energy equivalence* is proposed here. Based on this new hypothesis, a large damage theory is formulated, from which an anisotropic damage model is developed. Specializing the hypothesis for the isotropic damage and on the basis of the irreversible thermodynamics theory, a damage evolution model for ductile materials is formulated. The influence of the stress triaxiality and strain hardening exponent on the evolution process are analyzed. Using Dugdale's model for materials, damage distribution and size of damage zones just ahead of a macrocrack under Mode I loading are studied. Analytical results obtained are compared with those computed via a finite element analysis. Additionally, comparison of the size of plastic zones obtained by extending Dugdale's model for elastic-perfectly plastic materials to strain hardening materials is also made. Also, the effects of damage distribution and damage size on the stress intensity factor under Mode I loading are investigated. Three influence factors are considered: local fracture path deflections, a reduction in the modulus of elasticity and a release of residual stresses in the vicinity of a macrocrack. Shielding effects are produced in each of these situations.

# ACKNOWLEDGMENTS

The author would like to express his deepest gratitude and thanks to his supervisor, Dr. Ray P.S. Han, for his invaluable guidance, encouragement and advice throughout this research. The author would also like to thank his Examining Committee, Comprising of Drs. D. Ruth, E. Lajtai, N. Rajapakse, N. Bassim and G. Glinka for their helpful suggestions in this thesis.

The author wishes to thank the Department of Mechanical and Industrial Engineering, University of Manitoba for all the support they gave, the unforgettable Christmas parties they organized, the convenience and kindness the department secretaries, Gayle and Bev, offered during the author's Ph.D. program.

The author would like to express special thanks to his parents, sisters and brothers for their understanding and invaluable spiritual support.

Finally, the part of the financial support provided by the Graduate Study of the University of Manitoba and the Natural Science and Engineering Research Council of Canada (NSERC) are greatly appreciated.

# CONTENTS

ABSTRACT . . . . . ii

ACKNOWLEDGMENTS . . . . . iii

LIST OF TABLES . . . . . viii

LIST OF FIGURES . . . . . ix

CHAPTER 1 INTRODUCTION

1.1 Prologue . . . . . 1

1.2 Literature Survey . . . . . 4

1.3 Objective of Research . . . . . 11

1.4 Scope of Study . . . . . 11

1.5 Thesis Layout . . . . . 12

CHAPTER 2 BASIC CONCEPTS IN CONTINUUM DAMAGE MECHANICS

2.1 Damage Variables and Effective Stresses . . . . . 15

2.2 Damage Effect Tensor *M(D)* . . . . . 20

2.3 Experimental Measurement of Damage . . . . . 26

2.4 Ductile Damage versus Brittle Damage in the Fracture Process ..... 27

**CHAPTER 3 THE HYPOTHESIS OF INCREMENTAL COMPLEMENTARY ENERGY EQUIVALENCE AND THE THEORY OF LARGE ANISOTROPIC DAMAGE**

3.1 Hypotheses for Modeling Damage State Constitutive Equations ..... 29

3.2 The Theory of Large Anisotropic Damage ..... 34

3.3 Damage Effect Tensor $M(D)$ for Large Damage ..... 40

3.4 Transformation of Damage Tensor and Damage Effect Tensor ..... 42

3.5 Applications ..... 46

**CHAPTER 4 DAMAGE EVOLUTION IN DUCTILE MATERIALS**

4.1 Ductile Damage Evolution ..... 60

4.2 Irreversible Thermodynamics Theory for Damaged Materials ..... 62

4.3 A Damage Evolution Model ..... 66

4.4 Experiments and Predictions ..... 73

**CHAPTER 5 DAMAGE DISTRIBUTIONS AND DAMAGE ZONES JUST AHEAD OF A MACROCRACK**

5.1 Damage Evolution at a Macrocrack Tip ..... 78

5.2 Description of Nonlinear Behavior in Materials . . . . . 79

5.3 Damage Distribution in the Region of a Macrocrack Tip . . . . . 84

5.4 Size of the Damage Zone . . . . . 91

**CHAPTER 6 DAMAGE ZONES IN MATERIALS WITH STRAIN HARDENING BEHAVIOR**

6.1 Damage Distribution of a Strain Hardening Material with a Macrocrack . . . . . 100

6.2 Size of the Damage Zone along a Macrocrack . . . . . 114

**CHAPTER 7 DAMAGE PERFORMANCE IN THE VICINITY OF A MACROCRACK TIP**

7.1 Solid State and Damage . . . . . 121

7.2 Damage in the vicinity of a Macrocrack . . . . . 123

7.3 The Effects of Local Fracture Path Deflections on the SIF . . . . . 127

7.4 The Effects of a Reduction in the Modulus of Elasticity on the SIF . . . . 133

7.5 The Effect of a Release of Residual Stresses on the SIF . . . . . 139

7.6 Toughening of Damaged Materials . . . . . 144

**CHAPTER 8 SUMMARY, CONCLUSIONS AND FUTURE WORK**

8.1 Summary . . . . . 146

8.2 Conclusions . . . . . 147

8.3 RecommendationS for Future Work . . . . . 150

**BIBLIOGRAPHY** . . . . . 151

**APPENDIX: NOMENCLATURE** . . . . . 164

# LIST OF TABLES

*Table* 2.1 Damage Variables

*Table* 4.1 State Coupling and Uncoupling

*Table* 4.2 Mechanical Properties and Damage Thresholds

# LIST OF FIGURES


| | |
|---|---|
| *Figure* 1.1 | The Evolution of Structure Design and Analysis |
| *Figure* 2.1 | An Element in a Damaged Material |
| *Figure* 2.2 | Damage of a Bar under Uniaxial Tension: (a) Initial Undamaged State; (b) Current Damaged State; (c) Fictitious Undamaged State |
| *Figure* 2.3 | Principal Values of the Damage Tensor: (a) Current Damaged Configuration; (b) Fictitious Undamaged Configuration |
| *Figure* 2.4 | Measurement of Effective Young's Modulus |
| *Figure* 2.5 | Fracture in Metals |
| *Figure* 3.1 | The Hypothesis of Strain Equivalence |
| *Figure* 3.2 | The Hypothesis of Total Complementary Energy Equivalence |
| *Figure* 3.3 | The Hypothesis of Incremental Complementary Energy Equivalence |
| *Figure* 3.4 | Incremental Damage Equivalence for Isotropic Damage |
| *Figure* 3.5 | Piecewise Linear Damage of Materials |
| *Figure* 3.6 | Transformation of Cartesian Coordinate Systems |
| *Figure* 3.7 | Damage Variable $D_1$ Versus Young's Modulus Ratio |
| *Figure* 3.8 | Damage Variable $D_2$ Versus Poisson's Ratio |
| *Figure* 3.9 | Damage Variable $D_1$ Versus Strain |
| *Figure* 3.10 | Damage Variable $D_2$ Versus Strain |
| *Figure* 3.11 | Shaft under Pure Torsion |

*Figure* 3.12 Effective Shear Modulus Ratio Versus Strain

*Figure* 3.13 Elastic Perfectly-Plastic Behavior

*Figure* 3.14 Isotropic Damage Variable $D$ Versus Strain Ratio

*Figure* 4.1 Ductile Damage Evolution

*Figure* 4.2 Progression of Damage Evolution

*Figure* 4.3 Comparison of Theoretical Predictions with Experimental Results

*Figure* 4.4 Influence of Stress Triaxiality on the Damage Evolution

*Figure* 4.5 Damage Evolution of Materials with Different Strain Hardening Exponents

*Figure* 5.1 Damage Evolution at a Crack Tip

*Figure* 5.2 Unloading Paths: (a) Elastic Damage without Plastic Deformation;
(b) Plastic Deformation without Damage; and
(c) General Unloading Path.

*Figure* 5.3 A Physical Representation of Unloading Paths

*Figure* 5.4 Experimental Loading-unloading Paths

*Figure* 5.5 A Plate with a Macrocrack under Loading (Mode I)

*Figure* 5.6 Undamaged and Damaged Materials

*Figure* 5.7 $\sigma \sim \varepsilon$ Relationship for Elastic-Perfectly Plastic Materials

*Figure* 5.8 A Center-Cracked Specimen and Its Finite Element Model

*Figure* 5.9 Damage Distribution in the Region of a Crack Tip

*Figure* 5.10 Damage Distribution in the Damage Zone Along the Crack Tip

*Figure* 5.11 Dugdale Model with Damage

*Figure* 5.12 Effective Poisson's Ratio

*Figure* 5.13 Comparison of the Size of Damage Zones

*Figure* 6.1 Closed Curve $\Gamma^*$ at the Crack Tip

*Figure* 6.2 Comparison of Stress Predictions

*Figure* 6.3 Load Application Steps

*Figure* 6.4 Damage Distribution around a Crack Tip for $n = 0.1$

*Figure* 6.5 Damage Distribution around a Crack Tip for $n = 0.2$

*Figure* 6.6 Damage Distribution around a Crack Tip for $n = 0.5$

*Figure* 6.7 Damage Distribution in the Damage Zone along the Crack Tip at $\sigma_\infty = 0.6\sigma_Y$

*Figure* 6.8 Damage Distribution in the Damage Zone along the Crack Tip at $\sigma_\infty = 0.7\sigma_Y$

*Figure* 6.9 Damage Distribution in the Damage Zone along the Crack Tip at $\sigma_\infty = 0.8\sigma_Y$

*Figure* 6.10 Dugdale Model with Damage

*Figure* 6.11 Weighting Functions

*Figure* 6.12 Comparison of the Size of Damage Zones

*Figure* 7.1 Elementary Deformation and Damage

*Figure* 7.2 Voids or Microcracks along Grain Boundaries

*Figure* 7.3 Microcracks and Voids in the Vicinity of a Macrocrack under Mode I Loading

*Figure* 7.4 Statistical Distribution of Microcracks in the Vicinity of a Macrocrack

*Figure* 7.5 Crack Tip Advance Displacement and Applied Stress Intensity Factor

*Figure* 7.6 CTOD at Different Percentage of Microcrack Lengths ($B_o$: the scanned length of crack front, $C$: sum of the microcrack lengths measured in the direction of $B_o$)

*Figure* 7.7 Local Fracture Path Deflections

*Figure* 7.8 Stress Field of a Macrocrack

*Figure* 7.9 Macrocrack with Microcrack Path Deflections

*Figure* 7.10 Influence of Fracture Path Deflections on the SIF

*Figure* 7.11 Damage Zone

*Figure* 7.12 Influence of a Reduction in the Modulus on the SIF

*Figure* 7.13 Characteristic Tensile Stress-Strain Curves with Saturation Stage

*Figure* 7.14 Influence of a Release of Residual Stresses on the SIF

# CHAPTER ONE

## INTRODUCTION

### 1.1 Prologue

The evolution of structural analysis and design is schematically described in *Figure* 1.1. The earliest work simply relied upon previous attempts, proceeding in an essentially trial and error manner. It was not until the development of the concepts of stress and strain, and their incorporation into the mathematical theory of elasticity during the nineteenth century that quantitative procedures for analysis and design became possible. The application of concepts of elasticity to determine the strength of a material is shown as the second step in the figure.

Depicted as the third step is a consideration of stress concentrations in the stress analysis of an elliptical hole for a plate in tension. This concept relates the stress acting at the most highly stressed point on the edge of the hole to the remote stress. A key subsequent step was the connection of the stress intensity factor to Griffith's energy balance. This accomplishment resulted in the development of linear elastic fracture mechanics and is shown as the fourth step of the evolution.

The fifth step shown in the figure represents the more recent interest and activities of many researchers during the past two decades. This is an explicit recognition that microcracks or other defects do exist in every engineering structure, whether arising from initial defects in the material, from fabrication flaws, or from service conditions. The analysis of evolution, distribution and propagation of these defects makes it possible to predict and control them before they attain critical values. This new science is popularly known as *continuum damage mechanics* (CDM) and has now become a new branch of mechanics.

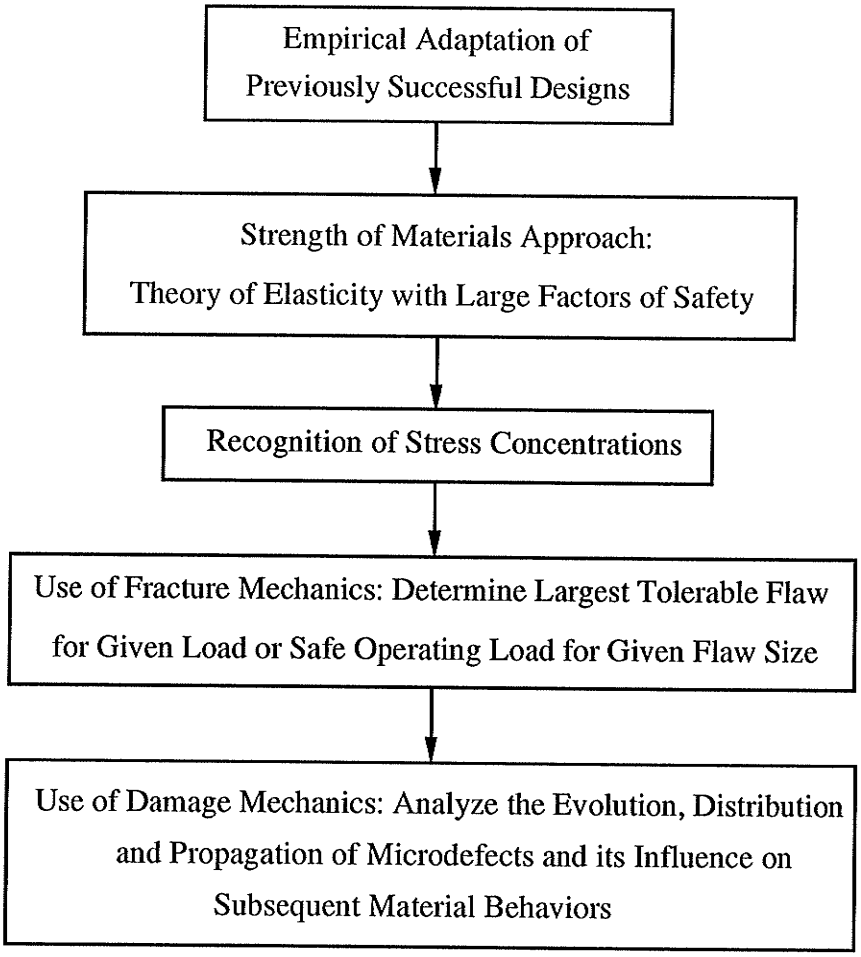



*Figure* 1.1: The Evolution of Structural Analysis and Design

As is well-known, engineering materials subjected to unfavorable mechanical and/or environmental conditions can result in a degradation of material properties and behavior due to the formation, accumulation and growth of microstructural defects. These material properties are the strength, rigidity and fracture toughness of the material, and the physical behavior include wave propagation velocities, heat and electric conductions, effects of magnetism and etc. The changes of the defects can be continuous or discontinuous, depending on the loading conditions and the material itself, leading ultimately to failure. At the microscale level this is the accumulation of microstresses in the neighbourhood of defects or interfaces and the breaking of atomic bonds in the material. At the mesoscale level, this is the growth and the coalescence of microcracks or microvoids which finally form a macrocrack. Thus, at the macroscale level, this is the growth of that macrocrack. Therefore, damage is attributed to the evolution and stable propagation of microcracks and voids in the material which in turn lead to macrocracks and a nonlinear stress-strain curve. There are two common approaches used to describe the influence of defects in the strength of a material. The first is the linear elastic fracture mechanics approach which considers the defects in a material as a single macrocrack and is based on conventional fracture parameters such as the J-integral, crack tip opening displacement (CTOD) and stress intensity factor (SIF). But there are many factors of microfracture in a heterogeneous material and this makes it difficult to model the behavior using the classical fracture mechanics in which each microcrack would have to be considered individually and result in micromechanical modelings. Although fewer assumptions are required and the elegance of the solutions make the micromechanical models interesting, the complexity of the rigorous models or the extensive simplifications necessary for practical models make the models impractical for large scale numerical implementation. Therefore, the second

method, CDM approach, is developed to analyze the evolution of the internal damage before the macrocracks become visible. CDM considers the defects of a material as continuously distributed microscopic damage and uses an appropriate internal state variable, namely, the damage variable to describe damage evolution and mechanical behavior of damaged materials. It discusses systematically the effects of damage on the mechanical properties of materials and structures, the damage itself on the subsequent development of damage under the influence of external conditions. CDM has now become an important branch of mechanics. An excellent account of the progress of CDM is outlined in [1] and [2].

## 1.2 Literature Survey

Since the first introduction of the concept of CDM by Kachanov [3] in the description of accelerating creep rates due to progressive material deterioration accompanied by the nucleation and propagation of microcracks and microvoids, many researchers have been trying to use it to solve practical engineering problems. For example, Ghrib and Tinawi [4] who used this concept to study the seismic response of concrete gravity dams; Jubran and Cofer [5] applied the method to evaluate the ultimate strength of a welded tubular connection (T-joint); Chow and co-workers used it to study ductile failure [6, 7], crack initiation [8], and crack propagations [9]; and so on. Meanwhile, some new damage terms are developed based on different damage principals. These terminology include:

(a) *Creep Damage* ([3], [10-12]): At high temperature and under the action of stress loadings, an accumulation and growth of microvoids in metal grains takes place (ductile

transgranular creep fracture). At the same time there occurs an accumulation and growth of microcracks on intergranular boundaries (brittle intergranular creep fracture).

(b) *Ductile Damage* ([13-16]): The same phenomenon, i.e., nucleation and growth of microvoids and microcracks, takes place in metals as the results of large plastic strains.

(c) *Fatigue Damage* ([17-20]): Under the action of cyclic loading a gradual deterioration of the structure of a material, caused by the accumulation and growth of microcracks and macrocracks, takes place.

(d) *Damage of Concrete* ([21-23]): Since concrete is a non-homogeneous material there are zones of weak mechanical resistance in it, which under loading, leads to the appearance of cracks.

(e) *Spall Damage* ([24-26]): Elastic and elastic-plastic damage due to impulsive loads. It is a uniform distribution of microscopic cavities and cracks, coupling between void growth and stress waves.

(f) *Corrosion Damage* ([27-31]): Pitting corrosion, intergranular corrosion, etc. Development of microcracks under stress in corrosive environments.

To derive the constitutive equations under the damage state, Lemaitre [10] proposed a hypothesis of the strain equivalence. This hypothesis is employed mainly in isotropic damage because it will result in asymmetry of the stiffness matrix when anisotropic damage is considered. As first reported by Cordebois and Sidoroff [32] that the damage developed in materials may be either isotropic or anisotropic even if the original material is isotropic. Different from Lemaitre's hypothesis, Sidoroff [33] suggested a hypothesis of the total complementary energy equivalence. Based on this energy equivalence hypothesis, Chow and Wang [34] proposed a generalized anisotropic damage theory. Using their model, the damage variables in the principal directions could be evaluated by conducting a

tensile test. Lee, Peng and Wang [35] proposed an anisotropic damage criterion which was achieved by introducing a damage strengthening concept just like the strain hardening concept in plasticity although the physical meaning is different. Using this criterion and Chow and Wang's anisotropic damage model [34], Chow and co-workers studied ductile fracture [6], crack initiation [8] and crack propagations [9]. Later, they analyzed the HRR fields for damaged materials [36]. This was achieved by describing the mechanical effects of the distributed microdefects in terms of the damage variable on the HRR field model for virgin materials. Toi and Che [37], Toi and Kiyosue [38] used Chow and Wang's theory [34] to model brittle microcracking in solids based on mesoscopic simulations for two and three dimensions. Luccioni, Oller and Danesi [39] tried to establish a plastic damaged model for anisotropic materials by assuming the existence of three spaces; a real damaged anisotropic space, a fictitious damaged isotropic space and a fictitious undamaged isotropic space. They solved the problem in the fictitious isotropic damaged space. However, all these models formulated on the basis of the elastic energy equivalence model proposed by Sidoroff [33], are restricted to small damage. Investigation into large damage is still very limited. Broberg [40] introduced a damage definition suitable for modeling large damage. When the damage is small, this definition reduces to the original Kachanov definition [3]. Luo, Mou and Han [41] proposed an incremental complementary elastic energy equivalence. Based on this assumption, they developed an anisotropic damage model. It has been shown that this hypothesis leads naturally to a theory for large anisotropic damage and that it reduces to the small damage model of Chow and Wang [34] when the damage is small.

Over the past decade, there has been a tremendous interest in ductile damage. Rousselier [43] considered ductile damage to be related to the density changes due to the inevitable

formation of microvoids during the plastic deformation process. However, this theory cannot yet be readily used for practical problems as it is difficult to measure the local changes in density. Lemaitre [13] developed a damage model to predict isotropic ductile damage by introducing a concept of the damage equivalent stress based on the thermodynamics. He found that the damage is linear with equivalent strain and quite dependent on the triaxiality by means of the damage equivalent stress. Tai and Yang [42] derived a void-damage model to analyze the growth and coalescence of microvoids for ductile damage. Thomson and Hancock [44] analyzed the ductile failure by void nucleation, growth and coalescence. They combined the observations of voids on metallographic sections with calculated deformation histories and the elliptical void growth equations to determine the local conditions for void nucleation and the strength of the particle-matrix interface. The influence of the stress triaxiality on the nucleation and coalescence were found. Sun et al. [45] implemented a local damage model into the finite element program ADINA to study the correlation between microscopical damage and macroscopical material damage in the analysis of ductile rupture of materials. Zheng, Luo and Zheng [15] formulated a microdamage evolution equation based on the irreversible thermodynamics and orthogonal flow rule. Then, by comparing with the microdamage evolution equation and invoking the principle of minimum strength, a macrodamage equation was obtained. In reality, the ductile damage can be caused by many different mechanisms, such as internal and external necking, nucleation and growth of microvoids, etc. Any of these mechanisms can cause the final fracture. Han and Mou [16] analyzed the void induced damage by using the effective stress concept and thermodynamics method. The effect of stress triaxiality on the damage evolutions have also been examined by Mou and Han [46].

Since macrocracks will dominate the material response when they form, the continuum damage mechanics is only applicable to the stage before the initiation of macrocracks. But the propagation of a macrocrack is still affected by the state of damage in the material, especially the damage in the vicinity area of the macrocrack tip. Numerical finite element analyses and experiment observations by Hayhurst, Dimmer and Morrison [47, 48] showed a strong concentration of damage ahead of a sharp macrocrack loaded in the opening mode of an infinite sheet (Mode I). This damage zone can cause the local fracture path very different from ideal cuts. These were also confirmed by the results of a microscopic examination [49]. As pointed out by Giovanola and Finnie [50], the validity of ductile fracture characterization based on the conventional fracture parameters is questionable. Also, Poe [51] indicated that it may not be possible to properly analyze the fracture process without an accurate knowledge of the size and nature of damage at the macrocrack tip. This is because these developing microdefects in the damage zone, interacting with the macrocrack and with each other, change the stress distribution in the vicinity of the macrocrack tip and therefore, affect crack propagations and conventional fracture parameters. For this reason, Chow and Lu [9] felt that the conventional fracture parameters cannot be considered as intrinsic material properties if the damage is not considered. Dugdale [52] calculated the length of the plastic zone in the direction of a macrocrack in Mode I for an elastic-perfectly plastic material. Janson [53] analyzed the stress distribution in the plastic zone by using the Dugdale model and the damage concept for an elastic-perfectly plastic material. However, in his work, he assumed the damage obeys a power relation and it is not too obvious how the exponent is obtained. Therefore, his model suffers from a lack of clear physical interpretation. Wu, Mai and Cotterell [54] established a model of fracture crack growth based on the modified Dugdale model and damage accumulation used by Budiansky and Hutchinson [55]. Using a Coffin-Manson

type law of plastic strain hysteresis energy for perfectly plastic material, they assumed that fatigue crack propagation is caused by damage accumulation due to cyclic plastic strain in the reversed plastic zone. Taylor, Chen and Kuszmaul [23] treated the dynamic fracture process in rock as a continuous accrual of damage and modeled the microcrack-induced damage accumulation in brittle rock under dynamic loading. In their model, they combined the theory of fracture mechanics with some statistical treatment to account for the random distribution of microcracks, and Budiansky and O'Connell's model [56] to determine the elastic miduli of a cracked solid was also employed. Chen [57] analyzed the continuum damage response of a center-cracked plain concrete panel in tension by assuming a Weibull statistical distribution of microcracks. Tai [58] investigated the damage variation at a macrocrack tip by using the effective plastic strains. The size of the damage zone is found to be dependent on the crack opening displacement, the critical recrystallization strain and the strain at damage initiation. But it is difficult to find an appropriate expression for the effective plastic strains for the materials. Chai [59] monitored the evolution of damage at the tip of macrocracks in adhesive bonds deforming in shear. Li and Du [60] analyzed the damage at a macrocrack tip in composite laminates. They tried to connect CDM with fracture mechanics by establishing some quantitative relations such as those between stress, energy release rate and damage variables, but no result was given in their work. Mou and Han [61] also analyzed the damage distributions and damage zones ahead of a macrocrack for elastic-perfectly plastic materials by using the isotropic case of their anisotropic large damage model [41]. This analysis has been extended to the prediction of damage distributions and damage zones for strain hardening materials with elastic damage [62].

The damage in the vicinity of a macrocrack causes a reduction in the modulus of elasticity in that area, whereas the reduction in the modulus will affect the SIF of the macrocrack to result in the so-called shielding phenomenon. In recent years, the shielding phenomenon has been a subject of several studies [63-75]. Evans and Fu [63, 64] studied the microcrack toughening associated with microstructural residual stresses arising from thermal contraction mismatch among randomly oriented grains. In their work, the concept of microcracking saturation was proposed which allowed the near tip crack field to be characterized by a SIF. Budiansky, Hutchinson and Lambropoulos [66], and Hutchinson [67] used this concept to consider the change of SIF due to strains arising from the release of residual stresses when microcracks are formed in the near tip area of a macrocrack. Shielding results for arbitrarily shaped microcrack zones were obtained for the case where the orientations of the microcracks are randomly distributed. Steif [68] analyzed cracktip shielding effects by modeling a semi-infinite macrocrack penetrating a circular inclusion which has a reduced modulus caused by microcracks. Shielding was also found for a wide range of material parameters. Employing a continuum damage mechanics approach, Chow and Lu [73] analyzed the macrocrack tip shielding in brittle solids. They found that by replacing the SIF by a near-tip SIF $K_{tip}$, the near-tip stress field can still be described by the classical singular solution, even for a material that has become anisotropic due to damage. They also concluded that isotropic damage is less effective than extremum anisotropic damage in macrocrack tip shielding. Mou and Han [74, 75] re-examined the damage performance in the vicinity of a macrocrack tip by considering damage distribution and damage size near the macrocrack tip. Effects due to local fracture path deflections, a reduction in the modulus of elasticity and a release of residual stresses during microcracking on SIF were studied in detail. The model used was based on the earlier

work of Mou and Han [46, 62] in which an approach was developed to predict damage distribution and the size of the damage zone under Mode I loading.

## 1.3 Objective of Research

The objective of the research is to develop a model to analyze large damage in continuum damage mechanics and use this model to study the damage evolution and damage distribution.

## 1.4 Scope of Study

The scope of the study encompasses the following areas:

- to formulate an incremental complementary energy approach to handle large damage,
- to include anisotropy in the model,
- to investigate damage evolution in ductile materials,
- to examine theoretically, damage distributions and damage zones ahead of a macrocrack under Mode I loading,
- to analyze the interaction between a macrocrack and damage zone, so as to be able to determine this interaction influence on the fracture characterizations under Mode I loading, and
- to carry out adequate model testing and verification by comparing its solutions with available experimental results, published results, finite element results, theoretical

results for simple limiting situations of (a) uniaxial tension, and (b) pure torsion, etc., to ensure the proposed theory is correctly formulated.

## 1.5 Thesis Layout

There are six main parts in this thesis: *Chapter 2*: Basic Concepts in Continuum Damage Mechanics; *Chapter 3*: The hypothesis of Incremental Complementary Energy Equivalence and the Theory of Large Anisotropic Damage; *Chapter 4*: Damage Evolution in Ductile Materials; *Chapter 5*: Damage Zones and Damage Distributions just ahead of a Macrocrack; *Chapter 6*: Damage Zones in Materials with Strain Hardening Behavior; *Chapter 7*: Damage Performance in the Vicinity of a Macrocrack Tip.

In *Chapter* 2, a general description of the continuum damage mechanics is presented. Damage variables, in the form of scalar, vector, second-order tensor and higher-order tensor are outlined. The concept of the effective stress is introduced. A general damage effect tensor is formulated which symmetrizes the effective stress. The common methods of experimental measurement of damage are also described.

In *Chapter* 3, two classical hypotheses for the deriving of the constitutive equations under damage state are presented: the hypothesis of strain equivalence and the hypothesis of total complementary energy equivalence. The advantages and disadvantages of these two hypotheses are described. Then, to overcome some disadvantages, the hypothesis of an incremental complementary energy equivalence is proposed which is then used to derive a large anisotropic damage model. This model reduces to the well-known small damage

model when the damage is small. Applications of the proposed damage model are illustrated by analyzing the cases of uniaxial tension, pure torsion and elastic perfectly-plastic behaved damage.

In *Chapter* 4, the irreversible thermodynamics theory coupled with the isotropic large damage model are used to develop a damage evolution model for ductile materials. The predictions of the damage evolution are then compared with experiment results. The predictions for materials with different strain hardening exponents and under different stress triaxiality are also given.

In *Chapter* 5, the nonlinear behavior of damaged materials are described. Damage zones and damage distributions ahead of a macrocrack in Mode I are analyzed by using Dugdale's model for materials with elastic perfectly-plastic behavior. The results are compared to those obtained via a finite element analysis. The sizes of the damage zones are also compared with those of the plastic zones predicted by Dugdale's model.

In *Chapter* 6, the study of chapter 5 is extended to strain hardening behaved damage materials. The formula of damage distribution and the size of damage zones are obtained. Comparisons with the finite element analysis are also conducted.

In *Chapter* 7, the damage performance in the vicinity of a macrocrack tip is examined. Special attention is paid to the effect of damage in the vicinity of a macrocrack tip on the stress intensity factor. The effects studied include local fracture path deflections, a reduction in the modulus of elasticity and a release of residual stresses during the

microcracking process. Damage distributions and the size of the damage zone ahead of a macrocrack are considered in the modeling.

Finally, in *Chapter* 8, an overall summary of the thesis is given and general conclusions from this doctoral research are drawn. Some future work is also suggested.

# CHAPTER TWO

## BASIC CONCEPTS IN CONTINUUM DAMAGE MECHANICS

In this chapter, an introduction to continuum damage mechanics is presented. The concepts of damage variables, effective stress and damage effect tensor are discussed. The chapter ends with a brief description on the experimental measurement of damage.

### 2.1 Damage Variables and Effective Stresses

In CDM, a damage variable is employed to describe the material deterioration. The damage variable can be a scalar, vector or tensor. The physical implications of the damage variable can be illustrated by considering a damage volume element at macroscale level as shown in *Figure* 2.1. Let $A$ be the overall cross-sectional area of the element before loading with its orientation defined by $\vec{n}$. After loading, the area $A$ becomes the effective area $\tilde{A}$. This is due to the material degradation caused by the presence of microcracks, voids and stress concentrations. If these microcracks and voids are assumed to be uniformly distributed in all directions, that is the damage is assumed to be isotropic, then the damage variable is defined as,

$$D = \frac{A - \tilde{A}}{A} \tag{1}$$

In addition this definition of the damage variable, Cordier and Van [76] defined $D$ as the percentage of broken grains relative to the total number of broken grains when the macrocrack is created. But the application of this definition is sustained some assumptions. Kempl [77] felt that quantities associated with failure are more appropriate indicators of damage than quantities associated with deformation. Therefore, he proposed the concept of a residual lifetime as a measure of damage. However, this kind of definition of damage is not suitable for the description of continuum solid mechanics states. From *Equation* (1), the relationship between the effective stress $\tilde{\sigma}$ and the usual Cauchy stress $\sigma$ is obtained as,

$$\tilde{\sigma} = \frac{1}{1-D}\sigma \tag{2}$$

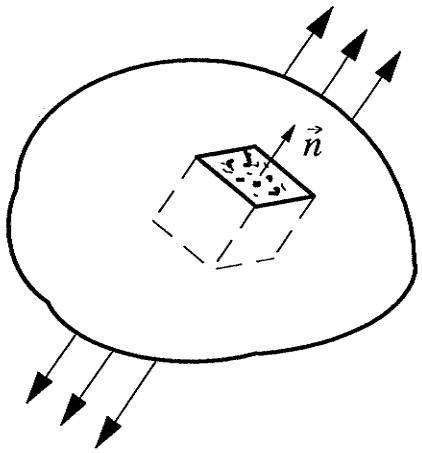



*Figure* 2.1: An Element in a Damaged Material

*Equations* (1) and (2) may also be physically illustrated for the case of a bar under uniaxial tension as depicted in *Figure* 2.2. Since $\tilde{A}$ is the effective load-carrying area of the current damage state, we can assume an equivalent fictitious undamaged bar subjected to the applied load $T$ with the cross-sectional area $\tilde{A}$ as shown in *Figure* 2.2(c).

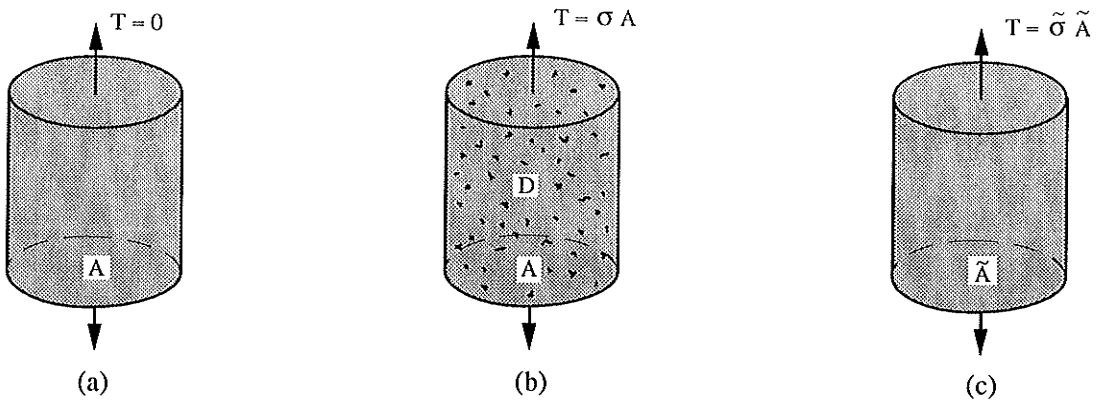
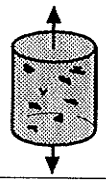
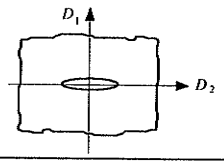
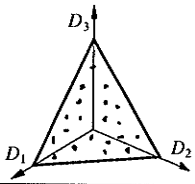



*Figure* 2.2: Damage of a Bar under Uniaxial Tension:
(a) Initial Undamaged State; (b) Current Damaged State;
(c) Fictitious Undamaged State

The scalar damage variable is adequate for modeling isotropic damage, i.e., for the damage characterized by the randomly distributed voids or by the homogeneous distribution of spherical cavities, but not applicable to damage with a marked directionality in void geometries or to damage with spherical cavities with a significant directionality in their spatial distribution. However, in the case of a small cavity density, the global deformation is almost isotropic and hence the scalar damage variable can also be employed for the constitutive equations of damaged materials. The implication and limitation of some scalar damage models were discussed in [78].

*Table* 2.1: Damage Variables

| Damage Variables | Applications | References | Figure Representation |
|---|---|---|---|
| Scalar | Creep<br>Void evolution<br>Fatigue failure<br>Elastic-plastic | [3], [10]<br>[13], [16]<br>[20]<br>[26] |  |
| Vector | Creep<br>Spalling<br>Elastic-brittle | [80]<br>[81]<br>[82], [83] |  |
| Second-order tensor | Creep<br>Elasticity<br>Elastic-plastic<br>General | [11]<br>[34], [41]<br>[79], [84], [85]<br>[35], [86], [87] |  |
| Higher-order tensor | Creep<br>Concrete<br>General | [88]<br>[89]<br>[90], [91] |  |

In most cases, even if the initial material properties are isotropic, the development of the material damage may be anisotropic. For this situation, a vector, a second or higher-order damage tensor has to be employed. *Table* 2.1 shows some examples of their applications. A vector damage variable can be used to describe the effects of the distributed plane cracks in the directions perpendicular to the plane of cracks. The magnitude of the vector represents either the area or the length of the crack and the direction represents the normal

to the plane of the crack. Although this is an improvement over the scalar representation, it still ignores the effect of the shape of the crack. Second and higher-order damage tensors can be used to describe the damage distributions and the mechanical effects of microscopic voids more accurately, but will result in greater mathematical complexities. One way to circumvent the mathematical complexities is to employ a symmetric second-order tensor as evident in a number of anisotropic damage models [6, 34, 41, 79, 84-87]. Suppose $\boldsymbol{D}$ is a symmetric second-order damage tensor and has the three principal values $D_1$, $D_2$ and $D_3$ corresponding to the three principal coordinates $X_1$, $X_2$, $X_3$. Then these values correspond to the reduction of the load-carrying areas of a tetrahedron in the $(X_1, X_2, X_3)$ coordinates as shown in *Figure* 2.3. That is,

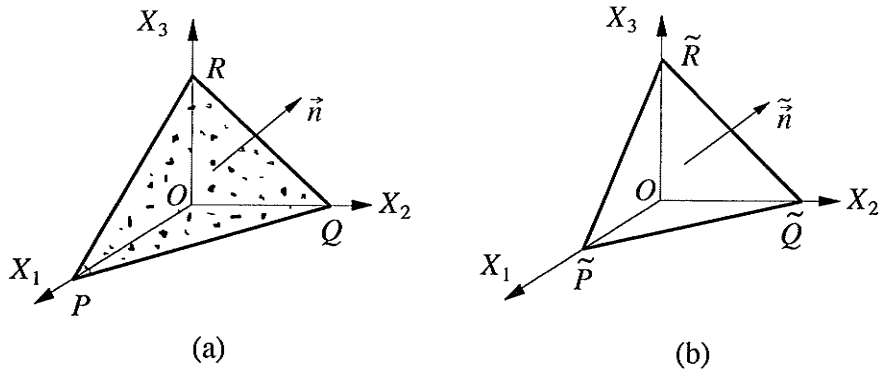



*Figure* 2.3: Principal Values of the Damage Tensor:
(a) Current Damaged Configuration; (b) Fictitious Undamaged Configuration

$$\vec{n} = \vec{X}_1,\ OQR \rightarrow O\tilde{Q}\tilde{R} \rightarrow D_1 = \frac{A_1 - \tilde{A}_1}{A_1}$$

$$\vec{n} = \vec{X}_2,\ ORP \rightarrow O\tilde{R}\tilde{P} \rightarrow D_2 = \frac{A_2 - \tilde{A}_2}{A_2}$$

$$\vec{n} = \vec{X}_3,\ OPQ \rightarrow O\tilde{P}\tilde{Q} \rightarrow D_3 = \frac{A_3 - \tilde{A}_3}{A_3}$$

For the anisotropic damage, the effective stress of *Equation* (2) can be expressed in a generalized form by,

$$\tilde{\sigma} = \boldsymbol{M}(\boldsymbol{D}) \bullet \sigma \tag{3}$$

or

$$\tilde{\sigma}_{ij} = M_{ijkl}\sigma_{kl}$$

where the $\bullet$ symbol denotes tensor product contracted over two indicates, and $M_{ijkl}$ are the components of $\boldsymbol{M}(\boldsymbol{D})$ which is a fourth-rank linear operator called the damage effect tensor of the fourth order. Note that $\boldsymbol{M}(\boldsymbol{D})$ reduces to a scalar $1/(1-D)$ when the damage is isotropic. As defined in *Equation* (3), although the Cauchy stress $\sigma$ is frame invariant, the effective stress $\tilde{\sigma}$ may not be symmetric or frame-invariant under the given transformation. It depends on the particular expression of $\boldsymbol{M}(\boldsymbol{D})$ that is used. However, if the effective stress is symmetrized, it can easily be shown that it satisfies the frame-invariance principle [92].

## 2.2 Damage Effect Tensor $\boldsymbol{M}(\boldsymbol{D})$

In general, it is easily seen from *Equation* (3) that the effective stress tensor is non-symmetric. To symmetrize the effective stress, the following relation is adopted:

$$\tilde{\sigma}_{ij} = \left(\delta_{ik} - D_{ik}\right)^{-1/2} \sigma_{kl} \left(\delta_{lj} - D_{lj}\right)^{-1/2} \tag{4}$$

*Equation* (4) is based on the geometric mean so as to make the effective stress symmetric. An alternative choice which is based on the arithmetic mean can be expressed as follows,

$$\tilde{\sigma}_{ij} = \frac{\sigma_{ik}\left(\delta_{kj} - D_{kj}\right)^{-1} + \left(\delta_{il} - D_{il}\right)^{-1}\sigma_{lj}}{2}$$

where the stress and the damage tensor are represented for a general state of damage, that is,

$$\left[\sigma_{ij}\right] = \begin{bmatrix} \sigma_{11} & \sigma_{12} & \sigma_{13} \\ \sigma_{12} & \sigma_{22} & \sigma_{23} \\ \sigma_{13} & \sigma_{23} & \sigma_{33} \end{bmatrix}, \qquad \left[D_{ij}\right] = \begin{bmatrix} D_{11} & D_{12} & D_{13} \\ D_{12} & D_{22} & D_{23} \\ D_{13} & D_{23} & D_{33} \end{bmatrix} \tag{5}$$

the symbol $\delta_{ij}$ is the Kronecker delta and $D_{ij}$ are less than 1. If *Equation* (4) is applied, then

$$\left[\delta_{ij} - D_{ij}\right]^{-1/2} = \frac{1}{\sqrt{\Theta}} \begin{bmatrix} \sqrt{\Delta_{22}\Delta_{33} - D_{23}^2} & \sqrt{D_{13}D_{23} + D_{12}\Delta_{33}} & \sqrt{D_{12}D_{23} + D_{13}\Delta_{22}} \\ \sqrt{D_{13}D_{23} + D_{12}\Delta_{33}} & \sqrt{\Delta_{11}\Delta_{33} - D_{13}^2} & \sqrt{D_{12}D_{13} + D_{23}\Delta_{11}} \\ \sqrt{D_{12}D_{23} + D_{13}\Delta_{22}} & \sqrt{D_{12}D_{13} + D_{23}\Delta_{11}} & \sqrt{\Delta_{11}\Delta_{22} - D_{12}^2} \end{bmatrix}$$

in which $\Theta$ is given by,

$$\Theta = \Delta_{11}\Delta_{22}\Delta_{33} - D_{23}^2\Delta_{11} - D_{13}^2\Delta_{22} - D_{12}^2\Delta_{33} - 2D_{12}D_{23}D_{13}$$

and

$$\Delta_{ij} = \delta_{ij} - D_{ij}$$

Then using *Equation* (4), the matrix representation for the effective stress tensor can be obtained. Rewriting the resulting effective stress matrix in the vector form $\{\sigma_{11} \quad \sigma_{22} \quad \sigma_{33} \quad \sigma_{12} \quad \sigma_{23} \quad \sigma_{13}\}^T$ and rearranging the terms, the following explicit $6\times6$ matrix representation for the damage effect tensor $\boldsymbol{M}(\boldsymbol{D})$ is obtained,

$$\left[M_{ij}(\boldsymbol{D})\right] = \frac{1}{\Theta}\begin{bmatrix} M_{11} & M_{12} & M_{13} & M_{14} & M_{15} & M_{16} \\ M_{21} & M_{22} & M_{23} & M_{24} & M_{25} & M_{26} \\ M_{31} & M_{32} & M_{33} & M_{34} & M_{35} & M_{36} \\ M_{41} & M_{42} & M_{43} & M_{44} & M_{45} & M_{46} \\ M_{51} & M_{52} & M_{53} & M_{54} & M_{55} & M_{56} \\ M_{61} & M_{62} & M_{63} & M_{64} & M_{65} & M_{66} \end{bmatrix} \tag{6}$$

where

$$M_{11} = \Delta_{22}\Delta_{33} - D_{23}^2$$

$$M_{21} = D_{13}D_{23} + D_{12}\Delta_{33}$$

$$M_{31} = D_{12}D_{23} + D_{13}\Delta_{22}$$

$$M_{41} = \sqrt{\left(\Delta_{22}\Delta_{33} - D_{23}^2\right)\left(D_{13}D_{23} + D_{12}\Delta_{33}\right)}$$

$$M_{51} = \sqrt{\left(D_{13}D_{23} + D_{12}\Delta_{33}\right)\left(D_{12}D_{23} + D_{13}\Delta_{22}\right)}$$

$$M_{61} = \sqrt{\left(\Delta_{22}\Delta_{33} - D_{23}^2\right)\left(D_{12}D_{23} + D_{13}\Delta_{22}\right)}$$

$$M_{12} = D_{13}D_{23} + D_{12}\Delta_{33}$$

$$M_{22} = \Delta_{11}\Delta_{33} - D_{13}^2$$

$$M_{32} = D_{12}D_{13} + D_{23}\Delta_{11}$$

$$M_{42} = \sqrt{\left(\Delta_{11}\Delta_{33} - D_{13}^2\right)\left(D_{13}D_{23} + D_{12}\Delta_{33}\right)}$$

$$M_{52} = \sqrt{\left(\Delta_{11}\Delta_{33} - D_{13}^2\right)\left(D_{12}D_{13} + D_{23}\Delta_{11}\right)}$$

$$M_{62} = \sqrt{\left(D_{13}D_{23} + D_{12}\Delta_{33}\right)\left(D_{12}D_{13} + D_{23}\Delta_{11}\right)}$$

$$M_{13} = D_{12}D_{23} + D_{13}\Delta_{22}$$

$$M_{23} = D_{12}D_{13} + D_{23}\Delta_{11}$$

$$M_{33} = \Delta_{11}\Delta_{22} - D_{12}^2$$

$$M_{43} = \sqrt{\left(D_{13}D_{23} + D_{12}\Delta_{33}\right)\left(D_{12}D_{13} + D_{23}\Delta_{11}\right)}$$

$$M_{53} = \sqrt{\left(\Delta_{11}\Delta_{22} - D_{12}^2\right)\left(D_{12}D_{13} + D_{23}\Delta_{11}\right)}$$

$$M_{63} = \sqrt{\left(\Delta_{11}\Delta_{22} - D_{12}^2\right)\left(D_{12}D_{23} + D_{13}\Delta_{22}\right)}$$

$$M_{14} = 2\sqrt{\left(\Delta_{22}\Delta_{33} - D_{23}^2\right)\left(D_{13}D_{23} + D_{12}\Delta_{33}\right)}$$

$$M_{24} = 2\sqrt{\left(\Delta_{11}\Delta_{33} - D_{13}^2\right)\left(D_{13}D_{23} + D_{12}\Delta_{33}\right)}$$

$$M_{34} = 2\sqrt{\left(D_{12}D_{23} + D_{13}\Delta_{22}\right)\left(D_{12}D_{13} + D_{23}\Delta_{11}\right)}$$

$$M_{44} = D_{13}D_{23} + D_{12}\Delta_{33} + \sqrt{\left(\Delta_{11}\Delta_{33} - D_{13}^2\right)\left(\Delta_{22}\Delta_{33} - D_{23}^2\right)}$$

$$M_{54} = \sqrt{\left(\Delta_{11}\Delta_{33} - D_{13}^2\right)\left(D_{12}D_{23} + D_{13}\Delta_{22}\right)} + \sqrt{\left(D_{12}D_{13} + D_{23}\Delta_{11}\right)\left(D_{13}D_{23} + D_{12}\Delta_{33}\right)}$$

$$M_{64} = \sqrt{\left(D_{13}D_{23} + D_{12}\Delta_{33}\right)\left(D_{12}D_{23} + D_{13}\Delta_{22}\right)} + \sqrt{\left(\Delta_{22}\Delta_{33} - D_{23}^2\right)\left(D_{12}D_{13} + D_{23}\Delta_{11}\right)}$$

$$M_{15} = 2\sqrt{\left(D_{13}D_{23} + D_{12}\Delta_{33}\right)\left(D_{12}D_{23} + D_{13}\Delta_{22}\right)}$$

$$M_{25} = 2\sqrt{\left(\Delta_{11}\Delta_{33} - D_{13}^2\right)\left(D_{12}D_{13} + D_{23}\Delta_{11}\right)}$$

$$M_{35} = 2\sqrt{\left(\Delta_{11}\Delta_{22} - D_{12}^2\right)\left(D_{12}D_{13} + D_{23}\Delta_{11}\right)}$$

$$M_{45} = \sqrt{\left(\Delta_{11}\Delta_{33} - D_{13}^2\right)\left(D_{12}D_{23} + D_{13}\Delta_{22}\right)} + \sqrt{\left(D_{13}D_{23} + D_{12}\Delta_{33}\right)\left(D_{12}D_{13} + D_{23}\Delta_{11}\right)}$$

$$M_{55} = D_{12}D_{13} + D_{23}\Delta_{11} + \sqrt{\left(\Delta_{11}\Delta_{33} - D_{13}^2\right)\left(\Delta_{11}\Delta_{22} - D_{12}^2\right)}$$

$$M_{65} = \sqrt{\left(D_{12}D_{23} + D_{13}\Delta_{22}\right)\left(D_{12}D_{13} + D_{23}\Delta_{11}\right)} + \sqrt{\left(\Delta_{11}\Delta_{22} - D_{12}^2\right)\left(D_{13}D_{23} + D_{12}\Delta_{33}\right)}$$

$$M_{16} = 2\sqrt{\left(\Delta_{22}\Delta_{33} - D_{23}^2\right)\left(D_{12}D_{23} + D_{13}\Delta_{22}\right)}$$

$$M_{26} = 2\sqrt{(D_{13}D_{23} + D_{12}\Delta_{33})(D_{12}D_{13} + D_{23}\Delta_{11})}$$

$$M_{36} = 2\sqrt{(\Delta_{11}\Delta_{22} - D_{12}^2)(D_{12}D_{23} + D_{13}\Delta_{22})}$$

$$M_{46} = \sqrt{(D_{13}D_{23} + D_{12}\Delta_{33})(D_{12}D_{23} + D_{13}\Delta_{22})} + \sqrt{(\Delta_{22}\Delta_{33} - D_{23}^2)(D_{12}D_{13} + D_{23}\Delta_{11})}$$

$$M_{56} = \sqrt{(D_{12}D_{23} + D_{13}\Delta_{22})(D_{12}D_{13} + D_{23}\Delta_{11})} + \sqrt{(\Delta_{11}\Delta_{22} - D_{12}^2)(D_{13}D_{23} + D_{12}\Delta_{33})}$$

$$M_{66} = D_{12}D_{23} + D_{13}\Delta_{22} + \sqrt{(\Delta_{11}\Delta_{22} - D_{12}^2)(\Delta_{22}\Delta_{33} - D_{23}^2)}$$

Obviously, ***M(D)*** is not symmetric. If the principal damage variables $D_1$, $D_2$ and $D_3$ are used, it can be easily verified that the damage effect tensor in *Equation* (6) reduces to the following diagonalized form:

$$\left[M_{ij}(D)\right] = \begin{bmatrix} \frac{1}{1-D_1} & 0 & 0 & 0 & 0 & 0 \\ 0 & \frac{1}{1-D_2} & 0 & 0 & 0 & 0 \\ 0 & 0 & \frac{1}{1-D_3} & 0 & 0 & 0 \\ 0 & 0 & 0 & \frac{1}{\sqrt{(1-D_1)(1-D_2)}} & 0 & 0 \\ 0 & 0 & 0 & 0 & \frac{1}{\sqrt{(1-D_2)(1-D_3)}} & 0 \\ 0 & 0 & 0 & 0 & 0 & \frac{1}{\sqrt{(1-D_3)(1-D_1)}} \end{bmatrix} \tag{7}$$

*Equation* (7) is exactly the form proposed by Sidoroff [33]. If the principal directions of the effective stresses and the material damage during loading are assumed to coincide with the conventional stresses, then *Equation* (4) becomes,

$$\begin{Bmatrix} \tilde{\sigma}_1 \\ \tilde{\sigma}_2 \\ \tilde{\sigma}_3 \\ \tilde{\sigma}_4 \\ \tilde{\sigma}_5 \\ \tilde{\sigma}_6 \end{Bmatrix} = \begin{Bmatrix} \sigma_1/(1-D_1) \\ \sigma_2/(1-D_2) \\ \sigma_3/(1-D_3) \\ 0 \\ 0 \\ 0 \end{Bmatrix}$$

Note that $\tilde{\sigma}_4 = \tilde{\sigma}_5 = \tilde{\sigma}_6 = 0$ which means that the effective shear stresses are zero and thus there is no shear stresses associated with area reductions.

## 2.3 Experimental Measurement of Damage

Damage variables relate to the overall area of defects in a specimen. Therefore the characteristics like orientation, density, shape etc. will affect the damage variable $D_i$. Several experimental methods can be used to measure damage quantitatively. They include direct measurements, variation of the elasticity modulus, variation of the microhardness, variation of density, electrical resistance, acoustic emission and etc. [93]. Note that the direct measurement and the variation of the elasticity modulus methods are usually employed for engineering materials. However, both of them are destructive methods. The direct measurement consists of the evaluation of the total defects areas lying on an element surface at mesoscale level. An example of this method can be found in [14] whose results have been used to verify the damage evolution model developed in [16]. The variation of density approach is not applicable when the anisotropic damage is to be considered since the measurement of density change can not provide any direction information. Therefore, it can only be used to evaluate isotropic damage, or used for the purpose of overall

evaluation of the damage in the material. The variation of the elasticity modulus technique may be used for any kind of damage as long as damage is uniformly distributed in the volume. By measuring the effective Young's modulus $\tilde{E}$ at unloading or reloading path (see *Figure* 2.4) and effective poisson's ratio, the damage variables in the principal directions $D_1$, $D_2$ and $D_3$ can be determined experimentally as shown by Chow and Wang [34]. The relationship of the damage variable with the effective Young's modulus will be discussed later.

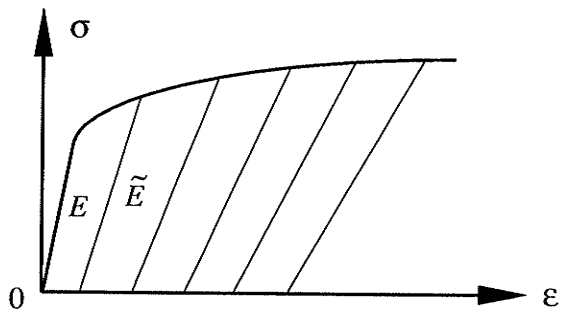
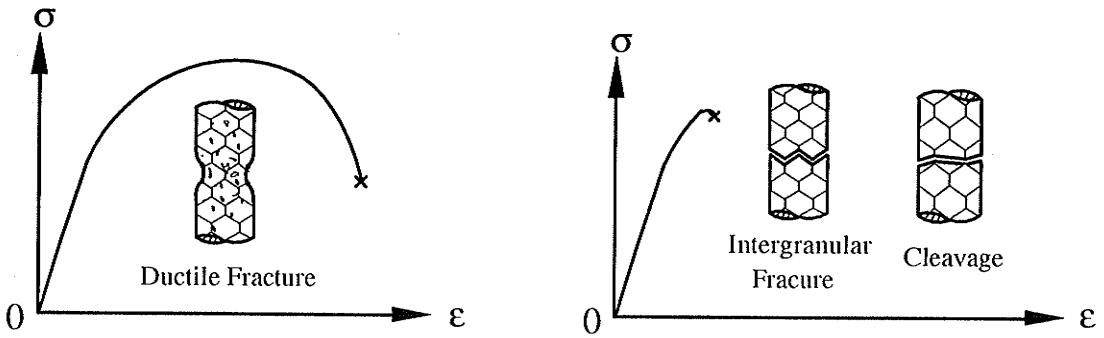



*Figure* 2.4: Measurement of Effective Young's Modulus

## 2.4 Ductile Damage versus Brittle Damage in the Fracture Process

*Figure* 2.5(a) and (b) schematically illustrates the uniaxial tensile stress-strain behavior in ductile and brittle materials. Ductile materials are characterized by a prolonged plastic deformation phase whereas brittle materials exhibit negligible plastic deformation. For a ductile material, the stress eventually reaches an instability point, where strain hardening

cannot keep pace with the loss in the cross sectional area, and a necked region forms beyond the maximum load. Microvoids nucleate at inclusions and the second phase particles, the voids grow together to form a macroscopic flaw, which leads ultimately to fracture. In ductile materials, if the second phase particles and inclusions are well bonded to the matrix, then void nucleation is often the critical step because fracture occurs soon after the voids are formed. If void nucleation occurs with little difficulty, the fracture properties are controlled by the growth and coalescence of voids. The failure will occur only after the growing voids reach a critical size (relative to their spacing) and a local plastic instability develops between voids. For a brittle material, the failure is typically by either cleavage or intergranular fracture. Cleavage is most likely when plastic flow is restricted. Therefore cleavage can be preceded by large scale plastic flow and ductile crack growth. Intergranular fracture may take place if microdefects or cavitation, microcracking and corrosion occur mainly on grain boundaries.




(a) Ductile Fracture

(b) Brittle Fracture

*Figure* 2.5: Fracture in Metals

# CHAPTER THREE

## THE HYPOTHESIS OF INCREMENTAL COMPLEMENTARY ENERGY EQUIVALENCE AND THE THEORY OF LARGE ANISOTROPIC DAMAGE

The central theme of this doctoral dissertation is introduced here by formulating the hypothesis of incremental complementary energy equivalence. Based on this hypothesis, a theory of large anisotropic damage is proposed. To verify and assess the model, several test examples are analyzed.

### 3.1 Hypotheses for Modeling Damage State Constitutive Equations

Three hypotheses are available for modeling constitutive equations under the damage state. They are as follows.

*(1) The Hypothesis of Strain Equivalence (J. Lemaitre and J. Chaboche, [94])*

The method of local states assumes the thermomechanical state at a point to be completely defined by a set of continuous state variables. In 1974, Lemaitre and Chaboche [94] argued that when this concept is applied at the microscale level, it implies that the constitutive equations (for computing strains) of a microvolume element are not modified

by a neighboring microvolume element containing a microcrack. Extrapolating to the mesoscale level, they proposed a strain equivalence hypothesis which states that the strains computed from the constitutive equations for a damaged material may be derived in the same way as for a virgin material by replacing the usual stress by the effective stress. This is graphically sketched in *Figure* 3.1. According to this hypothesis, the damage evolution is only characterized by a decrease in stress, with the strain remaining unchanged. But in reality, damage which is due to microcracks and voids and thus resulting in a loss of stiffness, must produce both stress and strain changes. However, the single biggest disadvantage of the Lemaitre and Chaboche's hypothesis is that it produces asymmetry in the stiffness matrix when anisotropic damage is modeled [34], unless some very strong restrictions on the form of the damage effect tensor are assumed. These drawbacks led others to consider alternative approaches to model damage.

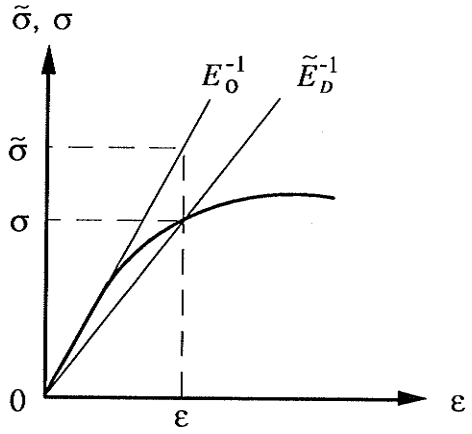



*Figure* 3.1: The Hypothesis of Strain Equivalence.

*(2) The Hypothesis of Total Complementary Energy Equivalence (F. Sidoroff [33])*

In 1980, Sidoroff [33] proposed the hypothesis of total complementary energy equivalence to overcome the asymmetry problem. He assumed that the total complementary energy for a damaged material $\Psi_c\left(\sigma, \tilde{\boldsymbol{E}}_D^{-1}, \boldsymbol{D}\right)$ is of the same form as that for an undamaged material $\Psi_c\left(\tilde{\sigma}, \boldsymbol{E}_o^{-1}, 0\right)$, with the exception that the stress is now replaced by the effective stress or

$$\Psi_c\left(\sigma, \tilde{\boldsymbol{E}}_D^{-1}, \boldsymbol{D}\right) = \Psi_c\left(\tilde{\sigma}, \boldsymbol{E}_o^{-1}, 0\right)$$

Since

$$\begin{aligned}\Psi_c\left(\tilde{\sigma}, \boldsymbol{E}_o^{-1}, 0\right) &= \frac{1}{2}\tilde{\sigma}^T \bullet \boldsymbol{E}_o^{-1} \bullet \tilde{\sigma} \\ &= \frac{1}{2}\sigma^T \bullet \boldsymbol{M}(\boldsymbol{D})^T \bullet \boldsymbol{E}_o^{-1} \bullet \boldsymbol{M}(\boldsymbol{D}) \bullet \sigma \\ &= \frac{1}{2}\sigma^T \bullet \tilde{\boldsymbol{E}}_D^{-1} \bullet \sigma\end{aligned}$$

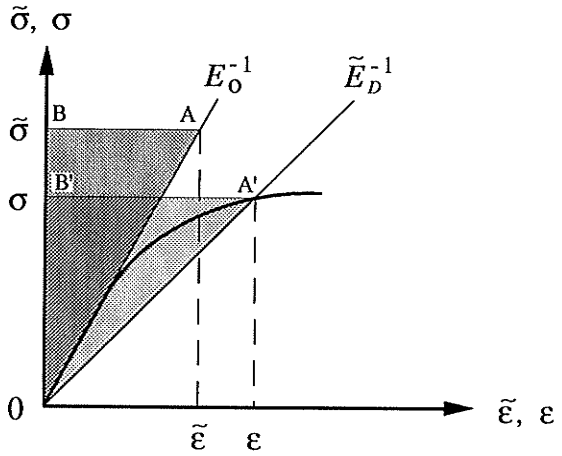



*Figure* 3.2: The Hypothesis of Total Complementary Energy Equivalence.

where *Equation* (3) has been used and $\tilde{\boldsymbol{E}}_D^{-1} = \boldsymbol{M}(\boldsymbol{D})^T \bullet \boldsymbol{E}_o^{-1} \bullet \boldsymbol{M}(\boldsymbol{D})$ is the effective modulus at damage state $\boldsymbol{D}$. Therefore this total energy equivalence can be schematically shown by *Figure* 3.2 where the areas *AB0* and *A'B'0* are assumed to be equal.

The concept of energy equivalence is more fundamental than the notion of strain equivalence. This is because energy is a more fundamental variable than strain (or stress) in describing a state of material, damaged or otherwise. Thermodynamically, deformation in solids is a process by which energy is transferred, stored, and/or dissipated. The first law of thermodynamics is a continuum postulate of the energy balance. The second law states that if an energy transfer is to occur naturally, it should be accompanied by an increase (or at least a non-decrease) in the entropy of the original state. Therefore, it is the concept of energy and not that of strain or stress, in rendering a logically simpler and more comprehensive way of characterizing real and irreversible physical processes.

Adopting Sidoroff's hypothesis, Chow and Wang [34] developed a model that is valid for anisotropic damage. They showed mathematically that symmetry in the stiffness matrix for the anisotropic damage is still retained. However, as we shall see, the models developed so far are not valid for large damage. As shown in *Figure* 3.2, the hypothesis of total complementary energy equivalence is based on the secant modulus line *A'0* and depending on the shape of the stress-strain curve, the resulting approximation of the area *A'B'0* can be crude. For example, the area formed by the triangle *A'B'0* can differ significantly from that bounded by the curve *0A'* and lines *0B'* and *A'B'*. To avoid this problem, we introduce the concept of an incremental area instead of a total area. This approach then allows us to arbitrarily choose the incremental step size and by making the step size very small, the

difference in areas between a triangle and that bounded by a curve can be made very small. However, the price to be paid is that a summation of all the incremental areas is now required. Further details of this approach is described next.

*(3) The Hypothesis of Incremental Complementary Energy Equivalence (A. Luo, Y. Mou and R. Han [41])*

The hypothesis of *incremental* complementary energy equivalence, first proposed by Luo, Mou and Han [41] in 1992, states that the incremental complementary elastic energy between the conventional stresses $\sigma_D$ and $\sigma_D + d\sigma_D$ for a damaged material characterized by a damage tensor $\boldsymbol{D} + d\boldsymbol{D}$, $\delta\Psi_c\left(d\sigma_D, \tilde{\boldsymbol{E}}^{-1}_{D+dD}, \boldsymbol{D} + d\boldsymbol{D}\right)$, as shown in *Figure* 3.3, is equivalent to the incremental complementary elastic energy between the effective stresses $\tilde{\sigma}_{D+dD}$ and $\tilde{\sigma}_{D+dD} + d\tilde{\sigma}_{D+dD}$ for a damaged material characterized by a damage tensor $\boldsymbol{D}$, $\delta\Psi_c\left(d\tilde{\sigma}_{D+dD}, \tilde{\boldsymbol{E}}^{-1}_{D}, \boldsymbol{D}\right)$. That is, the areas of $A'B'C'D'$ and $ABCD$ are equal, or

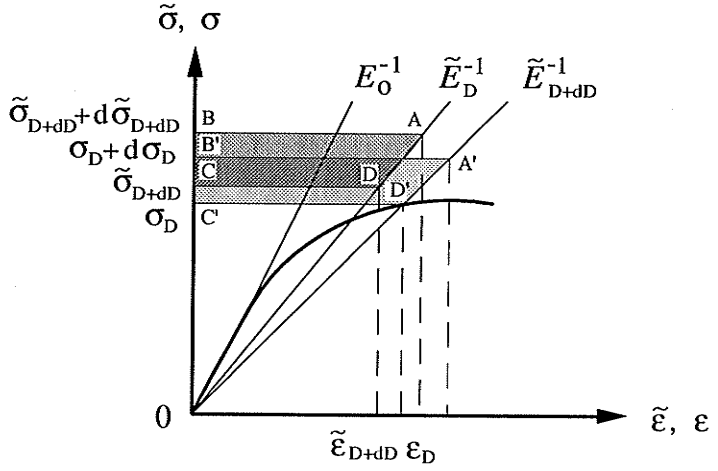



*Figure* 3.3: The Hypothesis of Incremental Complementary Energy Equivalence.

$$\delta\Psi_c\left(d\sigma_D, \tilde{E}^{-1}_{D+dD}, D+dD\right) = \delta\Psi_c\left(d\tilde{\sigma}_{D+dD}, \tilde{E}^{-1}_{D}, D\right) \tag{8}$$

For isotropic damage, the process is sketched in *Figure* 3.4, in which the damaged material is "transformed" from its damage to the fictitious undamaged states, through a series of sequential steps, $D+(dD)_1$, $D$, $D-(dD)_2, \cdots, 0$ (undamaged state).

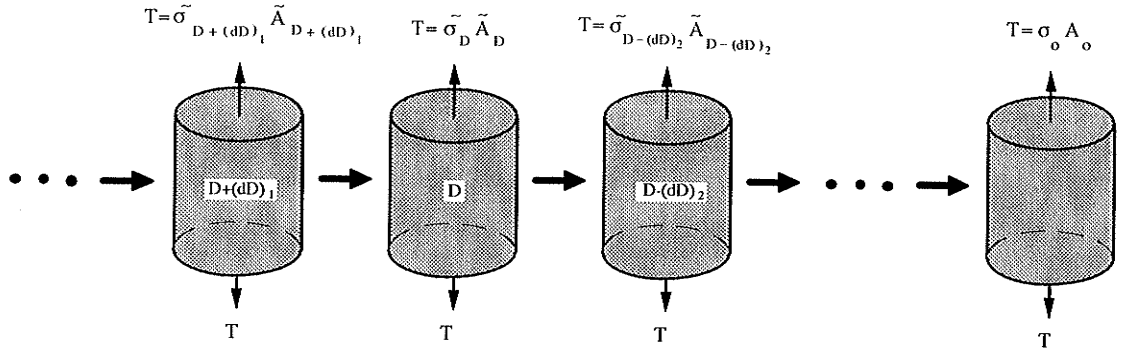



*Figure* 3.4: Incremental Damage Equivalence for Isotropic Damage.

Since the new hypothesis of Luo, Mou and Han [41] is applicable to large damage, it is more general than all previous others. The formulation of large damage based on this hypothesis is presented next.

## 3.2 The Theory of Large Anisotropic Damage

In the undamaged state, the linear elastic constitutive equation is,

$$\varepsilon^e = \boldsymbol{E}_o^{-1} \bullet \sigma \tag{9}$$

where $\varepsilon^e$, $\boldsymbol{E}_o^{-1}$ are respectively, the elastic strain and the elastic tensor. When a material is damaged, the constitutive relation becomes,

$$\varepsilon^e = \tilde{\boldsymbol{E}}_D^{-1} \bullet \sigma$$

in which $\tilde{\boldsymbol{E}}_D^{-1}$ is the effective elastic tensor. For small, incremental damage, the relation between the stress $\sigma$ and the effective stress $\tilde{\sigma}$ may be assumed to be similar to *Equation* (3) namely,

$$\tilde{\sigma}_{D+dD} = \boldsymbol{M}(d\boldsymbol{D}) \bullet \sigma_D \tag{10}$$

From *Figure* 3.3, we have,

$$\delta\Psi_c\left(d\sigma_D, \tilde{\boldsymbol{E}}_{D+dD}^{-1}, \boldsymbol{D} + d\boldsymbol{D}\right) = \frac{1}{2} d\sigma_D^T \bullet \tilde{\boldsymbol{E}}_{D+dD}^{-1} \bullet \left(2\sigma_D + d\sigma_D\right) \tag{11}$$

and together with *Equation* (10), we get,

$$\begin{aligned} \delta\Psi_c\left(d\tilde{\sigma}_{D+dD}, \tilde{\boldsymbol{E}}_D^{-1}, \boldsymbol{D}\right) &= \frac{1}{2} d\tilde{\sigma}_{D+dD}^T \bullet \tilde{\boldsymbol{E}}_D^{-1} \bullet \left(2\tilde{\sigma}_{D+dD} + d\tilde{\sigma}_{D+dD}\right) \\ &= \frac{1}{2} d\sigma_D^T \bullet \boldsymbol{M}(d\boldsymbol{D})^T \bullet \tilde{\boldsymbol{E}}_D^{-1} \bullet \boldsymbol{M}(d\boldsymbol{D}) \bullet \left(2\sigma_D + d\sigma_D\right) \end{aligned} \tag{12}$$

Invoking the proposed hypothesis and substituting *Equations* (11) and (12) into *Equation* (8) yields,

$$\tilde{\boldsymbol{E}}_{D+dD}^{-1} = \boldsymbol{M}(d\boldsymbol{D})^T \bullet \tilde{\boldsymbol{E}}_D^{-1} \bullet \boldsymbol{M}(d\boldsymbol{D}) \tag{13}$$

From thermodynamics, the constitutive relation is given by,

$$\begin{aligned}\varepsilon_D^e &= \frac{\partial\left[\delta\Psi_c\left(d\sigma_D, \tilde{E}_{D+dD}^{-1}, D+dD\right)\right]}{\partial\left(d\sigma_D\right)} \\ &= \left(M(dD)^T \bullet \tilde{E}_D^{-1} \bullet M(dD)\right) \bullet \sigma_D\end{aligned} \tag{14}$$

It is clear from *Equations* (13) and (14) that the constitutive relation between the stress and strain is,

$$\varepsilon_D^e = \tilde{E}_{D+dD}^{-1} \bullet \sigma_D \tag{15}$$

Multiplying each side of *Equation* (14) by $\left(M(dD)^T\right)^{-1}$ and simplifying via *Equation* (10), we have,

$$\begin{aligned}\left(M(dD)^T\right)^{-1} \bullet \varepsilon_D^e &= \tilde{E}_D^{-1} \bullet \left(M(dD) \bullet \sigma_D\right) \\ &= \tilde{E}_D^{-1} \bullet \tilde{\sigma}_{D+dD}\end{aligned} \tag{16}$$

The effective elastic strain $\tilde{\varepsilon}_{D+dD}^e$ can now be defined by,

$$\tilde{\varepsilon}_{D+dD}^e = \left(M(dD)^T\right)^{-1} \bullet \varepsilon_D^e$$

which implies that the constitutive relation for the damaged material at state $D+dD$ can be expressed in the form of effective stress and effective strain as follows,

$$\tilde{\varepsilon}_{D+dD}^e = \tilde{E}_D^{-1} \bullet \tilde{\sigma}_{D+dD} \tag{17}$$

Comparing *Equations* (9) and (17), it is obvious that to preserve the form of the constitutive equation at each stage of damage, it is necessary to replace strains and stresses by their effective counterparts. For example in going from an undamaged state, i.e. $\boldsymbol{D}=0$, to a damage increment state, i.e. $d\boldsymbol{D}$, the constitutive relation is,

$$\tilde{\varepsilon}^{e}_{d\boldsymbol{D}} = \boldsymbol{E}_o^{-1} \bullet \tilde{\sigma}_{d\boldsymbol{D}}$$

Thus, the incremental complementary energy equivalence can establish the relationship at each damage incremental step. It reflects the damage as a process of incremental material deterioration. Since we are dealing with incremental quantities, *Equation* (15) is applicable not only to small damage but also to large damage, assuming damage can be modeled as a series of small incremental damage. Note that small damage here refers to the situation where the damage variables $D_i << 1$. The derivations of the effective elastic tensor and the damage effect tensor for large damage are presented next. For ease of usage, standard tensor notations are used whenever possible. Thus, the 3-D stress and strain components can be conveniently expressed as,

$$\{\sigma\} = \begin{Bmatrix} \sigma_1 \\ \sigma_2 \\ \sigma_3 \\ \sigma_4 \\ \sigma_5 \\ \sigma_6 \end{Bmatrix} = \begin{Bmatrix} \sigma_{11} \\ \sigma_{22} \\ \sigma_{33} \\ \sigma_{12} \\ \sigma_{23} \\ \sigma_{13} \end{Bmatrix}, \quad \{\varepsilon\} = \begin{Bmatrix} \varepsilon_1 \\ \varepsilon_2 \\ \varepsilon_3 \\ \varepsilon_4 \\ \varepsilon_5 \\ \varepsilon_6 \end{Bmatrix} = \begin{Bmatrix} \varepsilon_{11} \\ \varepsilon_{22} \\ \varepsilon_{33} \\ 2\varepsilon_{12} \\ 2\varepsilon_{23} \\ 2\varepsilon_{13} \end{Bmatrix} \tag{18}$$

The elastic tensor $\boldsymbol{E}_o$ for an isotropic material is given by,

$$\left[E_{ij}\right]^{-1} = \frac{1}{E_o}\begin{bmatrix} 1 & -\nu & -\nu & 0 & 0 & 0 \\ -\nu & 1 & -\nu & 0 & 0 & 0 \\ -\nu & -\nu & 1 & 0 & 0 & 0 \\ 0 & 0 & 0 & 2(1+\nu) & 0 & 0 \\ 0 & 0 & 0 & 0 & 2(1+\nu) & 0 \\ 0 & 0 & 0 & 0 & 0 & 2(1+\nu) \end{bmatrix} \tag{19}$$

where $E_o$ is Young's modulus and $\nu$ is Poisson's ratio. Assuming damage is in the principal but unknown directions, then the damage effect tensor $M_{ij}(\boldsymbol{D})$ for small damage is given by *Equation* (7). Assuming identical form, the incremental damage effect tensor $M_{ij}(d\boldsymbol{D})$ can be written as,

$$\left[M_{ij}(d\boldsymbol{D})\right] = \begin{bmatrix} \frac{1}{1-dD_1} & 0 & 0 & 0 & 0 & 0 \\ 0 & \frac{1}{1-dD_2} & 0 & 0 & 0 & 0 \\ 0 & 0 & \frac{1}{1-dD_3} & 0 & 0 & 0 \\ 0 & 0 & 0 & \frac{1}{\sqrt{(1-dD_1)(1-dD_2)}} & 0 & 0 \\ 0 & 0 & 0 & 0 & \frac{1}{\sqrt{(1-dD_2)(1-dD_3)}} & 0 \\ 0 & 0 & 0 & 0 & 0 & \frac{1}{\sqrt{(1-dD_3)(1-dD_1)}} \end{bmatrix} \tag{20}$$

Next, we assume that the large damage can be discretized into a series of piecewise linear damage of up to $n$ steps as illustrated in *Figure* 3.5. The incremental damage variable $dD_{ik}$, $k = 1, 2, \cdots, n$, for the $i$th-direction when summed together, yields the large damage variable $D_i$ for that direction, i.e.,

$$D_i = \sum_{k=1}^{n} dD_{ik}\,, \quad (i = 1, 2, 3) \tag{21}$$

Substituting *Equations* (19) and (20) into *Equation* (13), we get the following effective elastic tensor,

$$\left[\tilde{E}_{ij}\right]_D^{-1} = \frac{1}{E_o}\begin{bmatrix} \dfrac{1}{\prod_{k=1}^{n}(1-dD_{1k})^2} & \dfrac{-\nu}{\prod_{k=1}^{n}(1-dD_{1k})(1-dD_{2k})} & \dfrac{-\nu}{\prod_{k=1}^{n}(1-dD_{1k})(1-dD_{3k})} \\ & \dfrac{1}{\prod_{k=1}^{n}(1-dD_{2k})^2} & \dfrac{-\nu}{\prod_{k=1}^{n}(1-dD_{2k})(1-dD_{3k})} \\ \text{symmetric} & & \dfrac{1}{\prod_{k=1}^{n}(1-dD_{3k})^2} \end{bmatrix}$$

$$\begin{bmatrix} 0 & 0 & 0 \\ 0 & 0 & 0 \\ 0 & 0 & 0 \\ \dfrac{2(1+\nu)}{\prod_{k=1}^{n}(1-dD_{1k})(1-dD_{2k})} & 0 & 0 \\ & \dfrac{2(1+\nu)}{\prod_{k=1}^{n}(1-dD_{2k})(1-dD_{3k})} & 0 \\ & & \dfrac{2(1+\nu)}{\prod_{k=1}^{n}(1-dD_{3k})(1-dD_{1k})} \end{bmatrix} \qquad (22)$$

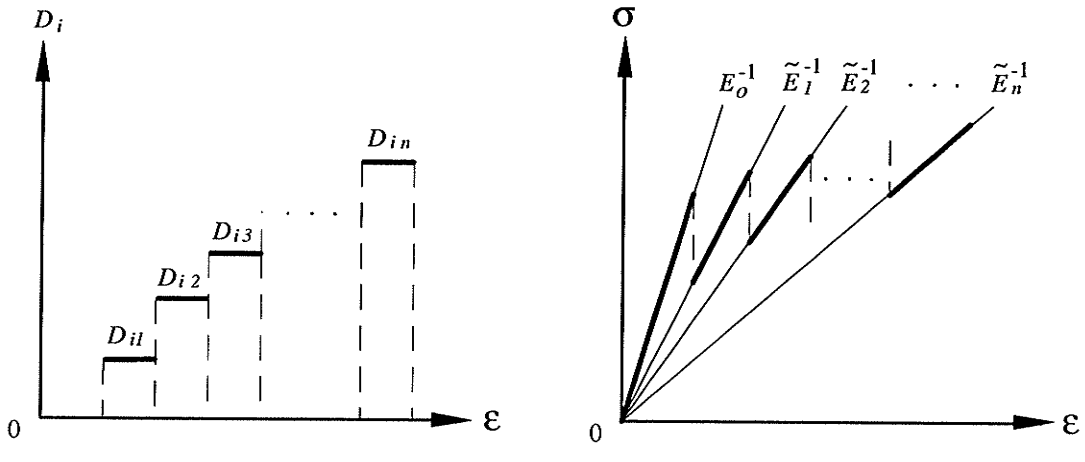



*Figure* 3.5: Piecewise Linear Damage of Materials

For continuous damage, $n \to \infty$, and if we assume equal damage steps, i.e., $dD_{i1} = dD_{i2} = \cdots = dD_{in}$, then $dD_{ik} = D_i/n$. *Equation* (22) becomes,

$$\left[\tilde{E}_{ij}\right]_D^{-1} = \frac{1}{E_o}\begin{bmatrix} \frac{1}{e^{-2D_1}} & \frac{-\nu}{e^{-(D_1+D_2)}} & \frac{-\nu}{e^{-(D_1+D_3)}} & 0 & 0 & 0 \\ \frac{-\nu}{e^{-(D_1+D_2)}} & \frac{1}{e^{-2D_2}} & \frac{-\nu}{e^{-(D_2+D_3)}} & 0 & 0 & 0 \\ \frac{-\nu}{e^{-(D_1+D_3)}} & \frac{-\nu}{e^{-(D_2+D_3)}} & \frac{1}{e^{-2D_3}} & 0 & 0 & 0 \\ 0 & 0 & 0 & \frac{2(1+\nu)}{e^{-(D_1+D_2)}} & 0 & 0 \\ 0 & 0 & 0 & 0 & \frac{2(1+\nu)}{e^{-(D_2+D_3)}} & 0 \\ 0 & 0 & 0 & 0 & 0 & \frac{2(1+\nu)}{e^{-(D_3+D_1)}} \end{bmatrix} \tag{23}$$

*Equation* (23) depicts the effective elastic tensor for large damage. Using this $\tilde{E}_D$, the constitutive equation for large damage can thus be written as,

$$\varepsilon^e = \tilde{E}_D^{-1} \bullet \sigma \tag{24}$$

### 3.3 Damage Effect Tensor $M(D)$ for Large Damage

To deduce the form of the damage effect tensor $\boldsymbol{M(D)}$ for large damage so that the effective stress tensor is symmetric, similar to *Equation* (4) we suggest the following relations which is based on the geometric mean in order to symmetrize the effective stress $\tilde{\sigma}$,

$$\tilde{\sigma}_{ij} = \left[e^{-D_{ik}} + \left(\delta_{ik} - 1\right)\right]^{-1/2} \sigma_{kl} \left[e^{-D_{lj}} + \left(\delta_{lj} - 1\right)\right]^{-1/2} \tag{25}$$

where the stress and damage tensors are represented for a general state of damage as given in *Equation* (5). Then the general expressions of $\boldsymbol{M}(\boldsymbol{D})$, similar to *Equation* (6) but $\Delta_{ij} = e^{-D_{ij}} + \delta_{ij} - 1$, can also be derived. Also, if the principal damage variables $D_1$, $D_2$ and $D_3$ are used, it can be easily seen that the damage effect tensor obtained from *Equation* (25) will be reduced to the following diagonalized form,

$$\left[\boldsymbol{M}_{ij}(\boldsymbol{D})\right] = \begin{bmatrix} \frac{1}{e^{-D_1}} & 0 & 0 & 0 & 0 & 0 \\ 0 & \frac{1}{e^{-D_2}} & 0 & 0 & 0 & 0 \\ 0 & 0 & \frac{1}{e^{-D_3}} & 0 & 0 & 0 \\ 0 & 0 & 0 & \frac{1}{e^{-(D_1+D_2)/2}} & 0 & 0 \\ 0 & 0 & 0 & 0 & \frac{1}{e^{-(D_2+D_3)/2}} & 0 \\ 0 & 0 & 0 & 0 & 0 & \frac{1}{e^{-(D_3+D_1)/2}} \end{bmatrix} \tag{26}$$

By comparing *Equation* (6) with *Equation* (26), we can define the damage variable for a large isotropic damage as,

$$D = \ln \frac{A}{\tilde{A}} \tag{27}$$

This definition was first proposed by Broberg [40], but here this definition arises naturally from the assumption of the incremental complementary energy equivalence. From *Equation* (27), the effective stress is,

$$\tilde{\sigma} = e^{D}\sigma$$

Note that the $M_{ij}(\boldsymbol{D})$ as presented in (26) allows the large effective elastic tensor $\tilde{\boldsymbol{E}}_{\boldsymbol{D}}$ in *Equation* (23) to be recovered by carrying out the following algebraic manipulation,

$$\tilde{\boldsymbol{E}}_{\boldsymbol{D}}^{-1} = \boldsymbol{M}(\boldsymbol{D})^{T} \bullet \boldsymbol{E}_{o}^{-1} \bullet \boldsymbol{M}(\boldsymbol{D})$$

If the damage variable is very small, i.e., $D_i << 1$, each term in $\boldsymbol{M}(\boldsymbol{D})$ can be expanded via a Taylor series expansion, namely, $e^{-D_i} = 1 - D_i + \frac{D_i^2}{2!} + \cdots$. Neglecting higher order terms, we get $e^{-D_i} \approx 1 - D_i$. Substituting into *Equation* (26), the small damage $\boldsymbol{M}(\boldsymbol{D})$ of *Equation* (7) is recovered. In a similar fashion, $\tilde{\boldsymbol{E}}$ for small damage is derived as,

$$\left[\tilde{E}_{ij}\right]_D^{-1} = \frac{1}{E}\begin{bmatrix} \frac{1}{(1-D_1)^2} & \frac{-\nu}{(1-D_1)(1-D_2)} & \frac{-\nu}{(1-D_1)(1-D_3)} & 0 & 0 & 0 \\ \frac{-\nu}{(1-D_1)(1-D_2)} & \frac{1}{(1-D_2)^2} & \frac{-\nu}{(1-D_2)(1-D_3)} & 0 & 0 & 0 \\ \frac{-\nu}{(1-D_1)(1-D_3)} & \frac{-\nu}{(1-D_2)(1-D_3)} & \frac{1}{(1-D_3)^2} & 0 & 0 & 0 \\ 0 & 0 & 0 & \frac{2(1+\nu)}{(1-D_1)(1-D_2)} & 0 & 0 \\ 0 & 0 & 0 & 0 & \frac{2(1+\nu)}{(1-D_2)(1-D_3)} & 0 \\ 0 & 0 & 0 & 0 & 0 & \frac{2(1+\nu)}{(1-D_3)(1-D_1)} \end{bmatrix} \tag{28}$$

which is precisely the form given by Chow and Wang [34].

## 3.4 Transformation of Damage Tensor and Damage Effect Tensor

The damage variables and damage effect tensor may be transformed to an arbitrary Cartesian rectangular coordinate system $(x_1', x_2', x_3')$ as shown in *Figure* 3.6. Assuming the direction cosines between the original coordinate system $(x_1, x_2, x_3)$ and the arbitrary coordinate system $(x_1', x_2', x_3')$ are related as follows,

| | $x_1$ | $x_2$ | $x_3$ |
|---|---|---|---|
| $x_1'$ | $g_{11}$ | $g_{12}$ | $g_{13}$ |
| $x_2'$ | $g_{21}$ | $g_{22}$ | $g_{23}$ |
| $x_3'$ | $g_{31}$ | $g_{32}$ | $g_{33}$ |

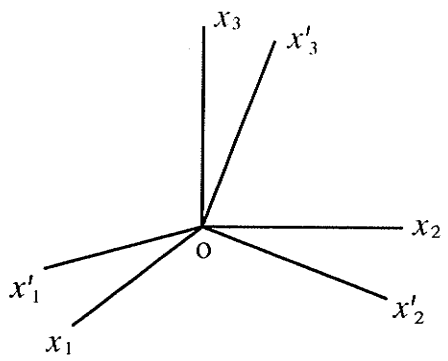



*Figure* 3.6: Transformation of Cartesian Coordinate Systems

then the transferred damage variables $D'_{ij}$ and damage effect tensor $M'_{ijkl}$ are given by,

$$D'_{ij} = g_{is}g_{jt}D_{st}$$

$$M'_{ijkl} = g_{is}g_{jt}g_{ku}g_{lv}M_{stuv}$$

where

$$[g_{ij}] = \left[\frac{\partial x'_i}{\partial x_j}\right] = \begin{bmatrix} g_{11} & g_{12} & g_{13} \\ g_{21} & g_{22} & g_{23} \\ g_{31} & g_{32} & g_{33} \end{bmatrix}$$

If $(x_1, x_2, x_3)$ is the principal coordinate system, then $D'_{ij}$ becomes,

$$\left[D'_{ij}\right] = \begin{bmatrix} D_1 g_{11}^2 + D_2 g_{12}^2 + D_3 g_{13}^2 & D_1 g_{11} g_{21} + D_2 g_{12} g_{22} + D_3 g_{13} g_{23} & D_1 g_{11} g_{31} + D_2 g_{12} g_{32} + D_3 g_{13} g_{33} \\ & D_1 g_{21}^2 + D_2 g_{22}^2 + D_3 g_{23}^2 & D_1 g_{21} g_{31} + D_2 g_{22} g_{32} + D_3 g_{23} g_{33} \\ \text{symmetric} & & D_1 g_{31}^2 + D_2 g_{32}^2 + D_3 g_{33}^2 \end{bmatrix}$$

*Equation* (6) shows the fourth order damage effect tensor $\boldsymbol{M}(\boldsymbol{D})$ written in a 6×6 matrix so that the effective stress tensor is still symmetric. To show that $\boldsymbol{M}(\boldsymbol{D})$ is applicable to any arbitrary coordinate systems, we will employ the vector form of stress as given by *Equation* (18). Rewriting the transformed effective stress $\tilde{\sigma}'_{ij} = g_{is} g_{jt} \tilde{\sigma}_{st}$ in the following form, we get:

$$\begin{aligned} \{\tilde{\sigma}'\} &= \left[\boldsymbol{G}_{ij}\right]\{\tilde{\sigma}\} = \left[\boldsymbol{G}_{ij}\right]\left(\left[\boldsymbol{M}_{ij}(\boldsymbol{D})\right]\{\sigma\}\right) \\ &= \left(\left[\boldsymbol{G}_{ij}\right]\left[\boldsymbol{M}_{ij}(\boldsymbol{D})\right]\left[\boldsymbol{G}_{ij}\right]^{-1}\right)\{\sigma'\} \\ &= \left[\boldsymbol{M}'_{ij}(\boldsymbol{D})\right]\{\sigma'\} \end{aligned}$$

where

$$\left[\boldsymbol{G}_{ij}\right] = \begin{bmatrix} g_{11}^2 & g_{12}^2 & g_{13}^2 & 2g_{11}g_{12} & 2g_{13}g_{12} & 2g_{11}g_{13} \\ g_{21}^2 & g_{22}^2 & g_{23}^2 & 2g_{22}g_{21} & 2g_{23}g_{22} & 2g_{23}g_{21} \\ g_{31}^2 & g_{32}^2 & g_{33}^2 & 2g_{31}g_{32} & 2g_{32}g_{33} & 2g_{33}g_{31} \\ g_{11}g_{21} & g_{12}g_{22} & g_{13}g_{23} & g_{12}g_{21} + g_{11}g_{22} & g_{13}g_{22} + g_{12}g_{23} & g_{13}g_{21} + g_{11}g_{23} \\ g_{21}g_{31} & g_{22}g_{32} & g_{23}g_{33} & g_{21}g_{32} + g_{22}g_{31} & g_{32}g_{23} + g_{22}g_{33} & g_{33}g_{21} + g_{31}g_{23} \\ g_{11}g_{31} & g_{12}g_{32} & g_{13}g_{33} & g_{12}g_{31} + g_{11}g_{32} & g_{12}g_{33} + g_{13}g_{32} & g_{13}g_{31} + g_{11}g_{33} \end{bmatrix}$$

and $\left[\boldsymbol{M}'_{ij}(\boldsymbol{D})\right]$ is defined as,

$$\left[M'_{ij}(D)\right]=\left[G_{ij}\right]\left[M_{ij}(D)\right]\left[G_{ij}\right]^{-1}$$

If $(x_1, x_2, x_3)$ is the principal coordinate system and $\left[M_{ij}(D)\right]$ is given by *Equation* (26), then the expressions of $\left[M'_{ij}(D)\right]$ are,

$$M'_{ij}=\sum_{k=1}^{3} g_{ik}g_{jk}e^{-D_k/2}\left(g_i g_j e^{-D_k/2}+2g_{i(k+1)}g_{j(k+1)}e^{-D_{k+1}/2}\right), \quad \text{for } i, j = 1, 2, 3$$

$$M'_{ii}=\sum_{k=1}^{3} e^{-D_k/2}\left[2g_{(i+1)k}g_{(i+2)k}e^{-D_k/2}+\left(g_{(i+1)k}g_{(i+2)(k+1)}+g_{(i+1)(k+1)}g_{(i+2)k}\right)^2 e^{-D_{k+1}/2}\right],$$

for $i = 4, 5, 6$

$$M'_{ij}=\sum_{k=1}^{3} e^{-D_k/2}\left[g_{(i+1)k}g_{(i+2)k}g_{jk}e^{-D_k/2}+g_{jk}g_{j(k+1)}\left(g_{(i+1)k}g_{(i+2)(k+1)}+g_{(i+1)(k+1)}g_{(i+2)k}\right)e^{-D_{k+1}/2}\right],$$

for $i = 4, 5, 6, j = 1, 2, 3$

$$M'_{54}=\sum_{k=1}^{3} e^{-D_k/2}\left[2g_{1k}g_{2k}g_{3k}^2 e^{-D_k/2}+\left(g_{2k}g_{3(k+1)}+g_{2(k+1)}g_{3k}\right)\left(g_{1k}g_{3(k+1)}+g_{1(k+1)}g_{3k}\right)e^{-D_{k+1}/2}\right],$$

$$M'_{6j}=\sum_{k=1}^{3} e^{-D_k/2}\left[2g_{1k}g_{2k}g_{3k}g_{(6-j)k}e^{-D_k/2}+\left(g_{3k}g_{(6-j)(k+1)}+g_{3(k+1)}g_{(6-j)k}\right)\left(g_{1k}g_{2(k+1)}+g_{1(k+1)}g_{2k}\right)e^{-D_{k+1}/2}\right]$$

for $j = 4, 5$

$$M'_{ji}=2M'_{ij}, \quad \text{for } i = 4, 5, 6,\ j = 1, 2, 3$$

$$M'_{ji}=M'_{ij}, \quad \text{for } i = 5, 6,\ j = 4, 5$$

Note that in these expressions, we used the notations $D_{n+3} = D_n$, and $g_{i(n+3)} = g_{in}$, where $n$ may be any integers. For example, $D_5 = D_{2+3} = D_2$ and $g_{25} = g_{2(2+3)} = g_{22}$. To verify the result, we note that for the case of isotropic damage, the following is recovered,

$$M'_{ij} = e^{D}\delta_{ij} = M_{ij}$$

It is very difficult to quantitatively define large damage since it depends on many factors which include the material itself, the level of loading, the amount and nature of defects, the evolution of damage, etc. However, because the large damage theory reverts to the small damage theory when the damage is small, it is better to use the large damage theory when in doubt. Based on this approach, one can perhaps quantitatively define large damage as follows: large damage is said to occur when the difference in the predictions of the two theories differ by more than 10%.

## 3.5 Applications

To demonstrate the method, the large damage theory is now applied to three cases: uniaxial tension, pure torsion and elastic perfectly-plastic material with elastic damage behavior. Damage variables are evaluated for each of the case, and comparisons with the small damage theory of Chow and Wang [34] are presented whenever possible.

*(1) Uniaxial Tension Model*

In accordance to the large damage theory for the anisotropic damage, the constitutive equations under tension are,

$$\varepsilon_1 = \frac{1}{E_o} e^{2D_1} \sigma_1 = \frac{1}{\tilde{E}} \sigma_1 \tag{29}$$

$$\varepsilon_2 = \frac{-\nu}{E_o e^{-(D_1+D_2)}} \sigma_1 = \frac{-\tilde{\nu}_{12}}{\tilde{E}} \sigma_1 \tag{30}$$

$$\varepsilon_3 = \frac{-\nu}{E_o e^{-(D_1+D_3)}} \sigma_1 = \frac{-\tilde{\nu}_{13}}{\tilde{E}} \sigma_1 \tag{31}$$

where $\tilde{E} = e^{-2D_1} E_o$, $\tilde{\nu}_{12} = e^{(D_2-D_1)}\nu$, $\tilde{\nu}_{13} = e^{(D_3-D_1)}\nu$ are the effective Young's modulus and Poisson's ratios respectively. Thus, the damage variables $D_1$, $D_2$ and $D_3$ can be evaluated from,

$$D_1 = -\frac{1}{2} \ln \frac{\tilde{E}}{E_o} \tag{32}$$

$$D_2 = D_1 - \ln \frac{\nu}{\tilde{\nu}_{12}} = -\ln \left( \frac{\nu}{\tilde{\nu}_{12}} \sqrt{\frac{\tilde{E}}{E_o}} \right) \tag{33}$$

$$D_3 = D_1 - \ln \frac{\nu}{\tilde{\nu}_{13}} = -\ln \left( \frac{\nu}{\tilde{\nu}_{13}} \sqrt{\frac{\tilde{E}}{E_o}} \right) \tag{34}$$

The corresponding constitutive equations derived from the small damage model are,

$$\varepsilon_1 = \frac{\sigma_1}{E_o (1-D_1)^2} = \frac{1}{\tilde{E}} \sigma_1 \tag{35}$$

$$\varepsilon_2 = \frac{-\nu}{E_o (1-D_1)(1-D_2)} \sigma_1 = \frac{-\tilde{\nu}}{\tilde{E}} \sigma_1 \tag{36}$$

$$\varepsilon_3 = \frac{-\nu}{E_o(1-D_1)(1-D_3)}\sigma_1 = \frac{-\tilde{\nu}}{\tilde{E}}\sigma_1 \tag{37}$$

where $\tilde{E} = (1-D_1)^2 E_o$, $\tilde{\nu}_{12} = \frac{1-D_1}{1-D_2}\nu$, $\tilde{\nu}_{13} = \frac{1-D_1}{1-D_3}\nu$. The damage variables associated with this model are therefore given by,

$$D_1 = 1 - \sqrt{\frac{\tilde{E}}{E_o}} \tag{38}$$

$$D_2 = 1 - \frac{\nu}{\tilde{\nu}_{12}}(1-D_1) = 1 - \frac{\nu}{\tilde{\nu}_{12}}\sqrt{\frac{\tilde{E}}{E_o}} \tag{39}$$

$$D_3 = 1 - \frac{\nu}{\tilde{\nu}_{13}}(1-D_1) = 1 - \frac{\nu}{\tilde{\nu}_{13}}\sqrt{\frac{\tilde{E}}{E_o}} \tag{40}$$

From the two sets of expressions for damage variable ***D***, it is clear that the small damage theory results given by *Equations* (38) to (40) can be easily recovered from the large damage theory results of *Equations* (32) to (34) via a Taylor series expansion and neglecting the higher order terms which is justifiable when the damage is small. Some plots showing the range of applicability of these two theories are presented next.

A plot of the damage variable $D_1$ predicted by the large damage and small damage theories versus the Young's modulus ratio $\tilde{E}/E_o$ is given in *Figure* 3.7. Observe that at large $\tilde{E}/E_o$ ratios, the two theories agree as expected, but they showed significant difference as the ratio decreases. The value of $D_1$ predicted by the two theories differ by at least 8.4% for damage measured at $\tilde{E}/E_o \leq 0.7$. In *Figure* 3.8, a plot of $D_2$ computed by the large

damage and small damage theories versus the Poisson's ratio parameter $\tilde{\nu}/\nu$ is presented. Once again, the overall trend is similar. Just as for $D_1$, the second damage variable $D_2$ computed by the two theories differ by at least 8.4% for damage measured at $\tilde{E}/E_o \leq 0.7$. The graph of the third damage variable $D_3$ is the same as $D_2$ and thus, not given here.

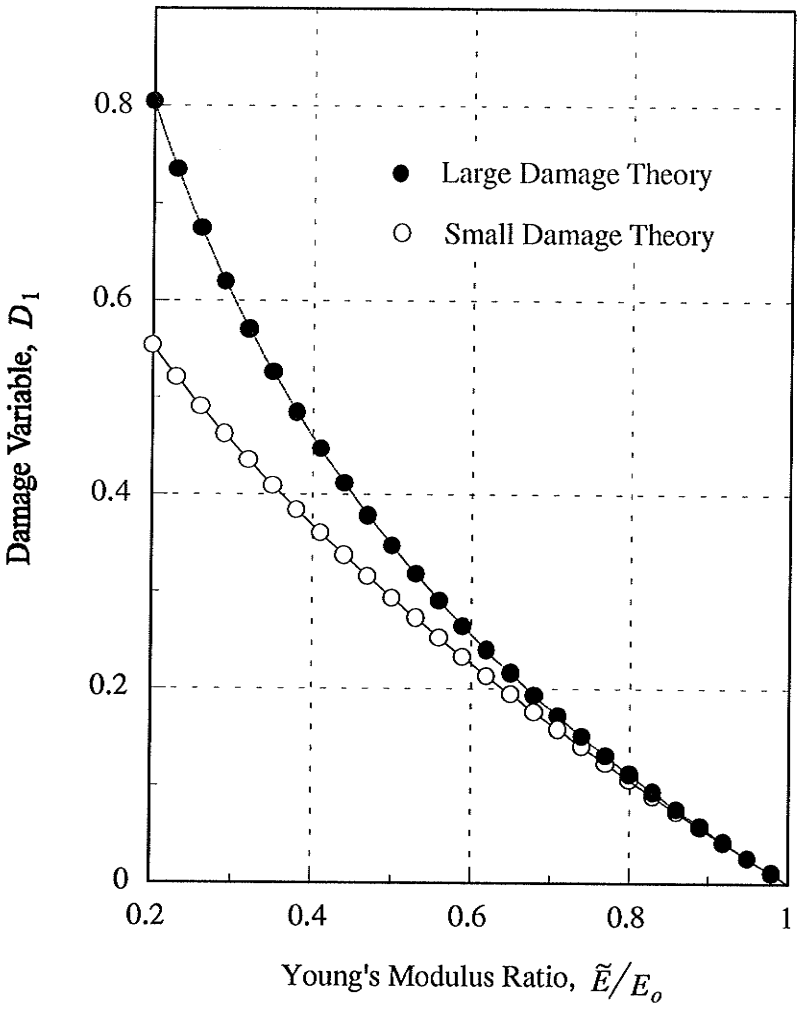



*Figure* 3.7: Damage Variable $D_1$ Versus Young's Modulus Ratio

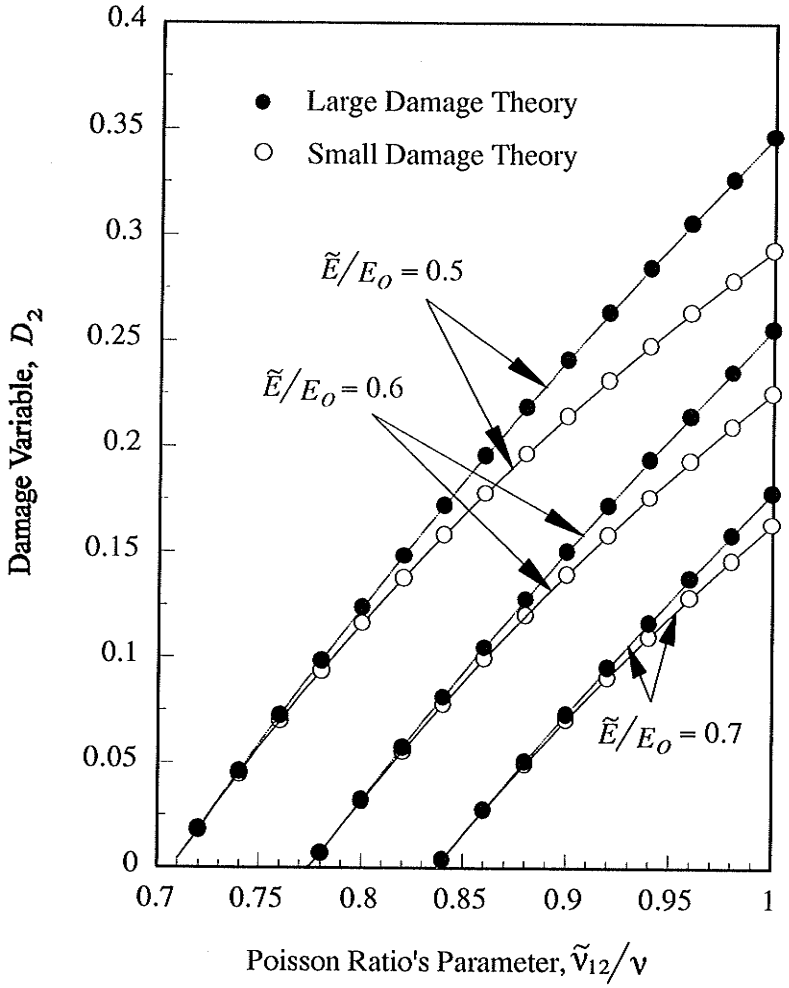



*Figure* 3.8: Damage Variable $D_2$ Versus Poisson's Ratio

Actual experimental data depicting anisotropic damage from an initially isotropic material prior to loading was presented by Chow and Wang [34]. It would be interesting to compare the two theories based on these experimental measurements. In their work, a series of uniaxial tension tests was carried out using specimens of aluminum alloy 2024-T3. They measured the effective variables $\tilde{E}$ and $\tilde{\nu}$, from which the damage variable $D$ can be computed. A plot of the damage variable $D_1$ versus strain $\varepsilon$ is presented in *Figure* 3.9. As expected, the two theories agree very well at small strains, but they differ by at

least 4% for $\varepsilon \geq 15\%$. A similar plot of $D_2$ versus $\varepsilon$ is shown in *Figure* 3.10. However, the difference here is not so dramatic, which is understandable since the test is a uniaxial tension test and thus, the damage is more pronounced in the loading direction, namely in $D_1$ direction. For isotropic material under uniaxial tension, the graph of $D_3$ is identical to $D_2$.

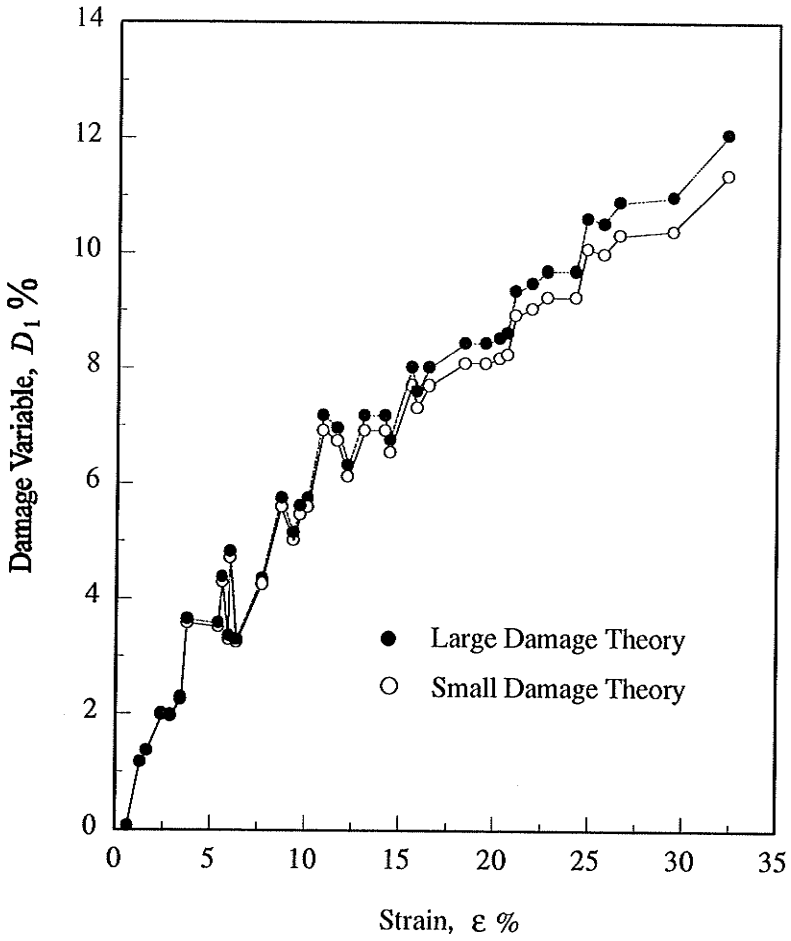



*Figure* 3.9: Damage Variable $D_1$ Versus Strain

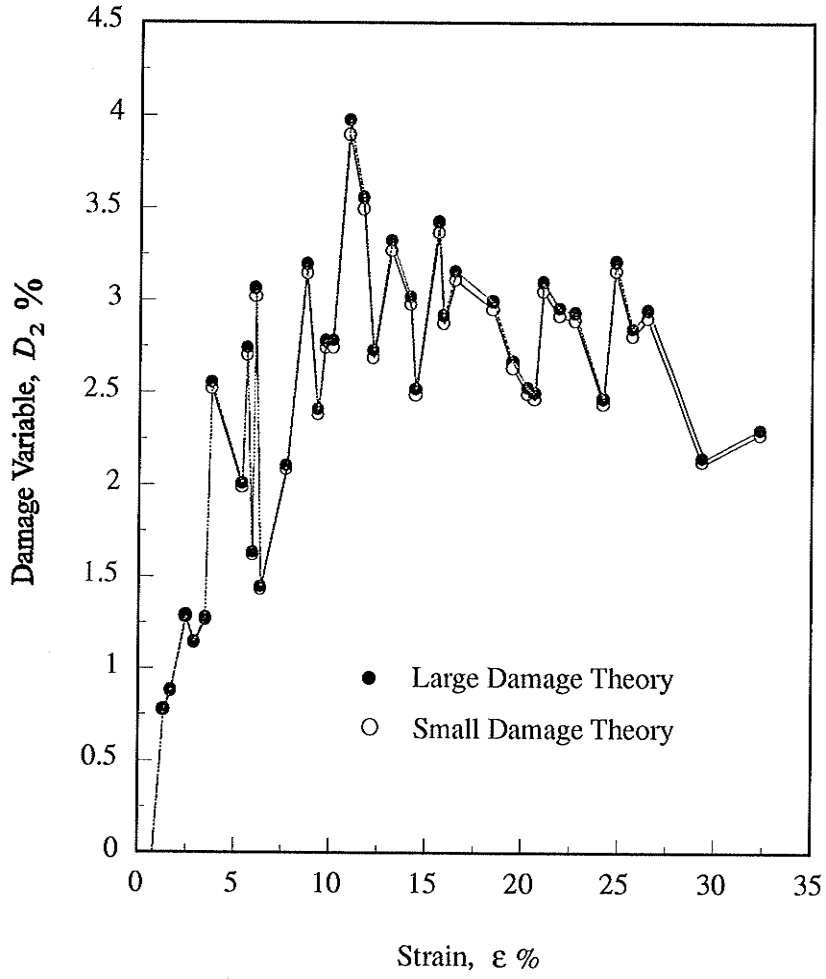



*Figure* 3.10: Damage Variable $D_2$ Versus Strain

*(2) Pure Torsion Model*

As a further application of the proposed large damage theory, a shaft under pure torsion $M$ as shown in *Figure* 3.11 is considered. The principal stresses under a maximum shear stress $\tau$ are $\sigma_1 = \tau$, $\sigma_2 = -\tau$, $\sigma_3 = 0$. The constitutive equation of *Equation* (24) can now be written in the following form,

$$\begin{Bmatrix} \varepsilon_1 \\ \varepsilon_2 \\ \varepsilon_{12} \end{Bmatrix} = \frac{1}{E_o} \begin{bmatrix} \frac{1}{e^{-2D_1}} & \frac{-\nu}{e^{-(D_1+D_2)}} & 0 \\ \frac{-\nu}{e^{-(D_1+D_2)}} & \frac{1}{e^{-2D_2}} & 0 \\ 0 & 0 & \frac{(1+\nu)}{e^{-(D_1+D_2)}} \end{bmatrix} \begin{Bmatrix} \tau \\ -\tau \\ 0 \end{Bmatrix} \tag{41}$$

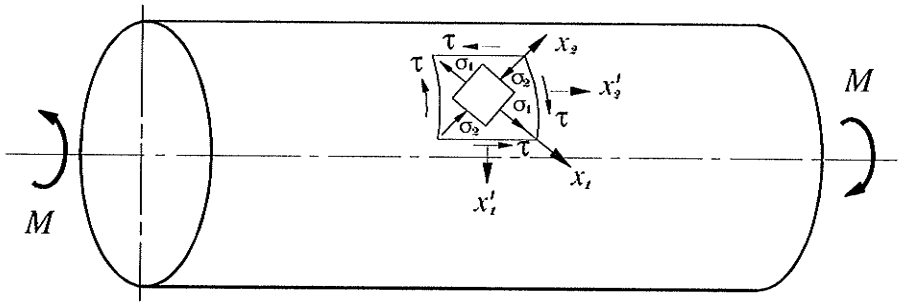



*Figure* 3.11: A Shaft under Pure Torsion

Solving for $D_1$, $D_2$ in *Equation* (41) yields,

$$D_1 = \frac{1}{2} \ln \frac{Y^2 X}{Y^2 - 1} \tag{42}$$

$$D_2 = \frac{1}{2} \ln \frac{X}{Y^2 - 1} \tag{43}$$

where

$$X = \frac{\tau}{E_o} (\varepsilon_1 + \varepsilon_2) \tag{44}$$

$$Y = \frac{1}{2} \left\{ -\nu \left( 1 + \frac{\varepsilon_1}{\varepsilon_2} \right) + \sqrt{\nu^2 \left( 1 + \frac{\varepsilon_1}{\varepsilon_2} \right)^2 - 4 \frac{\varepsilon_1}{\varepsilon_2}} \right\} \tag{45}$$

The effective Young's moduli and Poisson's ratios are now given by,

$$\tilde{E}_1 = E_o e^{-2D_1} = E_o \frac{Y^2 - 1}{Y^2 X} \tag{46}$$

$$\tilde{E}_2 = E_o e^{-2D_2} = E_o \frac{Y^2 - 1}{X} \tag{47}$$

$$\tilde{\nu}_{12} = \nu e^{D_2 - D_1} = \frac{\nu}{Y} \tag{48}$$

$$\tilde{\nu}_{21} = \nu e^{D_1 - D_2} = \nu Y \tag{49}$$

The effective shear modulus $\tilde{G}$ can be evaluated by a transformation of the damage tensor $\boldsymbol{D}$ and damage effect tensor $\boldsymbol{M}(\boldsymbol{D})$ from the principal stress axes system $(x_1, x_2, x_3)$ to the $(x_1', x_2', x_3')$ coordinate system. Alternatively, we could also transformed *Equation* (41) directly from the $(x_1, x_2, x_3)$ to $(x_1', x_2', x_3')$ systems as shown in *Figure* 3.11. The direction cosines for these two coordinate systems are,

$$g_{11} = \frac{\sqrt{2}}{2}, \quad g_{12} = -\frac{\sqrt{2}}{2}, \quad g_{13} = 0$$

$$g_{21} = \frac{\sqrt{2}}{2}, \quad g_{22} = -\frac{\sqrt{2}}{2}, \quad g_{23} = 0 \tag{50}$$

$$g_{32} = 0, \quad g_{32} = 0, \quad g_{33} = 1$$

From the transformed *Equation* (41), we get,

$$\frac{1}{\tilde{G}} = 2\left(\tilde{E}'_{33}\right)^{-1} = \left(\frac{1}{e^{-2D_1}} + \frac{1}{e^{-2D_2}} + \frac{2\nu}{e^{-(D_1+D_2)}}\right)\frac{1}{E_o}$$

Employing the relation

$$E_o = 2(1+\nu)G_o$$

we get the effective shear modulus $\tilde{G}$ for anisotropic damage, i.e.

$$\tilde{G} = \frac{2(1+\nu)G_o}{e^{2D_1} + e^{2D_2} + 2\nu e^{D_1+D_2}} \tag{51}$$

Note that for small damage, *Equation* (51) can be expanded in the exponential series and when higher order terms are ignored, the corresponding expression of Chow and Wang [34] are recovered,

$$\tilde{G} = \frac{2(1+\nu)G_o}{\frac{1}{(1-D_1)^2} + \frac{1}{(1-D_2)^2} + \frac{2\nu}{(1-D_1)(1-D_2)}} \tag{52}$$

A plot of $\tilde{G}/G$ versus the damage variables $D_1$, $D_2$ for $\nu = \frac{1}{2}$ is given in *Figure* 3.12. Observe that the same pattern is obtained, namely, as the damage gets bigger, the predictions of the two theories start to differ significantly.

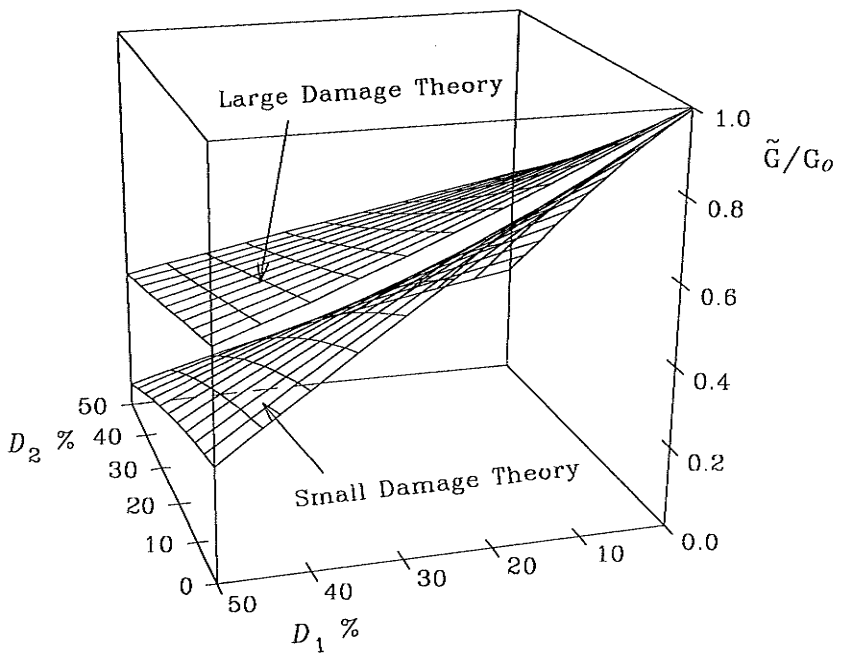



*Figure* 3.12: Effective Shear Modulus Ratio Versus Strain

*(c) Elastic Perfectly-Plastic Model*

Next, a large damage model of an elastic perfectly-plastic material with elastic damage as sketched in *Figure* 3.13 is outlined here. The undamaged constitutive equation for uniaxial tension is,

$$\sigma = \begin{cases} E_o \varepsilon, & \text{if } \varepsilon \le \varepsilon_o \\ E_o \varepsilon_o, & \text{if } \varepsilon \ge \varepsilon_o \end{cases} \tag{53}$$

where $\varepsilon_o$ is the strain at yield. The effective elastic modulus can be computed from *Equation* (23), and assuming isotropic material and isotropic damage, it is given by,

$$\tilde{E} = e^{-2D} E_o \tag{54}$$

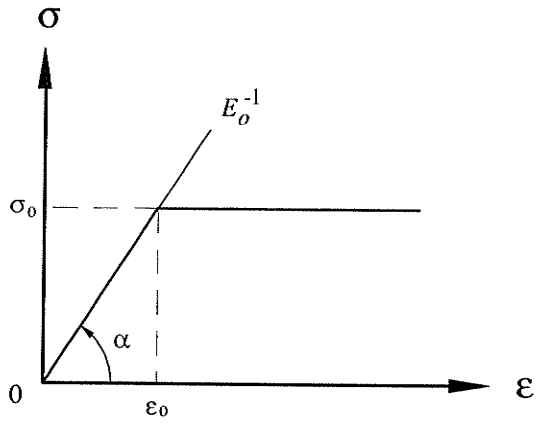



*Figure* 3.13: Elastic Perfectly-Plastic Behavior

Hence, the damage variable is,

$$D = -\frac{1}{2} \ln \frac{\tilde{E}}{E_o} \tag{55}$$

or, in terms of strains, the complete expression is,

$$D = \begin{cases} -\frac{1}{2} \ln \frac{\varepsilon_o}{\varepsilon}, & \text{for } \varepsilon \geq \varepsilon_o \\ 0, & \text{for } \varepsilon \leq \varepsilon_o \end{cases} \tag{56}$$

If the damage is small, *Equation* (56) reduces to,

$$D = \begin{cases} 1 - \sqrt{\varepsilon_o / \varepsilon}, & \text{for } \varepsilon \geq \varepsilon_o \\ 0, & \text{for } \varepsilon \leq \varepsilon_o \end{cases} \tag{57}$$

*Figure* 3.14 shows the variation of the damage variable $D$ with strain $\varepsilon$. Once again, significant difference between the large damage theory and the small damage theory begins to occur as the damage gets bigger. In particular, at $\varepsilon = 0.15$ the predictions of the two theories differ by 9.5%.

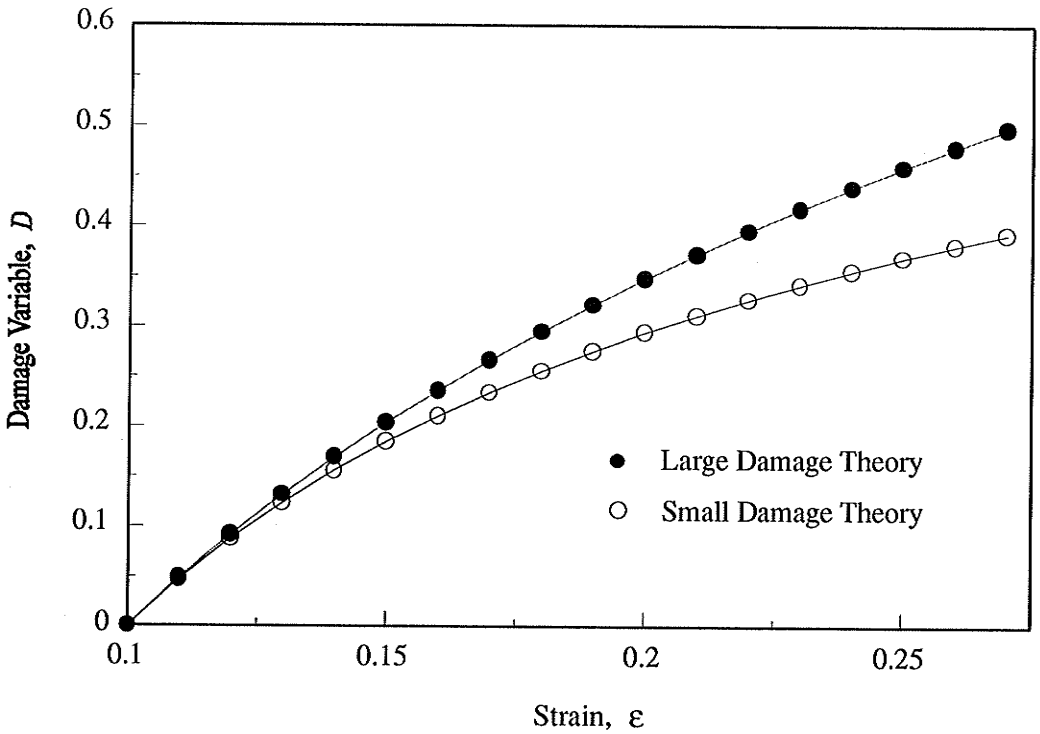



*Figure* 3.14: Isotropic Damage Variable $D$ Versus Strain Ratio

It is clear from the comparisons of these three cases that the hypothesis of total complementary energy equivalence is not applicable for large damage since large errors can occur when the damage becomes large. Also see comments in pages 32-33.

The formulations derived so far are mainly based on apriori knowledge of principal direction of damage tensor. This is because of the simplicity in derivation, clarity in physical meaning and practical practice in the measurement of damage in a specimen.

# CHAPTER FOUR

## DAMAGE EVOLUTION IN DUCTILE MATERIALS

The hypothesis of incremental complementary energy equivalence developed in the previous chapter together with the irreversible thermodynamics theory are now applied to study damage evolution in ductile materials. Comparison with experimental results are presented.

### 4.1 Ductile Damage Evolution

Due to the existence of discontinuities such as voids, microcracks, inclusions, etc., engineering materials are in general, inhomogeneous. In addition, when materials undergo plastic or local plastic deformation, the stresses and strains within the deforming materials are not uniformly distributed. As a result, macrocracks may first appear at locations of these defects. Many works [14, 17, 42, 95, 96] have shown that ductile fracture in metals is the end result of a sequence of three processes: void nucleation in the first phase, void growth in second phase and void coalescence with increase in plastic deformation in the third phase. At this stage, fracture occurs. These processes are graphically summarized in *Figure* 4.1.

In CDM, a continuous damage variable is used to describe the above degradation processes by interpreting as follows: damage generation when the damage is very small and is mainly caused by void nucleation, damage growth when the damage increases as the voids grow, damage instability when ductile fracture occurs due to void coalescence. These three phases of damage evolution are shown in *Figure* 4.2. It is therefore, highly desirable to develop a damage model for predicting the damage evolution in ductile materials. Note that for a material under loading, Phase 2 is the most important as the load capacity and life expectancy of a structure are dependent principally on it [97].

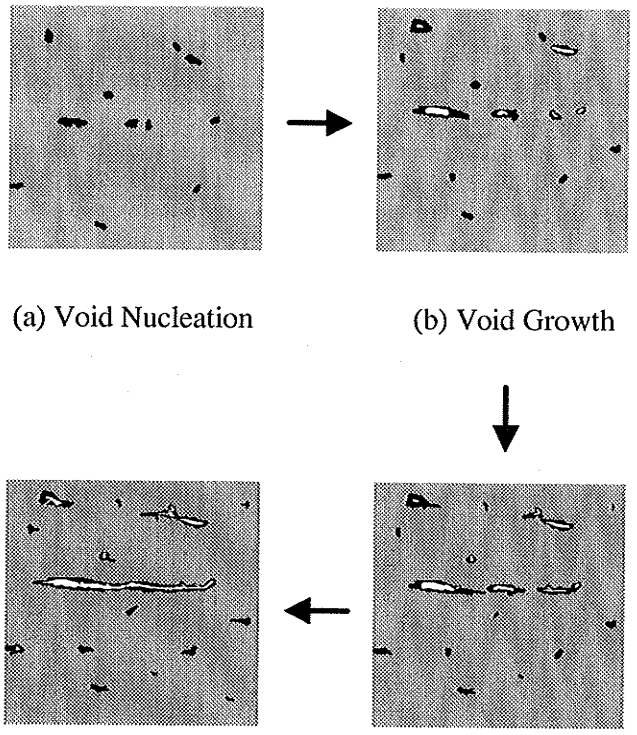



*Figure* 4.1: Ductile Damage Evolution

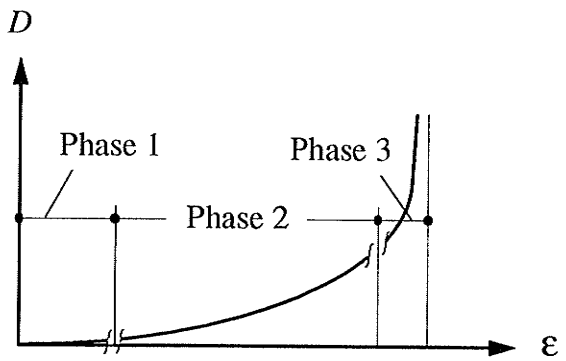



*Figure* 4.2: Progression of Damage Evolution

## 4.2 Irreversible Thermodynamics Theory for Damaged Materials

The irreversible thermodynamics theory is one of the basic theories in continuum mechanics. It has been successfully used to describe the damage strengthening criteria [84] and damage ductile fracture [13]. Although the basic theory is the same, Chow and Lu [84] emphasized the description of this theory on the damage strengthening criteria. In addition, Lemaitre [13] has also incorporated his strain equivalence hypothesis into the thermodynamics theory. However, it was found that for anisotropic damage, this resulted in an asymmetric stiffness matrix which is incorrect. In our proposed large damage model, due to the use of the complementary energy, this asymmetry situation does not arise. We formulated the general thermodynamics theory for damaged materials and then based on our large damage theory, developed the damage evolution model.

In an isothermal process, when a slowly changing (quasi-static) loading is applied to a solid, the energy transferred to the solid is either stored as an elastic strain energy or

dissipated by one or more mechanisms arising from the re-arrangement of the microstructures. For example, the nucleation and growth of microvoids and their ultimate coalescence into macrovoids is one of the approaches through which the imparted energy dissipates. It is well known that thermodynamics principles provide a more general approach to modeling dissipative phenomena. Damage evolution is an irreversible and evolving process governed by the second law of thermodynamics. An Irreversible thermodynamics theory for constitutive equations has been proposed as the most general framework for unifying the modeling of inelastic deformation and internal damage of materials [98, 99]. In particular, this theory can be extended to the unified theory of CDM by describing the internal state changes due to the material damage via the use of a proper internal state variables. Essentially, the damage variable $\boldsymbol{D}$ is treated as one of the internal state variables which influences the free energy of the system. Let the total strain tensor be decomposed into the elastic and inelastic strain tensors, $\varepsilon^e$, $\varepsilon^p$ respectively. That is,

$$\varepsilon = \varepsilon^e + \varepsilon^p$$

For most of the engineering materials, the Helmholtz free energy per unit mass $\psi^H$ is a function of internal state variables, i.e. $\psi^H\left(\varepsilon^e, r, \alpha, \boldsymbol{D}, T\right)$, where $r$, $\alpha$ and $T$ are the internal variables representing isotropic and kinematic hardening, and absolute temperature respectively. A state coupling of these parameters can exist, as evident from *Table* 4.1 [100], in which the state coupling of a 2024 aluminum alloy is depicted. Note that "1" denotes state coupling and "0" uncoupling. To determine whether we have state coupling or uncoupling, we can resort to qualitative microscopic considerations. For example, Lemaitre and Marquis [100] argued that the development of decohesion is affected by the interaction forces between atoms, and therefore, the elastic behavior is coupled with the

damage evolution. On the other hand, they indicated that the development of slips has no effects on these forces, and thus, no couplings between these two states. Taking into account the coupling and uncoupling states in *Table* 4.1, $\psi^H$ for an aluminum alloy can be expressed as,

$$\psi^H(\varepsilon^e, r, \alpha, \boldsymbol{D}, T) = \psi^e(\varepsilon^e, \boldsymbol{D}, T) + \psi_1^p(r, T) + \psi_2^p(\alpha, T) \tag{58}$$

in which $\psi^e, \psi_1^p, \psi_2^p$ are respectively the free energies due to the elastic strain and damage, isotropic hardening and kinematic hardening. From $\psi^H$ given by *Equation* (58), we can define the following generalized thermodynamic forces,

*Table* 4.1: State Coupling and Uncoupling (Lemaitre and Marquis [100])

| | $\varepsilon - \varepsilon^p$ | $T$ | $\alpha$ | $r$ | $\boldsymbol{D}$ |
|---|---|---|---|---|---|
| $\varepsilon - \varepsilon^p$ | | 1 | 0 | 0 | 1 |
| $T$ | 1 | | 0 | 1 | 0 |
| $\alpha$ | 0 | 0 | | 0 | 0 |
| $r$ | 0 | 1 | 0 | | 0 |
| $\boldsymbol{D}$ | 1 | 0 | 0 | 0 | |

$$\sigma = \rho \frac{\partial \psi^e}{\partial \varepsilon^e} \tag{59}$$

$$\boldsymbol{Y} = -\rho \frac{\partial \psi^{e}}{\partial \boldsymbol{D}} \tag{60}$$

$$\boldsymbol{R} = -\rho \frac{\partial \psi_{1}^{p}}{\partial r} \tag{61}$$

$$\boldsymbol{A} = -\rho \frac{\partial \psi_{2}^{p}}{\partial \alpha} \tag{62}$$

in which $\rho$ is the density of the material and, $\sigma, \boldsymbol{Y}, \boldsymbol{R}, \boldsymbol{A}$ are associated with elastic strain, damage, isotropic hardening and kinematic hardening respectively. Note that $\boldsymbol{Y}$ is also sometimes called the damage strain energy release rate. Then the entropy production rate density $\rho\dot{\Theta}$ can be written as,

$$\rho\dot{\Theta} = \boldsymbol{X} \bullet \dot{\boldsymbol{J}} \geq 0 \tag{63}$$

where $\boldsymbol{X}$ and $\dot{\boldsymbol{J}}$ are the thermodynamic conjugate force and flux vectors respectively, given by,

$$\begin{aligned} \boldsymbol{X} &= \left\{ \sigma, \boldsymbol{R}, \boldsymbol{A}, \boldsymbol{Y}, -\frac{1}{T}\mathrm{grad}T \right\} \\ \dot{\boldsymbol{J}} &= \left\{ \dot{\varepsilon}^{p}, \dot{r}, \dot{\alpha}, \dot{\boldsymbol{D}}, \boldsymbol{q} \right\}^{T} \end{aligned} \tag{64}$$

Here $\boldsymbol{q}$ denotes the heat flux vector. Substituting *Equation* (64) into *Equation* (63) yields,

$$\sigma \bullet \dot{\varepsilon}^{p} + \boldsymbol{R}\dot{r} + \boldsymbol{A}\dot{\alpha} + \boldsymbol{Y} \bullet \dot{\boldsymbol{D}} - \boldsymbol{q}\frac{1}{T}\mathrm{grad}T \geq 0 \tag{65}$$

Using Legendre transform, the complementary energy per unit mass $\psi^c$ can be expressed as,

$$\rho\psi^c(\sigma, r, \alpha, \boldsymbol{D}, T) = \sigma \bullet \varepsilon^e - \rho\psi^H\left(\varepsilon^e, r, \alpha, \boldsymbol{D}, T\right) \tag{66}$$

from which we can get the elastic strain, namely,

$$\varepsilon^e = \rho\frac{\partial\psi^c}{\partial\sigma} \tag{67}$$

Substituting *Equation* (66) into *Equations* (60)-(62) and noting that $\psi^H$ is made up of components indicated by *Equation* (58), we can get the following equations for the generalized thermodynamic forces in terms of the complementary energy per unit mass $\psi^c$:

$$\boldsymbol{Y} = \rho\frac{\partial\psi^c}{\partial\boldsymbol{D}} \tag{68}$$

$$\boldsymbol{R} = \rho\frac{\partial\psi^c}{\partial r} \tag{69}$$

$$\boldsymbol{A} = \rho\frac{\partial\psi^c}{\partial\alpha} \tag{70}$$

## 4.3 A Damage Evolution Model

Having formulated the general constitutive equations via thermodynamics principles, we can now derive a damage evolution model. Suppose there exists a dissipative potential $\psi^d$ associated with the entropy production rate. This implies from *Equation* (65) that $\psi^d$ is a function of the following variables; $\left(\dot{\varepsilon}^p, \dot{r}, \dot{\alpha}, \dot{\boldsymbol{D}}, \boldsymbol{q};\ \sigma, R, A, Y, T\right)$. To obtain the terms of the thermodynamic flux vector $\dot{\boldsymbol{J}}$, we can partial differentiate $\psi^d$ with respect to the corresponding conjugate variables of $\boldsymbol{X}$. Take for example, the damage evolution equation for the $\dot{\boldsymbol{D}}$ given by,

$$\dot{\boldsymbol{D}} = \frac{\partial \psi^d}{\partial \boldsymbol{Y}} \tag{71}$$

With the above general constitutive equations from the thermodynamics, we can now derive a damage evolution model. The elastic strain energy of the damaged material per unit mass is given by,

$$\rho\psi^e = \frac{1}{2}\tilde{E}_{ijkl}\varepsilon^e_{ij}\varepsilon^e_{kl}$$

in which $\tilde{\boldsymbol{E}}$ is the fourth-order tensor of effective modulus of elasticity. For isotropic damage the effective elasticity can be obtained from *Equation* (32), that is,

$$\tilde{E} = E\mathrm{e}^{-2\mathrm{D}}$$

where the hypothesis of incremental complementary energy equivalence has been employed. $\psi^e$ can also be calculated as the sum of shear strain energy and volume dilation energy with the tensor of elasticity written in terms of Young's modulus $E$ and Poisson's

ratio $\upsilon$. Let $\sigma'$ and $\varepsilon^{e\prime}$ be the stress deviator and strain deviator, $\sigma_H$ and $\varepsilon_H^e$ be the hydrostatic stress and hydrostatic strain, then there are following relations,

$$\varepsilon^{e\prime} = \frac{1+\upsilon}{\tilde{E}}\sigma' = \frac{1+\upsilon}{Ee^{-2D}}\sigma'$$

$$\varepsilon_H^e = \frac{1-2\upsilon}{\tilde{E}}\sigma_H = \frac{1-2\upsilon}{Ee^{-2D}}\sigma_H$$

where

$$\sigma'_{ij} = \sigma_{ij} - \sigma_H \delta_{ij}$$

$$\sigma_H = \frac{1}{3} tr(\sigma)$$

$$\varepsilon_{ij}^{e\prime} = \varepsilon_{ij} - \varepsilon_H \delta_{ij}$$

$$\varepsilon_H^e = \frac{1}{3} tr(\varepsilon^e)$$

in which $\delta_{ij}$ is the Kronecker delta. Thus the elastic strain energy becomes,

$$\begin{aligned} \rho\psi^e &= \frac{1}{2}\left[\frac{1+\upsilon}{Ee^{-2D}}\sigma'_{ij}\sigma'_{ij} + 3\frac{1-2\upsilon}{Ee^{-2D}}\sigma_H^2\right] \\ &= \frac{\sigma_{eq}^2}{2Ee^{-2D}}\left[\frac{2}{3}(1+\upsilon) + 3(1-2\upsilon)\left(\frac{\sigma_H}{\sigma_{eq}}\right)^2\right] \end{aligned} \tag{72}$$

where $\sigma_{eq}$ is the von Mises equivalent stress given by,

$$\sigma_{eq} = \left(\frac{3}{2}\sigma'_{ij}\sigma'_{ij}\right)^{1/2}$$

The general expression for the damage strain energy release rate $Y$ has been shown in *Equation* (60). For isotropic damage,

$$Y = -\rho \frac{\partial \psi^e}{\partial D}$$

Substituting *Equation* (72) into the above equation results,

$$\begin{aligned} Y &= -\frac{\sigma_{eq}^2 e^{2D}}{E}\left[\frac{2}{3}(1+\upsilon)+3(1-2\upsilon)\left(\frac{\sigma_H}{\sigma_{eq}}\right)^2\right] \\ &= -\frac{\sigma_{eq}^2 e^{2D}}{E} f\left(\frac{\sigma_H}{\sigma_{eq}}\right) \end{aligned} \tag{73}$$

where

$$f\left(\frac{\sigma_H}{\sigma_{eq}}\right) = \frac{2}{3}(1+\upsilon)+3(1-2\upsilon)\left(\frac{\sigma_H}{\sigma_{eq}}\right)^2$$

The constitutive equation for damage evolution is given by *Equation* (71) and for isotropic damage,

$$\dot{D} = \frac{\partial \psi^d}{\partial Y} \tag{74}$$

where we choose $\psi^d$ to be computed from,

$$\psi^d(Y, \dot{p}; p, D, T) = CS\left(-\frac{Y}{S}\right)^2 \frac{(p_c - p)^{n-1}}{p^{2n}} e^{-2D} \dot{p} \tag{75}$$

in which $p$ is the accumulated plastic strain defined by,

$$\dot{p} = \frac{dp}{dt} = \left( \frac{2}{3} \dot{\varepsilon}_{ij}^{p} \dot{\varepsilon}_{ij}^{p} \right)^{1/2}$$

Rupture occurs when $p=p_c$. The variables $S$, $C$ and $n$ are respectively, a temperature dependent constant, a material constant and a strain hardening exponent. According to the Ramberg-Osgood hardening law, we have,

$$\sigma_{eq} = Kp^{n} \tag{76}$$

in which $K$ is another material constant. Substituting *Equations* (73) and (75) into *Equation* (74) yields the following constitutive equation of damage evolution,

$$\dot{D} = -2 \frac{C\sigma_{eq}^{2}}{ES} f\left( \frac{\sigma_H}{\sigma_{eq}} \right) \frac{(p_c - p)^{n-1}}{p^{2n}} \dot{p}$$

By using *Equation* (76), then

$$\dot{D} = -2 \frac{CK^{2}}{ES} f\left( \frac{\sigma_H}{\sigma_{eq}} \right) (p_c - p)^{n-1} \dot{p} \tag{77}$$

or

$$dD = -\frac{Q}{ES} f\left( \frac{\sigma_H}{\sigma_{eq}} \right) (p_c - p)^{n-1} dp \tag{78}$$

where $Q = 2CK^2$ is a material dependent constant. Observe that *Equation* (77) is a differential model which is valid for any loading path. The material constant in *Equation* (77) can be determined by proportional loading test. In this case the stress triaxiality $\sigma_H/\sigma_{eq}$ can be considered as a constant with respect to time. Assuming the rapture happens at the rupture strain $p_c$ which corresponds to the damage threshold at failure $D_c$, i.e.,

$$D|_{p=p_c} = D_c$$

Integrating *Equation* (78) we get,

$$D_c - D = \frac{Q}{nES} f\left(\frac{\sigma_H}{\sigma_{eq}}\right)(p_c - p)^n \tag{79}$$

Let the initial condition of damage is $D|_{p=p_o} = D_o$, then from *Equation* (79) we have,

$$\frac{Q}{nES} = \frac{D_c - D_o}{(p_c - p_o)^n} f^{-1}\left(\frac{\sigma_H}{\sigma_{eq}}\right) \tag{80}$$

Furthermore in one-dimension case, we have

$$\frac{\sigma_H}{\sigma_{eq}} = \frac{1}{3}, \quad f\left(\frac{\sigma_H}{\sigma_{eq}}\right) = 1, \quad p \approx \varepsilon$$

then it is obtained from *Equation* (80) that,

$$\frac{Q}{nES} = \frac{D_c - D_o}{(\varepsilon_c - \varepsilon_o)^n}$$

where $\varepsilon_o$ and $\varepsilon_c$ are the one-dimension strains at initial damage threshold damage at failure. Thus *Equation* (78) and *Equation* (79) become,

$$dD = -n\frac{D_c - D_o}{(\varepsilon_c - \varepsilon_o)^n}(p_c - p)^{n-1} f\left(\frac{\sigma_H}{\sigma_{eq}}\right) \tag{81}$$

$$D = D_c - (D_c - D_o)\left(\frac{p_c - p}{\varepsilon_c - \varepsilon_o}\right)^n f\left(\frac{\sigma_H}{\sigma_{eq}}\right) \tag{82}$$

*Equation* (81) is a differential model and thus valid for any loading path, whereas *Equation* (82) is only valid for proportional loading. Observe that except for the strain hardening exponent *n*, it is not necessary to know all the other material constants in using *Equations* (81) and (82) for damage modeling. The parameters $D_c$, $D_0$, $\varepsilon_c$, $\varepsilon_0$ can be evaluated from a uniaxial tensile test. However, this is not true for $p_c$ and $p_0$ which are dependent on the stress triaxiality ratio $\sigma_H/\sigma_{eq}$, Lemaitre [13] assumed that this dependence is the same for both quantities, and that the ratio $p_o/p_c$ does not depend on the triaxiality ratio. It is further assumed that this ratio is equal to its value in the one-dimension case, namely,

$$\frac{p_o}{p_c} = \frac{\varepsilon_o}{\varepsilon_c}$$

In view of the above equation and noting that $D|_{p=p_o} = D_o$, we have after solving for $p_c$ in *Equation* (82),

$$p_c = \varepsilon_c f^{\frac{-1}{n}}\left(\frac{\sigma_H}{\sigma_{eq}}\right) \tag{83}$$

With *Equation* (83), all the material constants in *Equations* (81) and (82) can be determined by a uniaxial tension test. It is seen that all the parameters in *Equations* (81) and (82) have definite physical meaning and that makes the model very useful for handling practical applications in damage evolution analysis.

## 4.4 Experiments and Predictions

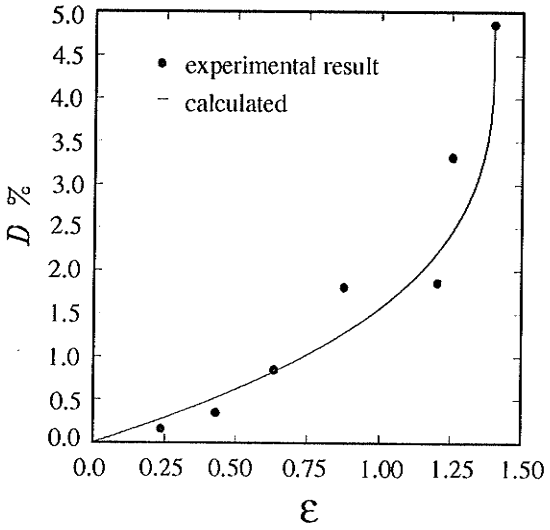
In order to assess the performance of the proposed model, some comparisons with experimental results are necessary. We would like to refer to the work of Roy et. al. [14], who studied the nucleation and growth of voids during tensile straining of some spheroidized carbon steels. The relationships between the fraction of voids and plastic strain for some carbon steels were obtained. Some mechanical properties and damage thresholds are given in *Table* 4.2. With these parameters, the damage evolution in the case of one dimension has be evaluated by using the model developed in this thesis.

*Table* 4.2: Mechanical Properties and Damage Thresholds (Roy et. al. [14])

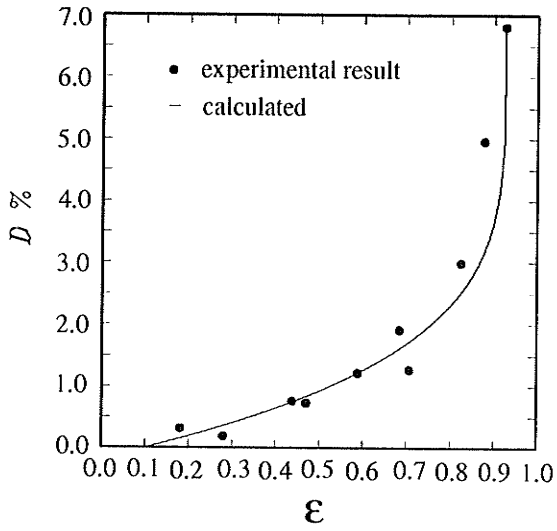
| Steels | T(°C) | $n$ | $D_o$% | $D_c$% | $\varepsilon_o$ | $\varepsilon_c$ |
|---|---|---|---|---|---|---|
| 1015 | 22 | 0.31 | 0 | 4.853 | 0 | 1.40 |
| 1045 | 22 | 0.22 | 0 | 6.805 | 0.10 | 0.925 |
| 1090 | 22 | 0.19 | 0 | 4.907 | 0 | 0.645 |

Depicted in *Figures* 4.3(a)–(c) are some comparisons of damage evolution predictions for steel 1015, 1045 and 1090 with the experiment results of Roy et. al. [14]. Observe from the graphs that good agreement between the theoretical predictions and the experiment results are obtained. It can also be seen from these figures that the damage increases approximately linearly during the void growth phase until it reaches the damage instability phase, i.e. fracture, where the damage increases rapidly.

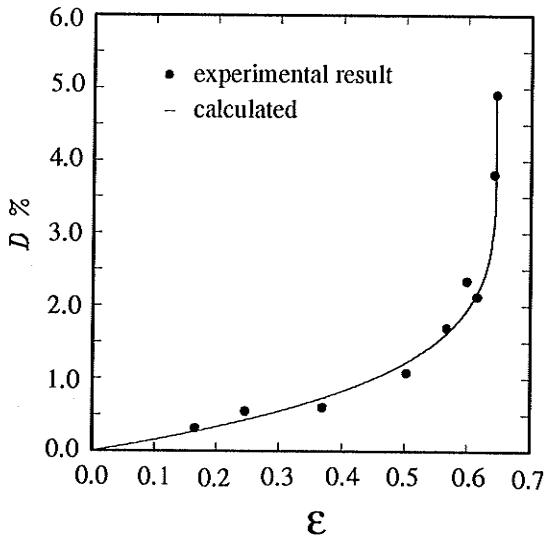
*Figures* 4.4(a)-(c) illustrate the influence of the stress triaxiality ratio on the damage evolution of these three kinds of steel. Observe that at a higher stress triaxiality ratio, the damage evolution is greater. For modeling of other materials, we have plotted in *Figures* 4.5(a)-(d) the damage evolution with different strain hardening exponents under varying stress triaxiality ratios where we have assumed $\varepsilon_o = 0$ and constant stress triaxiality ratio during loading. It can be seen from this figure that the stress triaxiality ratio has a strong influence on the damage evolution. Also, as the ratio increases, the span of Phase 2 during damage evolution reduces rather significantly and this, unfortunately implies a faster rate of damage.




(a) steel 1015

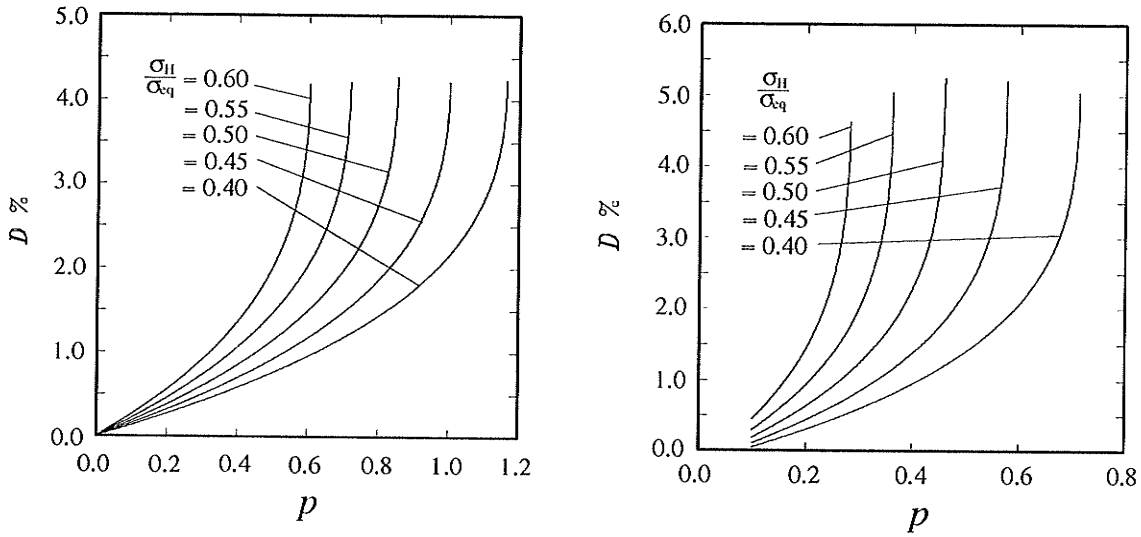



(b) steel 1045



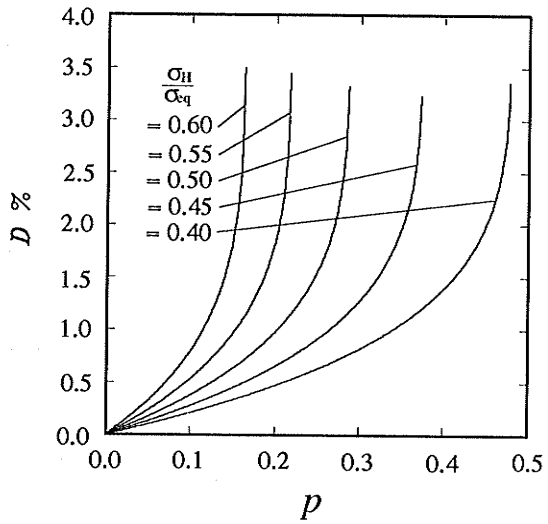

(c) steel 1090

*Figure* 4.3: Comparison of Theoretical Predictions with Experimental Results




(a) steel 1015

(b) steel 1045




(c) steel 1090

*Figure* 4.4: Influence of Stress Triaxiality on the Damage Evolution

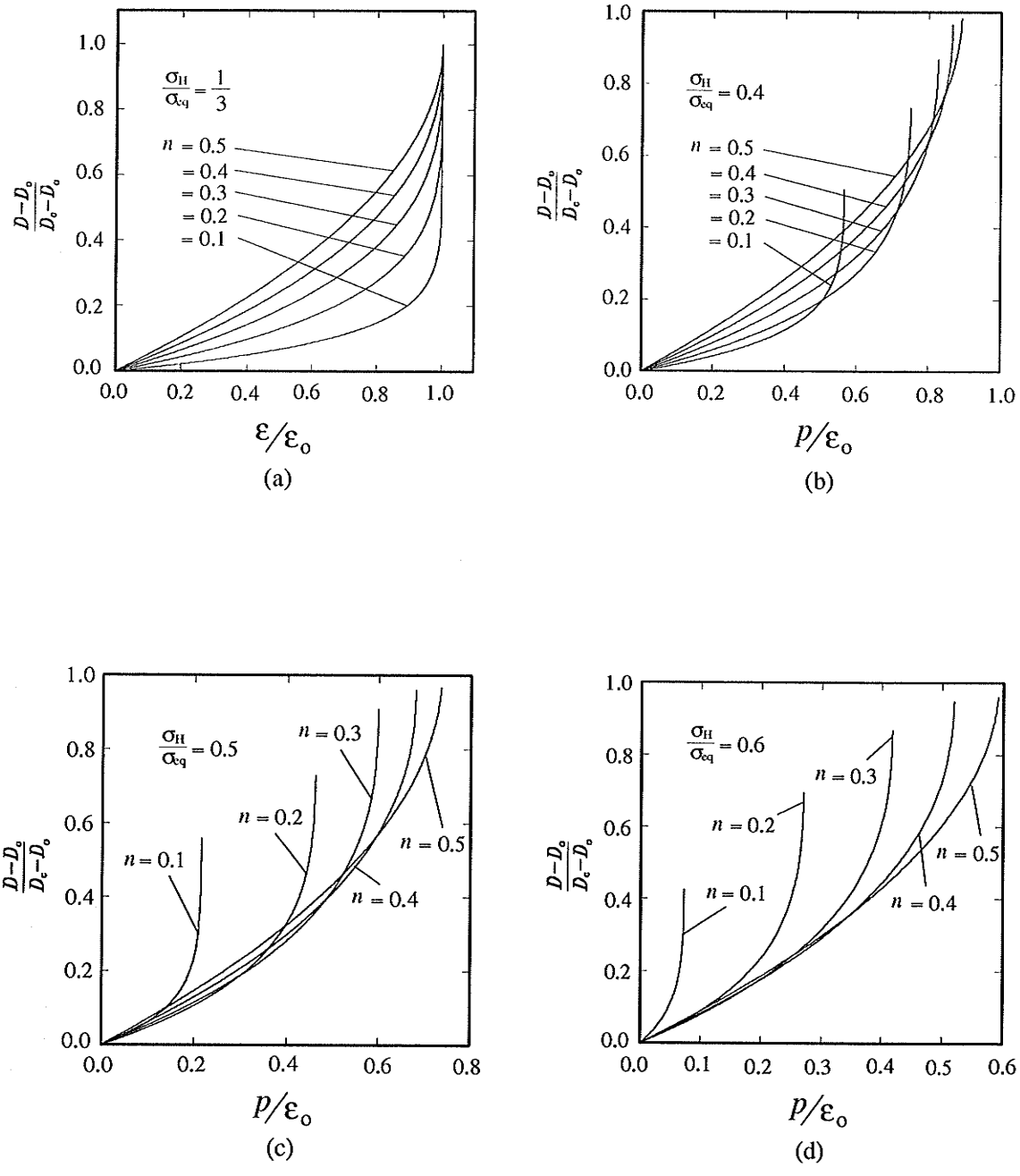



*Figure* 4.5: Damage Evolution of Materials with Different Strain Hardening Exponents

# CHAPTER FIVE

## DAMAGE DISTRIBUTIONS AND DAMAGE ZONES JUST AHEAD OF A MACROCRACK

In this chapter, damage zones and damage distributions just ahead of a macrocrack under Mode I loading are analyzed via the proposed hypothesis. Comparison with finite element analysis for damage and Dugdale's model for plastic zones are made.

### 5.1 Damage Evolution at a Macrocrack Tip

As presented in *Chapter* 4, ductile fracture in metals is the end result of a sequence of three processes; void nucleation, void growth and void coalescence. In particular, this process occurs in the region just ahead of a macrocrack tip as depicted in *Figure* 5.1. The void nucleates mainly during the second phase by particle fracture or by interfacial decohesion. Further growth occurs with the increase of plastic deformations. The true stress in the ligaments between neighboring voids increases as the ligaments become progressively thinner. This leads to void coalescence and subsequently, internal necking between neighboring voids takes place until a ductile fracture occurs.

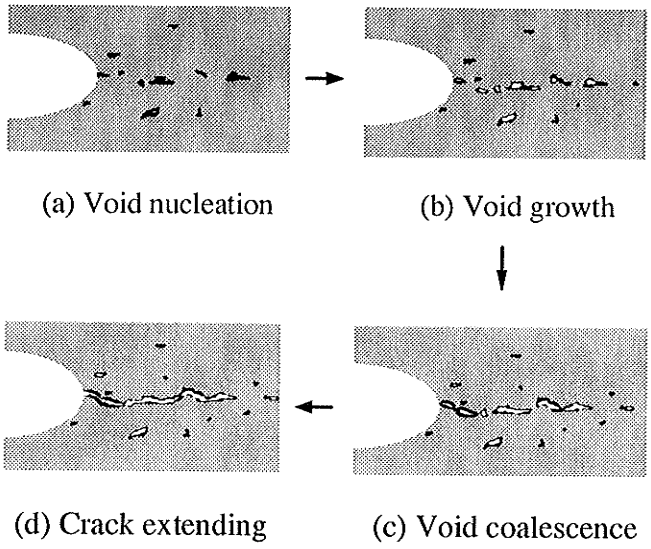
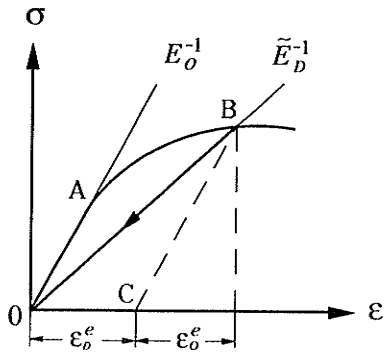



*Figure* 5.1: Damage Evolution at a Macrocrack Tip.

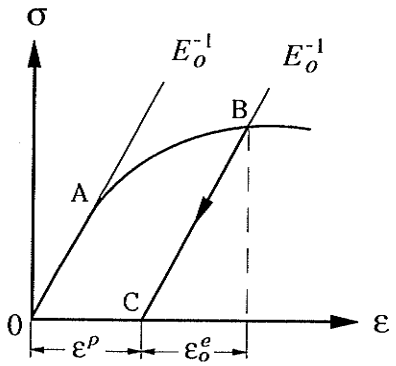
## 5.2 Description of the Nonlinear Behavior in Materials

The nonlinear behavior of materials is attributed to the presence of plastic flow. However, if damage is considered, the nonlinear behavior is the result of damage or plastic flow or both. Damage is caused by microcracks and voids through the process of nucleation, void growth and coalescence, and thus, affects the elastic properties of the material. On the other hand, plastic flow produces a permanent deformation in the material. This nonlinear phenomenon is observed by the loading and unloading curves of a specimen as sketched in *Figures* 5.2(*a*)-(*c*). Note that in these figures the unloading path *BC* is always parallel to elastic loading path *OA*. In *Figure* 5.2(*a*), the material exhibits only elastic deformations, but with damage. Hence, its elastic modulus is reduced to $\tilde{E}_D$. At point *B*, the strain $\varepsilon$ is given by the sum of the elastic damage strain $\varepsilon_D^e$ and the elastic strain of the undamaged material $\varepsilon_0^e$. That is,

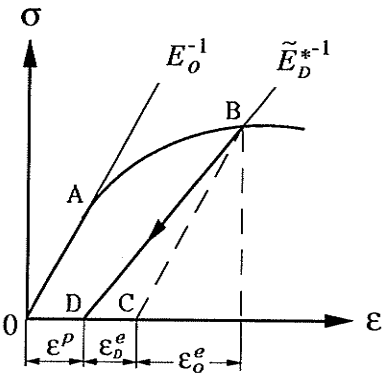
$$\varepsilon = \varepsilon_D^e + \varepsilon_o^e$$




(a) Elastic Damage without Plastic Deformation




(b) Plastic Deformation without Damage




(c) General Unloading Path

*Figure* 5.2: Unloading Paths

In *Figure* 5.2(*b*), a body undergoes elasto-plastic deformation but without damage during the entire loading path $O \rightarrow A \rightarrow B$. Hence, the elastic modulus remains unchanged. At point $B$, the strain consists of elastic and plastic deformations, namely,

$$\varepsilon = \varepsilon_o^e + \varepsilon^p$$

*Figure* 5.2(*c*) depicts a general unloading path in which all three kinds of deformation exist at point $B$; elastic deformation, elastic damage and plastic deformation. Hence

$$\varepsilon = \varepsilon_o^e + \varepsilon_D^e + \varepsilon^p$$

The elastic modulus in this case is $\tilde{E}_D^*$ and it is obvious that,

$$E_o > \tilde{E}_D^* > \tilde{E}_D$$

is true. In particle-reinforced materials, the particles may fracture. Therefore, decreases in strain hardening can be observed when the particle volume fraction or particle size is increased. This is due to the accelerated damage in the form of particle cracking in higher volume fraction and/or larger particle size materials as has been found by Hunt, Brockenbrough and Magnusen [97]. A physical interpretation of the three cases in *Figure* 5.2 is depicted in *Figure* 5.3, where a specimen under tensile loading $T$ is considered. We have assumed that voids, microcracks and other defects of the material can be represented by an equivalent void. Hence, if $L_o$ and $\Delta L^l$, $\Delta L^u$, $\Delta L_D^l$, $\Delta L_D^u$ denote the original length, the undamaged incremental lengths during loading and unloading, and the damaged incremental lengths during loading and unloading respectively, then we have,

$$\Delta L_D^l > \Delta L^l > \Delta L^u$$

$$\Delta L_D^l > \Delta L_D^u$$

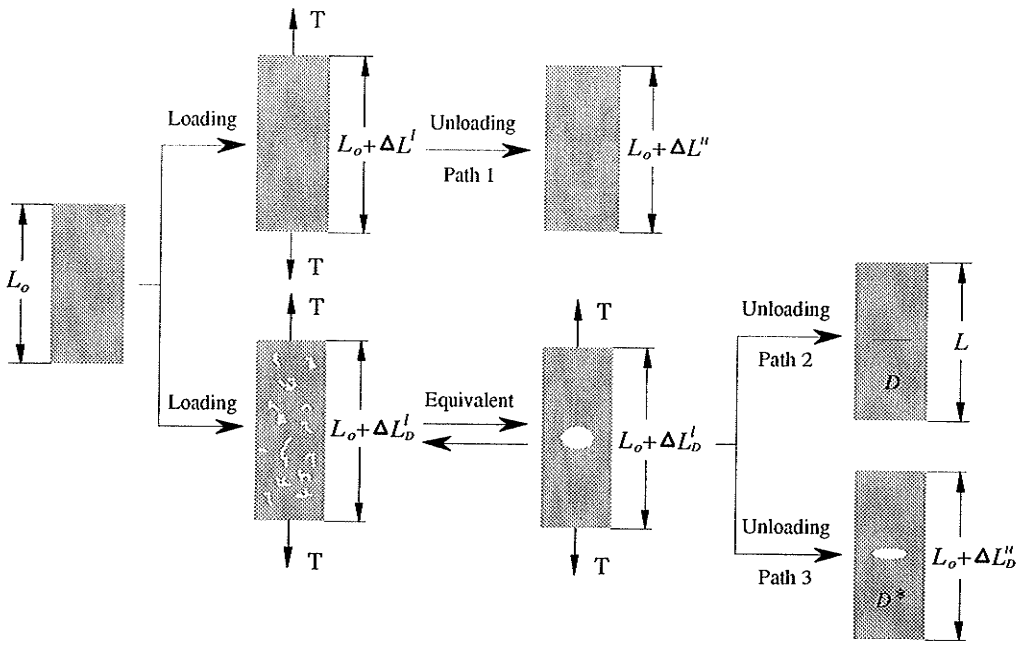
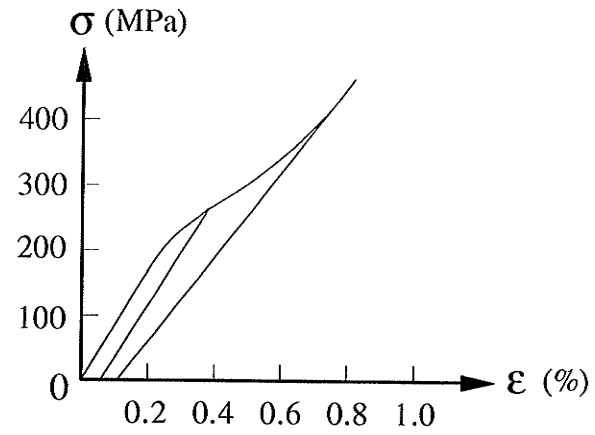


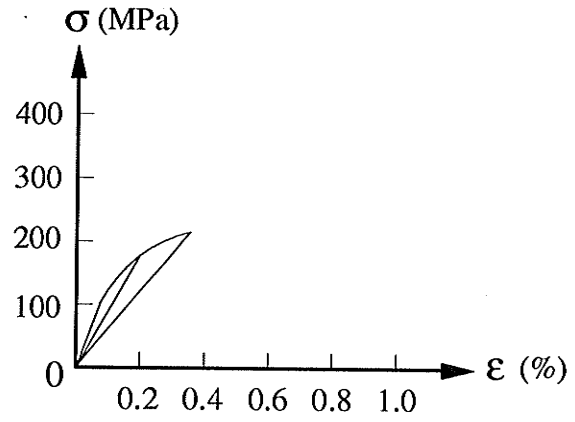

*Figure* 5.3: A Physical Representation of Unloading Paths.

In *Figure* 5.3, Paths 1, 2, and 3 correspond to the unloading curves of *Figures* 5.2 (*b*), (*a*) and (*c*) respectively. Note that in Path 2, the equivalent void during loading is completely recovered during unloading. This phenomenon is that of damage *deactivation* and is different from the concept of damage *healing* [101] which represents the amount of damage decrement when compressed.

*Figure* 5.4 shows the experimental results of typical loading-unloading stress-strain curves [102]. Observe that *Figure* 5.4(*a*) clearly represents the situation in *Figures* 5.2(*b*) and 5.2(*c*) described earlier while *Figure* 5.4(*b*) depicts the case of *Figure* 5.2(*a*).




(*a*) C/SiC




(*b*) SiC/SiC

*Figure* 5.4: Experimental Loading-unloading Paths [102]

## 5.3 Damage Distribution in the Region of a Macrocrack Tip

According the hypothesis of the incremental complementary energy equivalence, the relation between the damage variable and the effective Young's modulus for isotropic damage as discussed in *Chapter* 3 is

$$\tilde{E}_D^{-1} = e^{2D} E_o^{-1}$$

or

$$D = \frac{1}{2} \ln\left(\frac{E_o}{\tilde{E}_D}\right) \tag{84}$$

where $E_o$ is the Young's modulus and $\tilde{E}_D$ is the effective Young's modulus at the damage state $D$. The effective stress is

$$\tilde{\sigma}_D = e^D \sigma_o$$

Therefore

$$D = \ln\left(\frac{\tilde{\sigma}_D}{\sigma_o}\right) \tag{85}$$

Consider a plate with a central crack under Mode I loading as shown in *Figure* 5.5. The crack length is assumed to be small compared with the overall width of the sheet. Also, the thickness of the sheet is assumed to be small compared with the crack length, in order to preserve the state of plane stress.

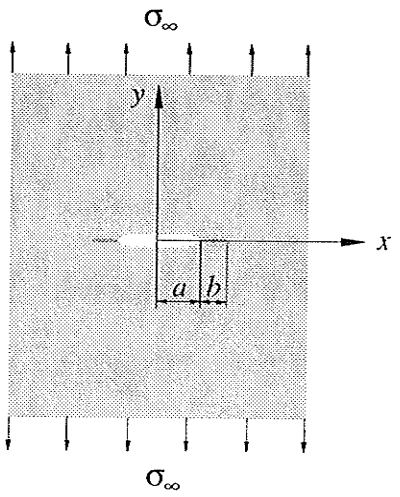
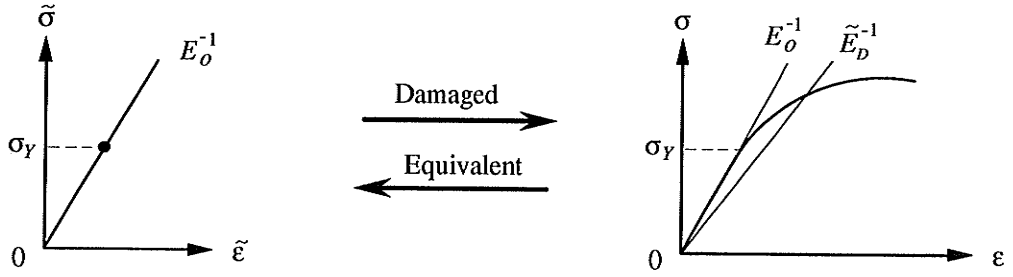



*Figure* 5.5: A Plate with a Macrocrack under Loading (Mode I)

In accordance to linear elasticity, an undamaged material exhibits linear constitutive law. Typically, due to damage, strain hardening occurs as the loading continues past the proportional limit. This is illustrated in *Figure* 5.6.




(a) Equivalent Linear Elastic Material

(b) Damaged Material

*Figure* 5.6: Undamaged and Damaged Materials.

The equation for damage distribution can be developed from the damage definition and the property of the material. In the following, the damage distribution along a macrocrack under Mode I loading is formulated for elastic-perfectly plastic materials, and the results are then compared with those predicted from a finite element analysis. *Figure* 5.7 shows an elastic-perfectly plastic material with $\sigma \sim \varepsilon$ relationship and yield stress $\sigma_Y$, and the following equation at the damage state $D$ holds:

$$E_o \varepsilon_o = \tilde{E}_D \varepsilon$$

or

$$\frac{\tilde{E}_D}{E_o} = \frac{\varepsilon_o}{\varepsilon} \tag{86}$$

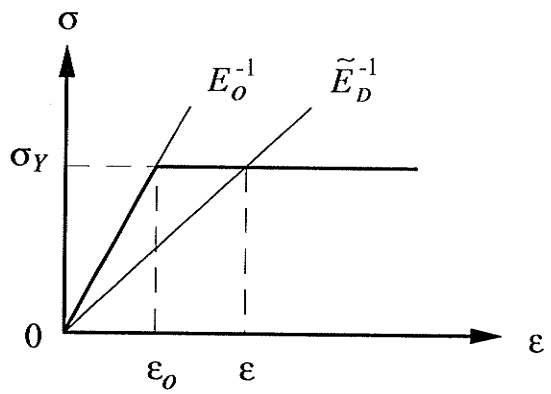



*Figure* 5.7: $\sigma \sim \varepsilon$ Relationship for Elastic-Perfectly Plastic Materials.

In view of *Equation* (86), *Equation* (84) becomes,

$$D = \frac{1}{2} \ln\left(\frac{\varepsilon}{\varepsilon_o}\right) \tag{87}$$

The experimental results of Rooke and Bradshaw [103] show that the strain in the plastic zone varies in accordance to $\varepsilon \propto (x-a)^{-1}$ for $x > a$. Utilizing this information for the loading case studied here (Mode I), we have:

$$\varepsilon = \frac{C_o}{x-a} \tag{88}$$

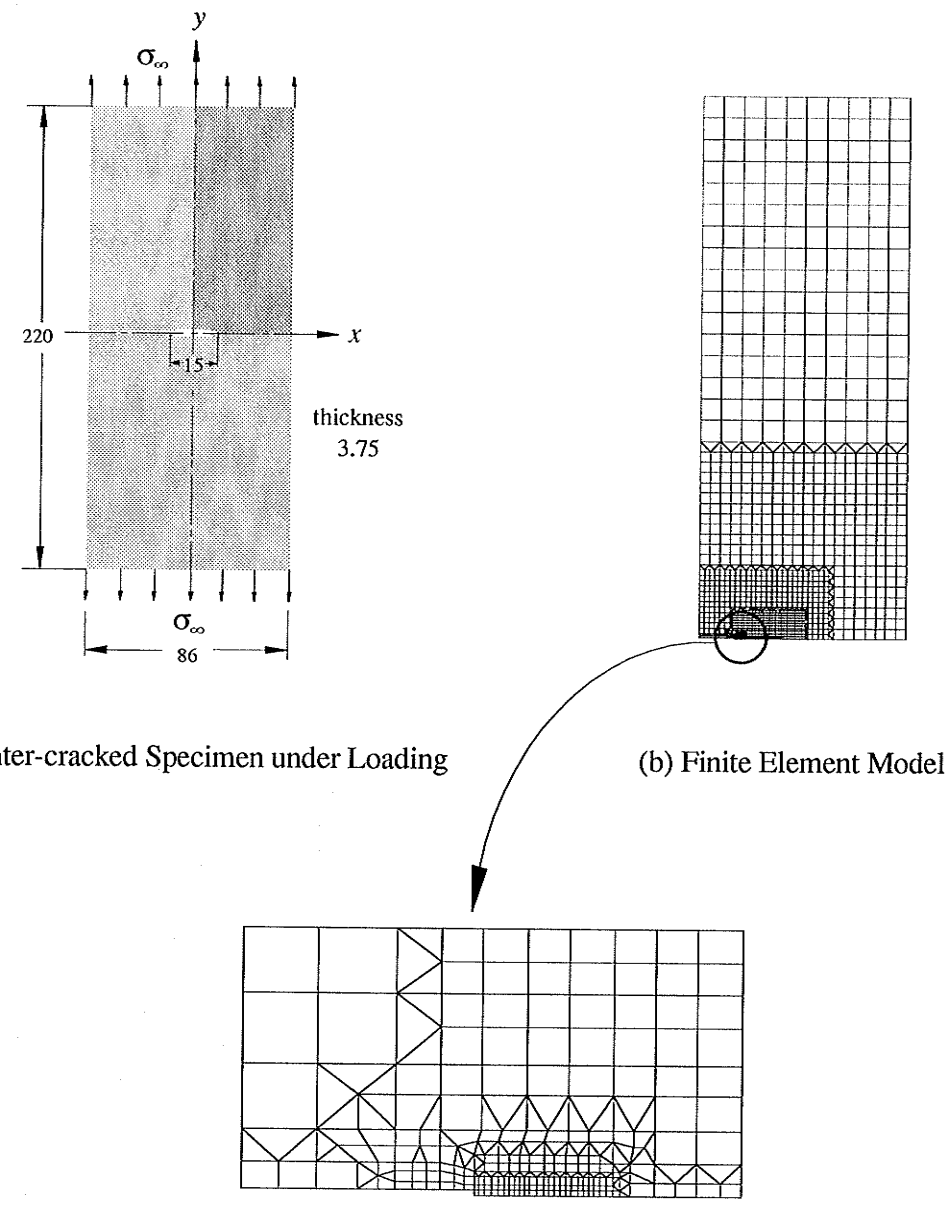
where $C_o$ is a constant and $a$ is the half length of the initial crack. Thus, the damage distribution along the crack tip can be expressed as,

$$D = \frac{1}{2}\ln\frac{C_o}{\varepsilon_o(x-a)} = D_b + \frac{1}{2}\ln\frac{b}{x-a} \tag{89}$$

where $b$ is the length of the damage zone in $x$-direction, and $D_b$ is the damage at the $x=a+b$ (or $x=c$) boundary of the damage zone as sketched in *Figure* 5.5. Note that $D_b$ is the damage when the void growth begins and is loading path-dependent.

To assess the proposed model, a finite element analysis of the plate shown in *Figure* 5.5 is now given. The purpose is to evaluate numerically, the damage distribution in the region of a crack tip. *Figure* 5.8 shows the dimensions of the plate and its finite element model. Observe that due to the symmetry of geometry and loading, only one quarter of the plate needs to be discretized. Both 3-node and 4-node isoparametric elements are employed in the model. To determine the degree of discretization of the finite element mesh, the von Mises stress of all elements connected at a node are computed. If the relative difference between them is less than a prescribed value, which for our case, is selected to be 3%, then the mesh is assumed to be sufficiently accurate. For the region around the crack tip, a

much finer mesh is used. Hence, the total number of elements and nodes employed in the model are 1398 and 1335 respectively.

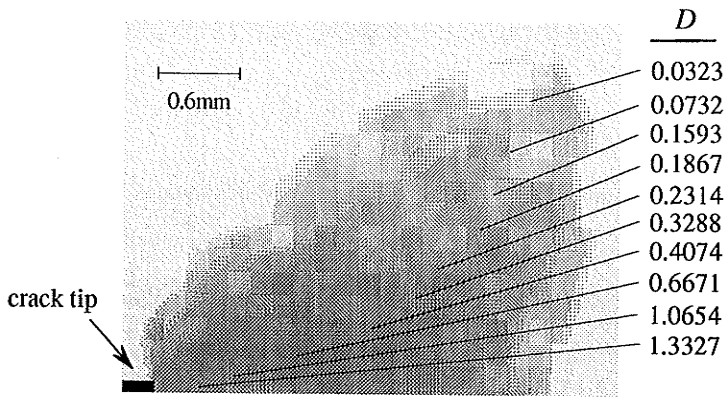



(a) Center-cracked Specimen under Loading

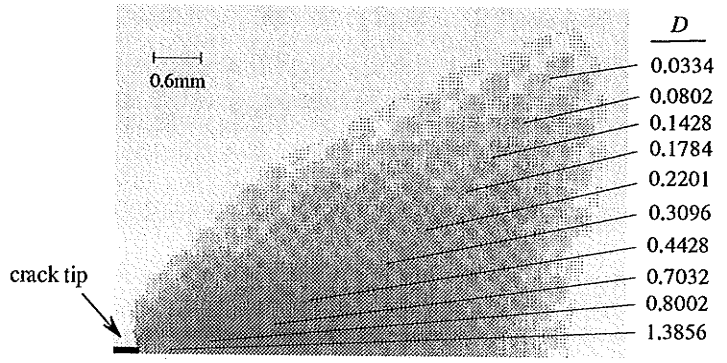
(b) Finite Element Model

(c) Mesh around the Crack Tip

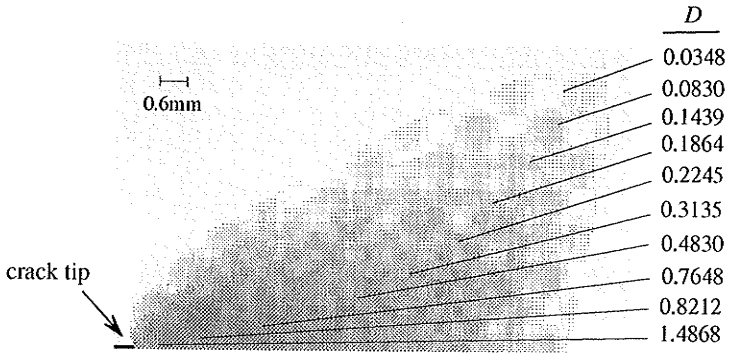
*Figure* 5.8: A Center-Cracked Specimen and Its Finite Element Model.




(*a*) $\sigma_\infty = 0.6\sigma_Y$

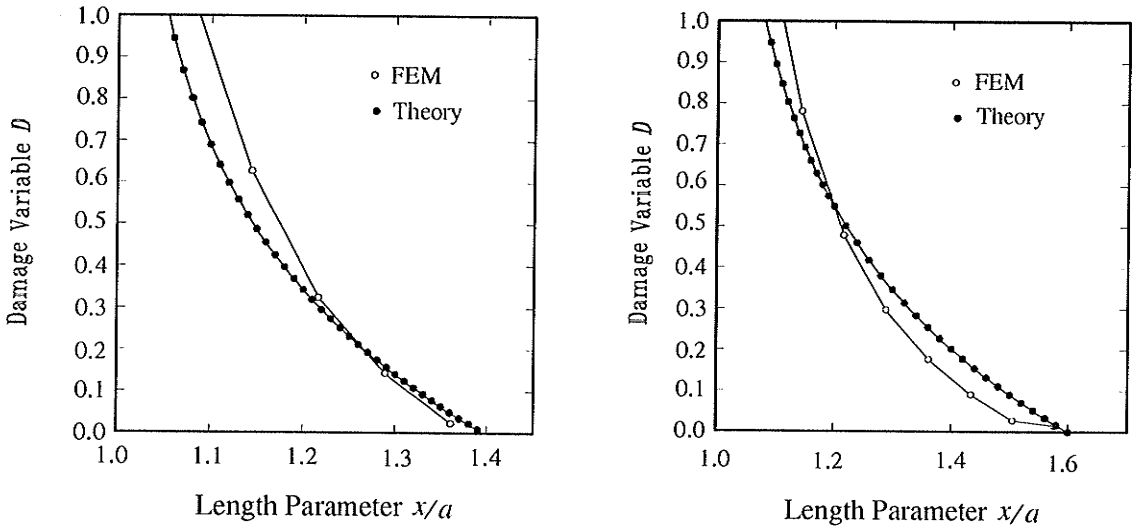



(*b*) $\sigma_\infty = 0.7\sigma_Y$




(*c*) $\sigma_\infty = 0.8\sigma_Y$

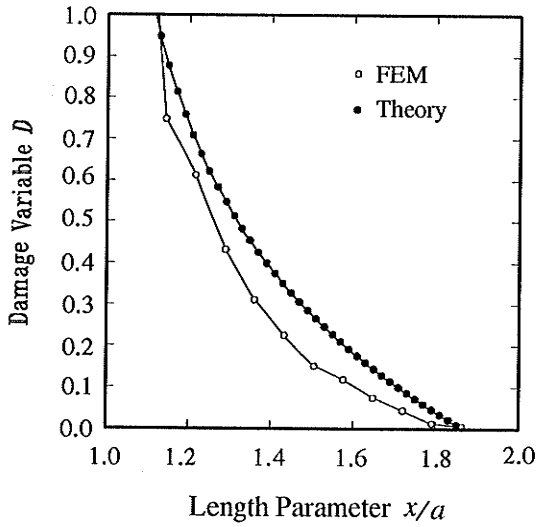
*Figure* 5.9: Damage Distribution in the Region of a Crack Tip




(a) $\sigma_\infty = 0.6\sigma_Y$




(b) $\sigma_\infty = 0.7\sigma_Y$




(c) $\sigma_\infty = 0.8\sigma_Y$

*Figure* 5.10: Damage Distribution in the Damage Zone Along the Crack Tip.

An elastic material behavior is assumed. However, when the material is damaged, it exhibits a perfectly plastic behavior as given in *Figure* 5.7. Three loading cases are analyzed, namely $\sigma_\infty = 0.6\sigma_Y$, $\sigma_\infty = 0.7\sigma_Y$, $\sigma_\infty = 0.8\sigma_Y$. The damage distribution around the crack tip is then calculated via *Equation* (85). The results are summarized in *Figure* 5.9. Observe that the damage pattern around the crack tip for different loading magnitudes are similar in shape, but as expected, the damage zones get larger with increasing loads. This is evident in the sketch of *Figure* 5.9*(a)-(c)*. To gauge the relative size of the damage zones, a variable length scale of 0.6mm is indicated on the top left corner of each figure. The maximum damage variable increases from 1.3327 to 1.4868 as the loading increases from $0.6\sigma_Y$ to $0.8\sigma_Y$. In *Section* 5.4, we will discuss the size of the damage zone along the crack direction.

*Figure* 5.10 shows the damage distribution along the $x$-axis of the damage zone as predicted by *Equation* (89) for the three loading cases. In this equation, $D_b$=*0* is assumed and $b$ calculated by the finite element analysis for the three loading cases are 2.98, 4.54, 7.00 respectively. It is seen that the theoretical predictions agree closely with the finite element results. Therefore, the expression in *Equation* (89) can be used to compute the damage distribution along the crack tip.

## 5.4 Size of the Damage Zone

Dugdale [52] obtained the size of the plastic zone for Mode I loading, for an elastic-perfectly plastic material. In his model, the length of the plastic zone is assumed to be

much greater than the thickness of the sheet but still very small compared to the other geometric parameters. He also postulated that the effect of yielding is to increase the crack length by the extent of the plastic zone in which the stress in loading direction has attained $\sigma_Y$. In this work, Dugdale's model is employed to calculate the size of the damage zone by replacing $\sigma_Y$ with the effective stress $\tilde{\sigma}$. That is,

$$\tilde{\sigma} = e^D \sigma_Y \tag{90}$$

The stress outside the damage zone consists of two parts $\sigma = \sigma_{y_1} + \sigma_{y_2}$. The former is due to the external load $\sigma_\infty$, and the latter is due to the load on the crack face of the damage zone as shown in *Figure* 5.11. These two stress components can be determined via the Westergaard stress function $\Psi$ which is a complex function of the variable $z=x+iy$. The general expressions for stress computation using $\Psi$ are,

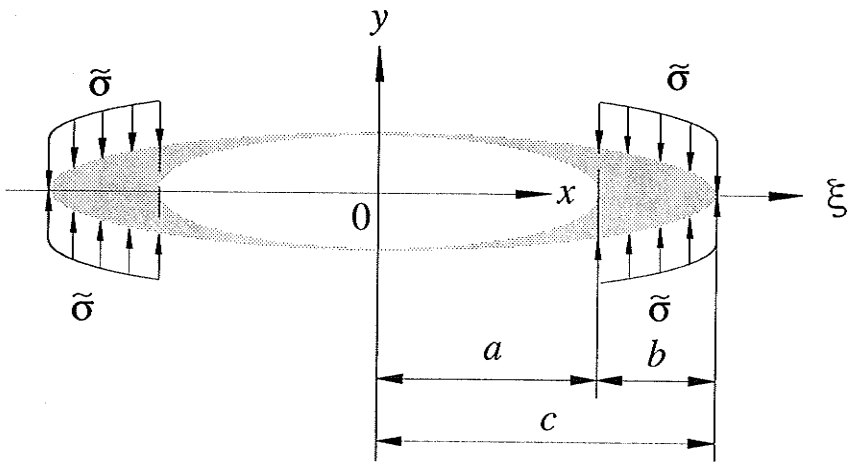



*Figure* 5.11: Dugdale Model with Damage.

$$\sigma_x = \Re\ \Psi - y\Im\ \Psi'$$

$$\sigma_y = \Re\ \Psi + y\Im\ \Psi' \qquad (91)$$

$$\tau_{xy} = -y\Re\ \Psi'$$

where $\Psi'$ is the derivative of $\Psi$ with respect to $z$, and $\Re$ and $\Im$ refer to the real and imaginary parts of $\Psi$. For the case of uniaxial loading $\sigma_\infty$ and using *Equation* (91), Westergaard [104] showed that the stress $\sigma_{y_1}$, along the $x$-axis is given by,

$$\sigma_{y_1}(x) = \sigma_\infty \sqrt{\frac{c}{2\xi}} \qquad (92)$$

where $\xi$ is the abscissa originating at $x=a+b$ as drawn in *Figure* 5.11. To obtain an expression for $\sigma_{y_2}$, first we assume that the damage zone is loaded by a pair of continuously varying forces $\tilde{\sigma}(x)dx$ along the $x$-axis which result in a stress $d\sigma'_{y_2}$ outside the zone. Based on this assumption and using Westergaard's stress function as obtained by Irwin [105], we have,

$$d\sigma'_{y_2} = -\frac{2}{\pi}\sqrt{\frac{c}{2\xi}}\frac{1}{\sqrt{c^2 - x^2}}\tilde{\sigma}(x)dx \qquad (93)$$

To derive the actual stress $d\sigma_{y_2}$ from $d\sigma'_{y_2}$, we need to take into account the presence of voids inside the damage zone. This can be conveniently achieved via an influence function $w(x)$. That is,

$$d\sigma_{y_2} = w(x)d\sigma'_{y_2} \tag{94}$$

Due to voids in the length $dx$, an effective loading length $d\tilde{x}$ should be used instead. Budiansky and O'Connell [56] studied the elastic moduli of a randomly arrayed penny-shaped cracks in an isotropic elastic solid and obtained the following damage variable in terms of the effective Poisson's ratio $\tilde{\nu}$ and the effective void dimension parameter $\tilde{d}$,

$$\frac{\tilde{E}_D}{E_o} = 1 - \frac{\tilde{d}}{f(\tilde{\nu})} \tag{95}$$

where

$$f(\tilde{\nu}) = \frac{45}{16(1+\tilde{\nu})(5-4\tilde{\nu})} \tag{96}$$

Note that the effective void dimension parameter $\tilde{d}$ provides information on the voids in a given area. It is assumed by Grady and Kipp [106] that $\tilde{d}$ can be described by the following expression,

$$\tilde{d} = Nd$$

where $d$ is the average void dimension in the area under consideration and $N$ is the number of voids per unit area. To describe $N$, a Weibull statistical function which has been used to provide a satisfactory quantification of the inherent microcracks leading to tensile fracture [107], can be employed. Thus the effective loading length $d\tilde{x}$ can be expressed as,

$$d\tilde{x} = w(x)dx = (1-\tilde{d})dx \tag{97}$$

From *Equations* (84), (89) and (95), we get an expression for the effective void dimension $\tilde{d}$ as,

$$\tilde{d} = \left(1 - e^{-2D_b - \ln\frac{b}{x-a}}\right) f(\tilde{\nu})$$

Once again, if $D_b = 0$ is assumed, then

$$\tilde{d} = \left(1 - \frac{x-a}{b}\right) f(\tilde{\nu}) \tag{98}$$

In view of *Equation* (97), the weighting function in *Equation* (94) is given by,

$$w(x) = 1 - \left(1 - \frac{x-a}{b}\right) f(\tilde{\nu}) \tag{99}$$

The stress outside the damage zone due to loading in the damage zone $\sigma_{y_2}$ is thus computed using *Equations* (94) and (99). That is,

$$\sigma_{y_2} = \int w(x) d\sigma'_{y_2} = -\frac{2}{\pi}\sqrt{\frac{c}{2\xi}} \int_a^c w(x) \sqrt{\frac{1}{c^2 - x^2}}\tilde{\sigma}(x)dx \tag{100}$$

The total stress is now given by the summation of *Equations* (92) and (100),

$$\sigma(x) = \sigma_{y_1} + \sigma_{y_2} = \sqrt{\frac{c}{2\xi}}\left(\sigma_\infty - \frac{2}{\pi}\int_a^c w(x)\frac{1}{\sqrt{c^2 - x^2}}\tilde{\sigma}(x)dx\right) \tag{101}$$

Since $\sigma(x)$ is finite at the boundary of the damage zone, viz., at $x=c$ (or $\xi$ =0), the following condition in *Equation* (101) must hold,

$$\sigma_{\infty} - \frac{2}{\pi} \int_a^c w(x) \frac{1}{\sqrt{c^2 - x^2}} \tilde{\sigma}(x) dx = 0 \tag{102}$$

from which the size of the damage zone can be computed. To carry out the integration in *Equation* (102), a non-dimensional variable $\lambda$ is introduced by letting $x=a+b(1-\lambda)=c-b\lambda$. Then $D$ and $w(x)$ can be expressed as,

$$D = D_b + \frac{1}{2} \ln \frac{1}{1-\lambda} \tag{103}$$

$$w(x) = 1 - \lambda f(\tilde{v}) \tag{104}$$

Substituting *Equations* (90) and (103-104) into *Equation* (102) and assume $D_b = 0$ yields,

$$\sigma_{\infty} - \sigma_Y \frac{2}{\pi} \sqrt{\frac{b}{2c}} \int_0^1 \left(1 - \lambda f(\tilde{v})\right) \lambda^{-½} (1-\lambda)^{-½} \left(1 - \frac{b}{2c}\lambda\right)^{-½} d\lambda = 0$$

and after integration, we have,

$$\frac{\sigma_{\infty}}{\sigma_Y} - \frac{2}{\pi} \sqrt{\frac{b}{2c}} \left[ \left(1 - f(\tilde{v})\right) B\left(\frac{1}{2}, \frac{1}{2}\right) F\left(\frac{1}{2}, \frac{1}{2}; 1; \frac{b}{2c}\right) \right.$$

$$\left. + f(\tilde{v}) B\left(\frac{1}{2}, \frac{3}{2}\right) F\left(\frac{1}{2}, \frac{1}{2}; 2; \frac{b}{2c}\right) \right] = 0$$

where $B(p, q)$ and $F(\alpha, \beta; \gamma; z)$ are the beta and hypergeometric functions [108] defined as follows,

$$B(p, q) = \frac{1}{q}\sum_{k=0}^{\infty}(-1)^k \frac{q(q-1)\cdots(q-k)}{k!(p+k)} \tag{105}$$

$$F(\alpha, \beta; \gamma; z) = \frac{\Gamma(\gamma)}{\Gamma(\alpha)\Gamma(\beta)} \sum_{n=0}^{\infty} \frac{\Gamma(\alpha+n)\Gamma(\beta+n)}{\Gamma(\gamma+n)} \frac{z^n}{n!} \tag{106}$$

Hence, the non-dimensionalized damage zone can be computed from,

$$\frac{c}{a} = 1 + \frac{\left(\pi \frac{\sigma_\infty}{\sigma_Y}\right)^2}{2\left[\left(1 - f(\tilde{\nu})\right)H_1 + f(\tilde{\nu})H_2\right]^2 - \left(\pi \frac{\sigma_\infty}{\sigma_Y}\right)^2} \tag{107}$$

where

$$H_1 = B\left(\frac{1}{2}, \frac{1}{2}\right) F\left(\frac{1}{2}, \frac{1}{2}; 1; \frac{1}{2} - \frac{a}{2c}\right)$$

and

$$H_2 = B\left(\frac{1}{2}, \frac{3}{2}\right) F\left(\frac{1}{2}, \frac{1}{2}; 2; \frac{1}{2} - \frac{a}{2c}\right)$$

*Figure* 5.12 shows the variation of the effective Poisson's ratio $\tilde{\nu}$ with strain, for aluminum alloy 2024-T3 [34]. Observe that this variation is very small which is true for

most engineering materials. Therefore, it is reasonable to assume that the effective Poisson's ratio has a nominal variation around 0.3, namely, $\tilde{\nu} = 0.3$.

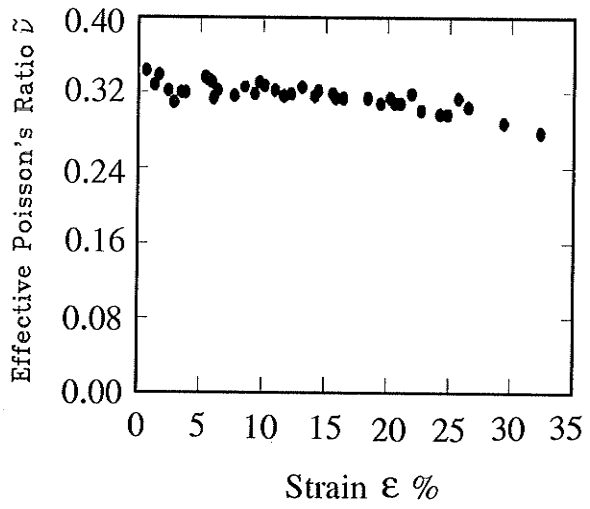



*Figure* 5.12: Effective Poisson's Ratio (Chow and Wang [34])

*Figure* 5.13 shows a comparison of the damage zone computed by *Equation* (107) with the finite element predictions for varying ratios of the external loading $\sigma_\infty$ to yield stress $\sigma_Y$. The agreement with the finite element analysis is very good. It would be interesting to also compare Dugdale's plastic zone in this plot. Using the concept of SIF, the expression for Dugdale's plastic zone is given by,

$$\frac{c}{a} = \sec\left(\frac{\pi}{2}\frac{\sigma_\infty}{\sigma_Y}\right)$$

The result is plotted in *Figure* 5.13. Notice that Dugdale's plastic zone is comparatively larger than the damage zone predicted by the proposed model.

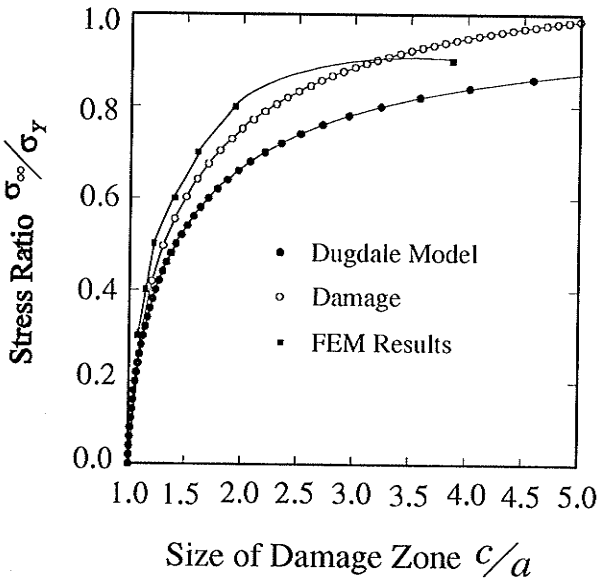



*Figure* 5.13: Comparison of the Sizes of Damage Zones.

# CHAPTER SIX

## DAMAGE ZONES IN MATERIALS WITH STRAIN HARDENING BEHAVIOR

In this chapter, the work in the previous Chapter 5 is now extended to include strain hardening materials with elastic damage. As before, comparison with finite element analysis for damage and Dugdale's model for plastic zones are also given.

### 6.1 Damage Distribution of a Strain Hardening Material with a Macrocrack

In the foregoing chapter, the damage distribution in the region of a crack tip under Mode I loading has been analyzed via *Equation* (84). It is assumed here that the unloading path corresponds to elastic damage without plastic deformation as shown in *Figure* 5.2(*a*). Also, the stress-strain curve of the material is assumed to follow a uniaxial stress-strain relation of the Ramberg-Osgood type given by,

$$\sigma = \begin{cases} E_o \varepsilon, & \text{if } \sigma \le \sigma_Y; \\ \sigma_Y (\varepsilon/\varepsilon_o)^n, & \text{if } \sigma \ge \sigma_Y, \end{cases} \tag{108}$$

where $\sigma_Y$ is the initial yield stress which is often taken as the flow stress to account for the strain hardening effects, $\varepsilon_o = \sigma_Y / E$ is the strain in tension, and $n$ $(1 \ge n \ge 0)$ is the strain

hardening exponent. When $n$=1, the linearly elastic behavior is recovered from *Equation* (108), and in the limit $n \to 0$, the elastic-perfectly plastic case is recovered. In CDM, *Equation* (108) can be written in the following form,

$$\sigma = \begin{cases} E_o \varepsilon, & \text{if } \sigma \le \sigma_Y; \\ \tilde{E}_D \varepsilon, & \text{if } \sigma \ge \sigma_Y, \end{cases} \tag{109}$$

where from *Equations* (108) and (109), the effective Young's modulus $\tilde{E}_D$ is given by,

$$\frac{\tilde{E}_D}{E_o} = \left( \frac{\varepsilon_o}{\varepsilon} \right)^{1-n} \tag{110}$$

Substituting *Equation* (110) into *Equation* (84) yields,

$$D = \frac{1-n}{2} \ln \left( \frac{\varepsilon}{\varepsilon_o} \right) \tag{111}$$

The stress distribution $\sigma(x)$ along a crack under Mode I loading can be formulated by an experimental study or by a finite element analysis. In Wang and Chow [36], they analyzed HRR fields for damaged materials. In their work, they obtained similar stress expression as derived by Hutchinson [109]. That is,

$$\begin{aligned} \sigma_{rr} &= C r^{S-2} \breve{\sigma}_{rr}(\theta) \\ \sigma_{\theta\theta} &= C r^{S-2} \breve{\sigma}_{\theta\theta}(\theta) \\ \sigma_{r\theta} &= C r^{S-2} \breve{\sigma}_{r\theta}(\theta) \end{aligned} \tag{112}$$

in which $C$ is a constant and $\breve{\sigma}_{rr}(\theta)$, $\breve{\sigma}_{\theta\theta}(\theta)$, $\breve{\sigma}_{r\theta}(\theta)$ are stress amplitudes. From the path independence of $J$-integral, Hutchinson [109] showed that for virgin materials,

$$S = \frac{2n'+1}{n'+1} \tag{113}$$

where $n' = 1/n$. However, Wang and Chow [36] argued that this property of the path independence of $J$-integral is violated when damage near the macrocrack tip is considered. They not only justified this theoretically but also numerically.

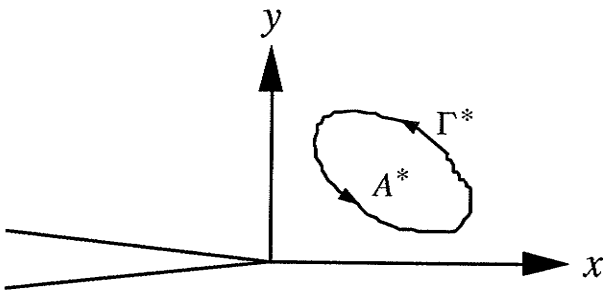



*Figure* 6.1: Closed Curve $\Gamma^*$ at the Macrocrack Tip

Consider an arbitrary closed curve $\Gamma^*$ as shown in *Figure* 6.1. If $W$ is the strain energy density, then following the same analysis as outlined for virgin materials, they showed that,

$$J^* = \oint_{\Gamma^*} W dy - \sigma_{ij} n_j u_{i,x} ds$$

$$= \iint_{A^*} \frac{\partial W}{\partial D} \frac{\partial D}{\partial x} dxdy \neq 0$$

which implies that the path independence does not prevail when considering damage around the macrocrack tip. Instead of *Equation* (113), they suggested the following formula,

$$S = \frac{2G+1}{G+1} \tag{114}$$

where $G = n' + m$ and $m$ is a material constant. If $m \approx 0.5$ is chosen (just as in Wang and Chow's work [36]), then the exponent in the stresses of *Equation* (112) becomes,

$$S - 2 = -\frac{1}{G+1} = -\frac{1}{n'+m+1}$$

$$= -\frac{2n}{2+3n}$$

Therefore we can write the stress distribution along the crack in the following expression,

$$\sigma(x) = C_o \left( \frac{1}{x-a} \right)^{\frac{2n}{2+3n}} \tag{115}$$

where $C_o$ is a constant to be determined later and $a$ is the half length of the crack. Comparing *Equation* (115) with *Equation* (108), the following strain distribution is derived,

$$\frac{\varepsilon(x)}{\varepsilon_o} = \frac{C_o}{\sigma_Y} \left( \frac{1}{x-a} \right)^{\frac{2}{2+3n}} \tag{116}$$

Substituting *Equation* (116) into *Equation* (111), we arrived at the following expression of damage distribution along a crack for strain hardening materials,

$$D = \frac{1-n}{2} \ln\left[ \frac{C_o}{\sigma_Y} \left( \frac{1}{x-a} \right)^{\frac{2}{2+3n}} \right] \tag{117}$$

Using the damage value $D_b$ at the boundary of the damage zone, i.e. $x = a+b$, where $b$ is the length of the damage zone in $x$-direction and $x$ is the abscissa as sketched in *Figure* 5.5, the constant $C_o$ can be found. If $D_b = 0$ is assumed, then from *Equation* (117), we get,

$$C_o = \sigma_Y b^{\frac{2}{2+3n}}$$

Substituting the expression of $C_o$ back into *Equations* (115)-(117), yields,

$$\sigma(x) = \sigma_Y \left( \frac{b}{x-a} \right)^{\frac{2n}{2+3n}} \tag{118}$$

$$\varepsilon(x) = \varepsilon_o \left( \frac{b}{x-a} \right)^{\frac{2}{2+3n}} \tag{119}$$

$$D = \frac{1-n}{2+3n} \ln\left( \frac{b}{x-a} \right) \tag{120}$$

Note that for an elastic-perfectly plastic material, $n = 0$ and the strain distribution of *Equation* (119) along a crack is found to vary as $\varepsilon(x) \propto (x-a)^{-1}$ which is consistent with the experimental results by Rooke and Bradshaw [103].

Again, the finite element model of the plate given in *Figure* 5.5, is used to assess the proposed model. The comparison includes a numerical evaluation of the damage distribution in the region of a crack tip. Once again, the three loading cases are analyzed, namely, $\sigma_\infty = 0.6\sigma_Y$, $\sigma_\infty = 0.7\sigma_Y$, $\sigma_\infty = 0.8\sigma_Y$. The strain hardening exponent chosen are $n$ = 0.1, 0.2 and 0.5. As shown in *Figure* 6.2, the load is applied by five steps. *Figure* 6.3 shows the comparison of the stress distribution of *Equation* (118) with the finite element results. The same finite element model of *Figure* 5.8 is used. A good agreement of stress distribution is observed.

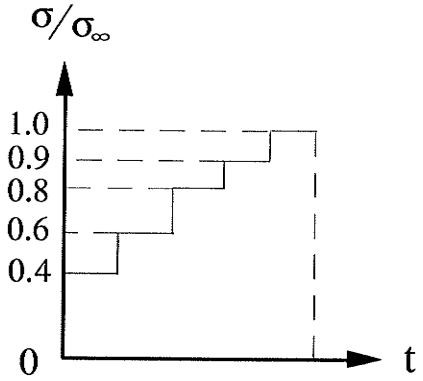
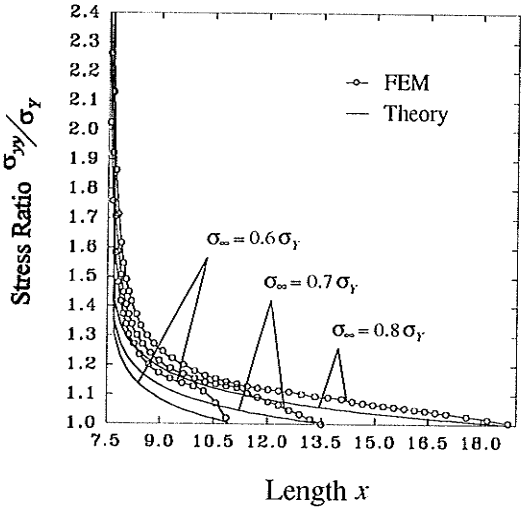


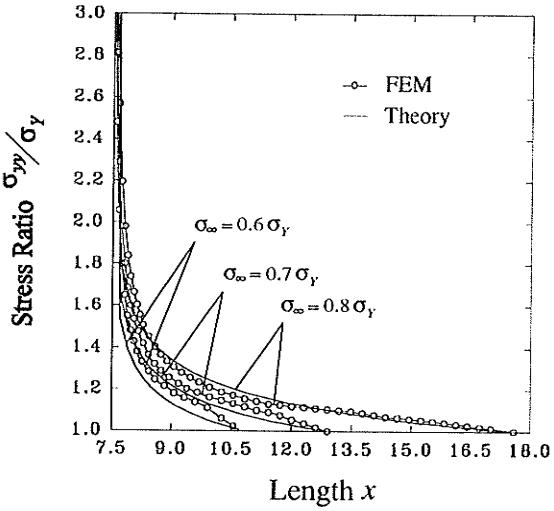

*Figure* 6.2: Load application steps

At each load step, the damage around the crack tip is calculated using the incremental complementary energy equivalence model sketched in *Figure* 3.3 and represented by the following equation,

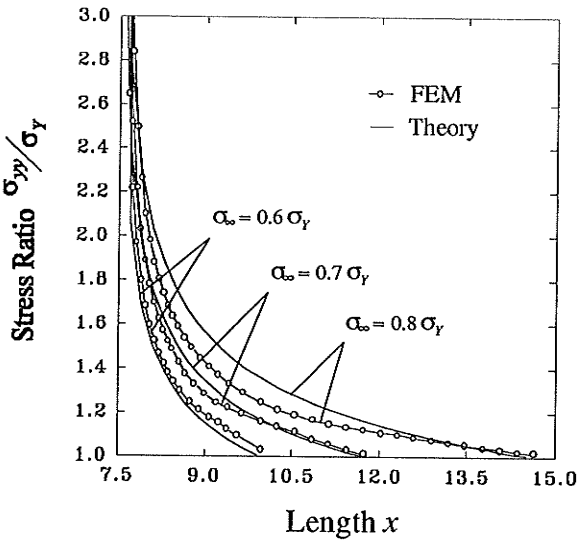
$$\delta\psi_c\left(d\sigma_D, \tilde{E}^{-1}_{D+dD}, D+dD\right) = \delta\psi_c\left(d\tilde{\sigma}_{D+dD}, \tilde{E}^{-1}_{D}, D\right) \qquad (121)$$




(*a*) $n$=0.1




(*b*) $n$=0.2

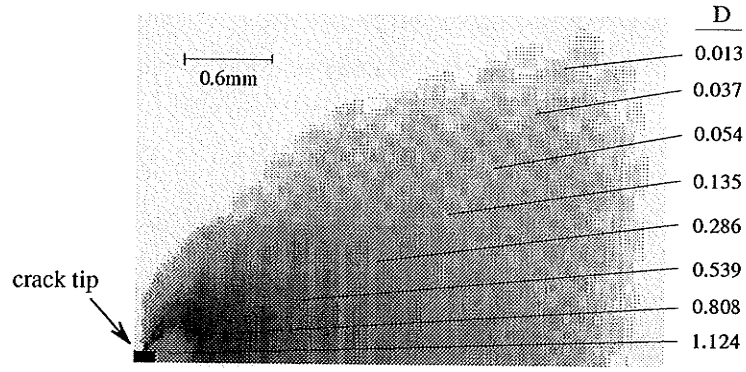



(*c*) $n$=0.5

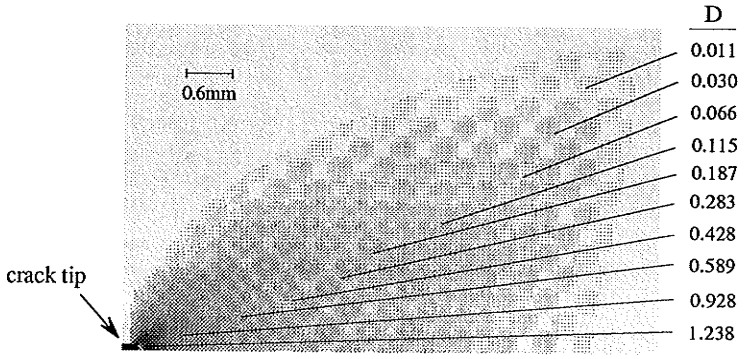
*Figure* 6.3: Comparison of stress predictions

Here the stress increment between the load steps is taken as $d\sigma_D$. The results are summarized in *Figures* 6.4 to 6.6. Observe that the damage pattern around the crack tip for different loading magnitudes are similar in shape, and as expected, the damage zones get larger with increasing loads. To gauge the relative size of the damage zones, a variable length scale of 0.6mm is indicated on the top left corner of each figure. The maximum damage variable increases from 1.124 to 1.353, 0.980 to 1.225 and 0.560 to 0.727 for $n$=0.1, 0.2, 0.5 respectively as the loading increases from $0.6\sigma_Y$ to $0.8\sigma_Y$.

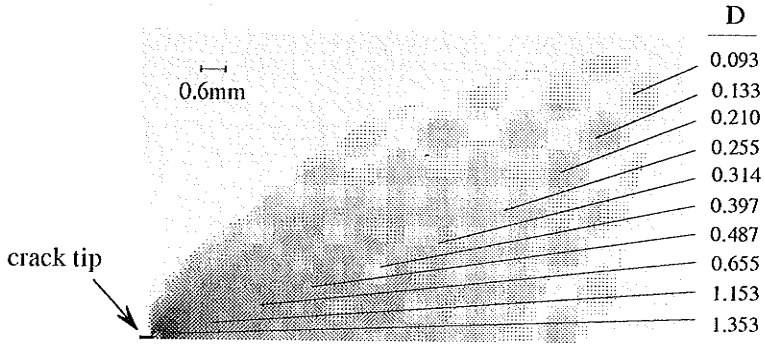
*Figures* 6.7 to *Figure* 6.9 show the damage distribution along the $x$-axis of the damage zone as predicted by *Equation* (120) for the three loading cases. In this equation, the values of $b$ calculated by the finite element analysis are used. It is seen that the theoretical predictions agree closely with the finite element results, especially for the case of $n$=0.5. Therefore, the expression in *Equation* (120) can be used to compute the damage distribution along the crack tip. In the next section, this equation is also employed to evaluate the size of the damage zone.




(*a*) $\sigma_\infty = 0.6\sigma_Y$

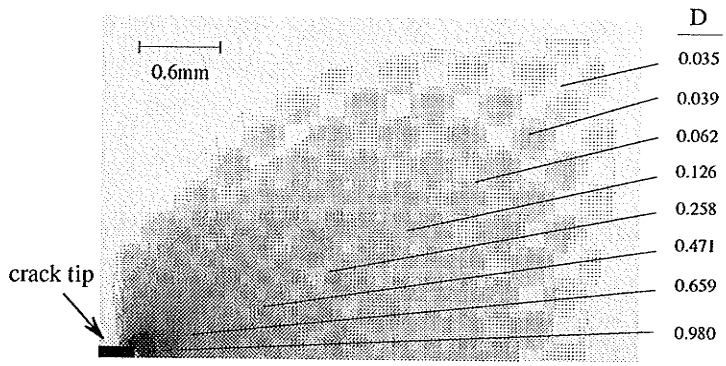



(*b*) $\sigma_\infty = 0.7\sigma_Y$

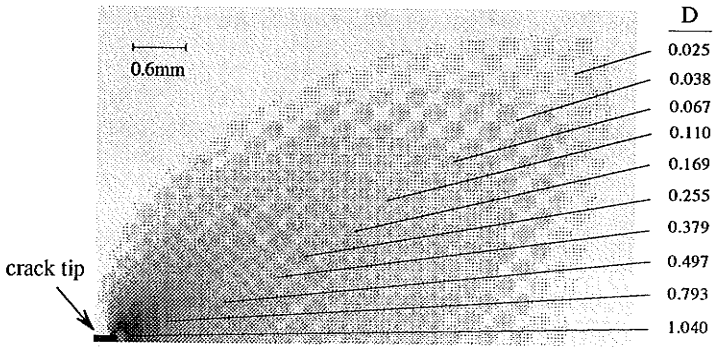



(*c*) $\sigma_\infty = 0.8\sigma_Y$

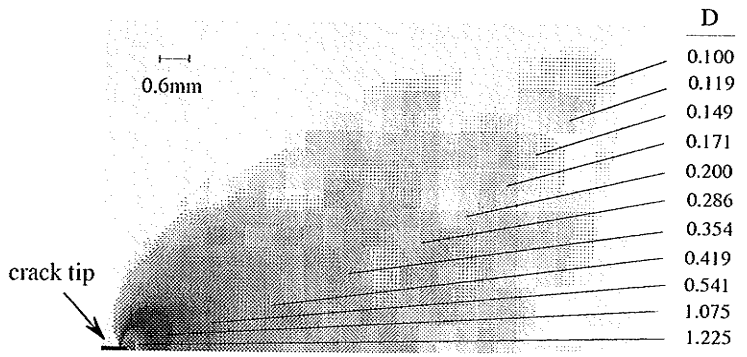
*Figure* 6.4: Damage Distribution around a Crack Tip for $n$=0.1




(*a*) $\sigma_\infty = 0.6\sigma_Y$

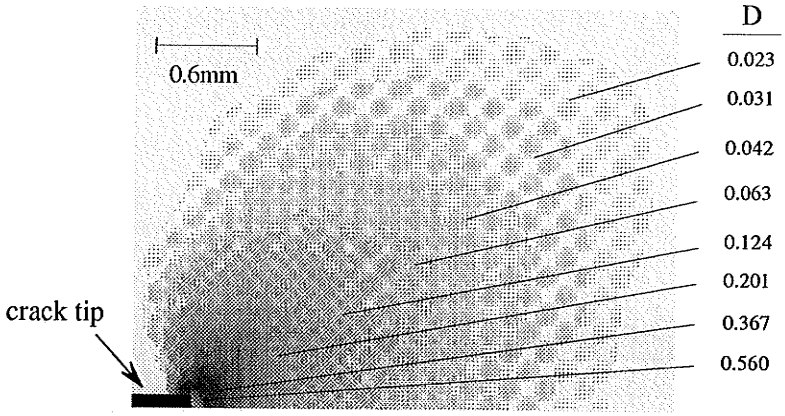



(*b*) $\sigma_\infty = 0.7\sigma_Y$

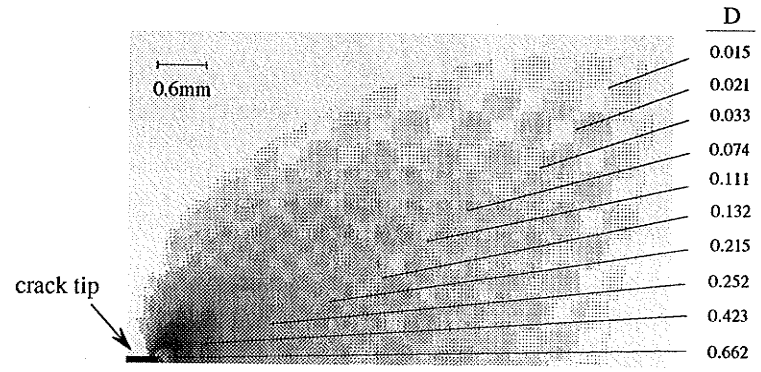



(*c*) $\sigma_\infty = 0.8\sigma_Y$

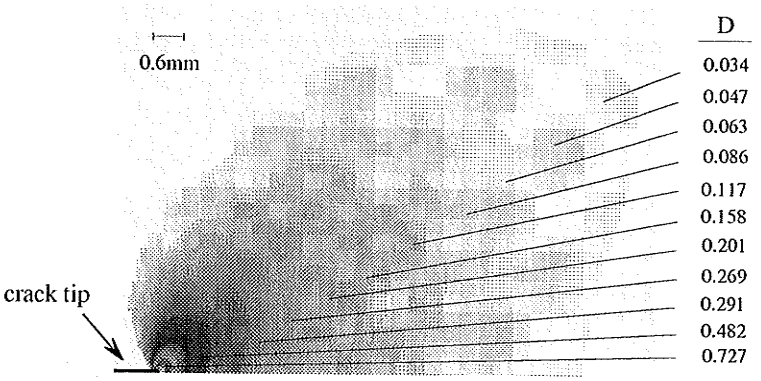
*Figure* 6.5: Damage Distribution around a Crack Tip for $n$=0.2




(*a*) $\sigma_\infty = 0.6\sigma_Y$

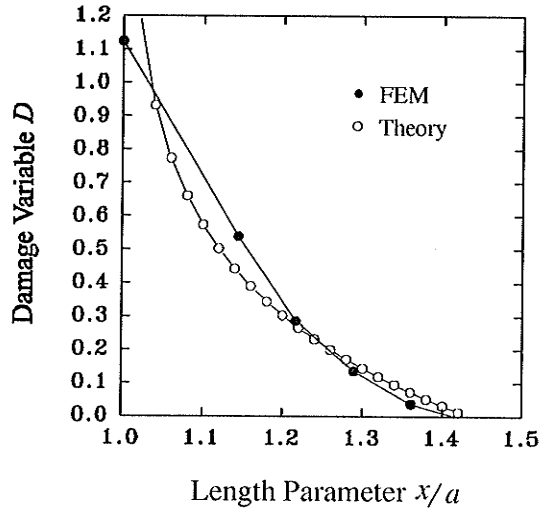



(*b*) $\sigma_\infty = 0.7\sigma_Y$

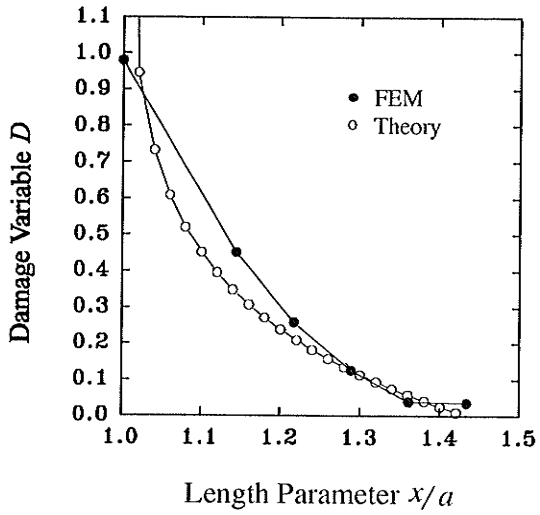



(*c*) $\sigma_\infty = 0.8\sigma_Y$

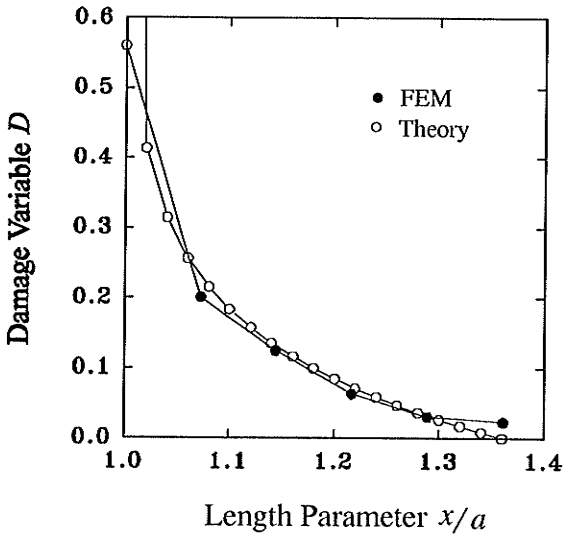
*Figure* 6.6: Damage Distribution around a Crack Tip for $n$=0.5




(*a*) $n$=0.1

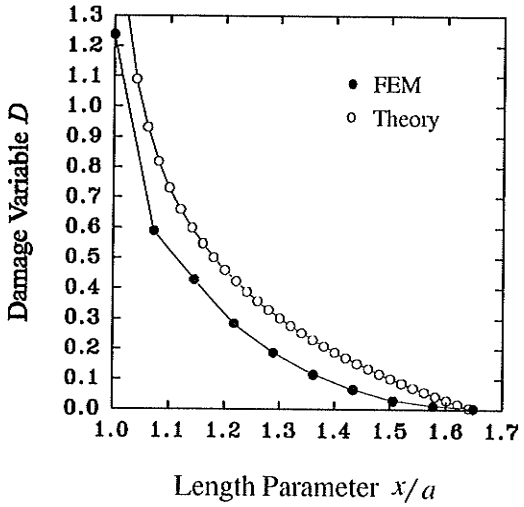



(*b*) $n$=0.2

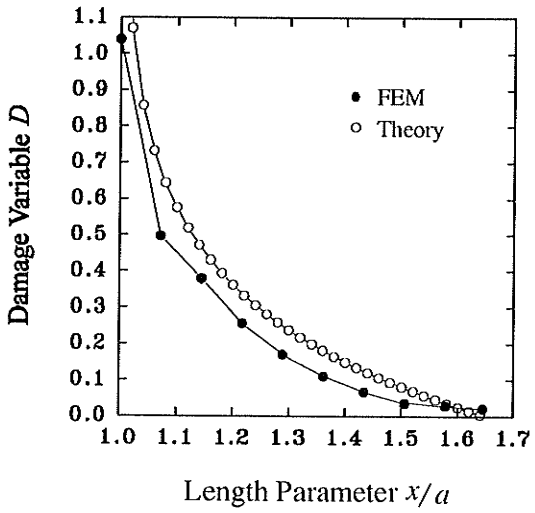



(*c*) $n$=0.5

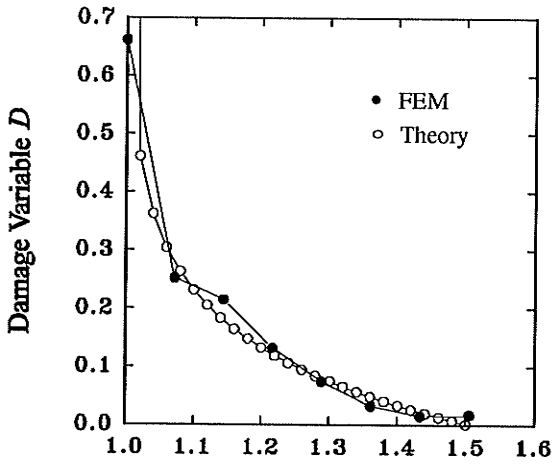
*Figure* 6.7: Damage Distribution in the Damage Zone along the Crack Tip at $\sigma_\infty = 0.6\sigma_Y$




(*a*) $n$=0.1

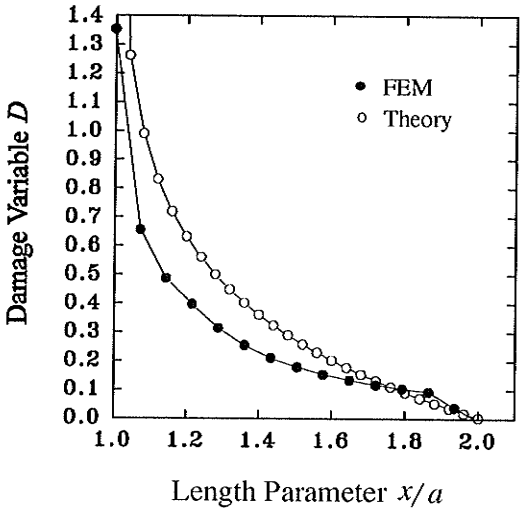



(*b*) $n$=0.2

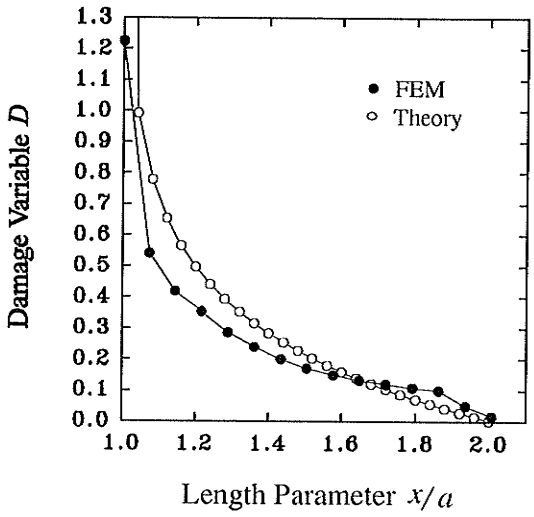



(*c*) $n$=0.5

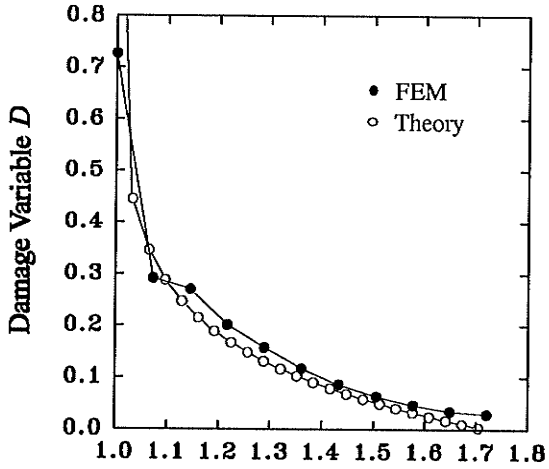
*Figure* 6.8: Damage Distribution in the Damage Zone along the Crack Tip at $\sigma_\infty = 0.7\sigma_Y$




(*a*) $n$=0.1




(*b*) $n$=0.2




(*c*) $n$=0.5

*Figure* 6.9: Damage Distribution in the Damage Zone along the Crack Tip at $\sigma_\infty = 0.8\sigma_Y$

## 6.2 Size of the Damage Zone along a Macrocrack

In *Chapter* 5, the size of damage zone was analyzed using the Dugdale model for elastic-perfectly plastic materials under elastic damage. Now a similar method is employed here to formulate the size of damage zone along a crack under Mode I loading, for strain hardening materials. We employ Dugdale model to calculate the size of the damage zone by replacing $\sigma(x)$ with the effective stress $\tilde{\sigma}(x)$. That is,

$$\tilde{\sigma}(x) = e^{D}\sigma(x) \tag{122}$$

The stress outside the damage zone consists of two parts $\sigma = \sigma_{y_1} + \sigma_{y_2}$. The former is due to the external load $\sigma_\infty$, and the latter is due to the load on the crack face of the damage zone as illustrated in *Figure* 6.10. The expressions of $\sigma_{y_1}$ and $\sigma_{y_2}$ are the same as those given by *Equations* (92) and (94), namely,

$$\sigma_{y_1}(x) = \sigma_\infty \sqrt{\frac{c}{2\xi}}$$

$$d\sigma_{y_2} = w(x)d\sigma'_{y_2} \tag{123}$$

where $\xi$ is the abscissa originating at $x=a+b$ as drawn in *Figure* 6.10. Note that the weighting function which depends on the effective void dimension $\tilde{d}$ is different. The

expression for $\tilde{d}$ is obtained by substituting *Equation* (84) into *Equation* (89) and comparing with *Equation* (120), we get,

$$\tilde{d} = \left(1 - \left(\frac{x-a}{b}\right)^{\frac{2(1-n)}{2+3n}}\right) f(\tilde{\nu})$$

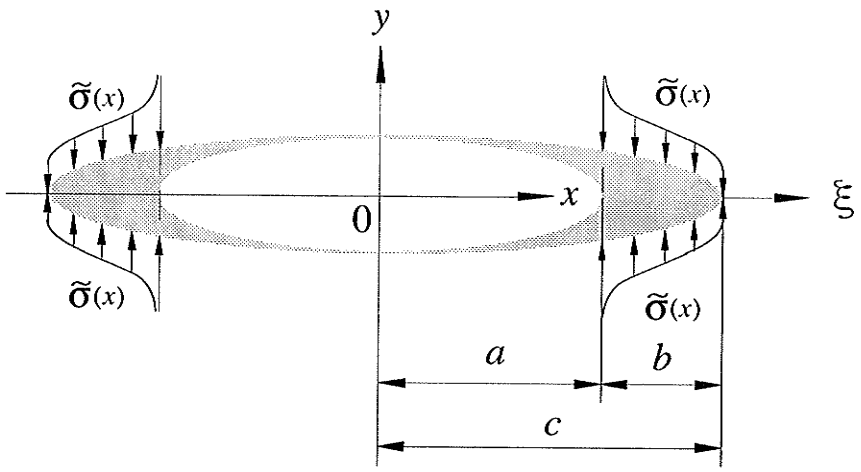



*Figure* 6.10: Dugdale model with damage

Hence, the weighting function in *Equation* (123) is given by,

$$w(x) = 1 - \left(1 - \left(\frac{x-a}{b}\right)^{\frac{2(1-n)}{2+3n}}\right) f(\tilde{\nu}) \tag{124}$$

A sketch of this weighting function is shown in *Figure* 6.11 for a prescribed $\tilde{\nu} = 0.3$ but different $n$.

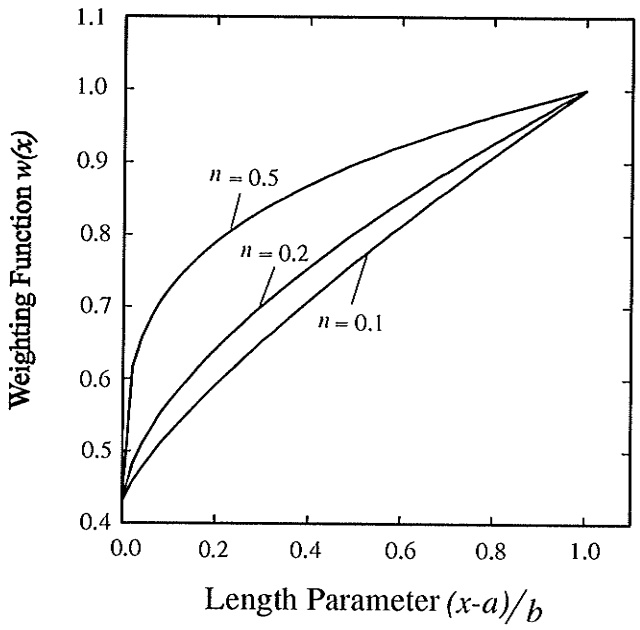



*Figure* 6.11: Weighting Functions

The stress outside the damage zone but due to loading in the damage zone $\sigma_{y_2}$ can be computed using *Equations* (100) and (124). Introducing a non-dimensional variable $\lambda$ by letting $x=a+b(1-\lambda)=c-b\lambda$, then $D$ and $w(x)$ can be expressed as,

$$D=\frac{1-n}{2+3n}\ln\frac{1}{1-\lambda} \tag{125}$$

$$w(x)=1-f(\tilde{\nu})+(1-\lambda)^{2(1-n)/2+3n}f(\tilde{\nu}) \tag{126}$$

Similarly, using the condition that the stress $\sigma(x)$ must be finite at the boundary of the damage zone, that is *Equation* (102) and substituting *Equations* (122) and (125-126) into it results,

$$\sigma_\infty - \sigma_Y \frac{2}{\pi}\sqrt{\frac{b}{2c}}\left[\int_0^1 (1-f(\tilde{\nu}))\lambda^{-1/2}\,(1-\lambda)^{-(n+1)/(2+3n)}\left(1-\frac{b}{2c}\lambda\right)^{-1/2} d\lambda\right.$$

$$\left. + \int_0^1 f(\tilde{\nu})\lambda^{-1/2}\,(1-\lambda)^{(1-3n)/(2+3n)}\left(1-\frac{b}{2c}\lambda\right)^{-1/2} d\lambda\right] = 0$$

Upon integration, we have,

$$\frac{\sigma_\infty}{\sigma_Y} - \frac{2}{\pi}\sqrt{\frac{b}{2c}}\left[(1-f(\tilde{\nu}))B\left(\frac{1}{2},\ \frac{1+2n}{2+3n}\right)F\left(\frac{1}{2},\ \frac{1}{2};\ \frac{1}{2}+\frac{1+2n}{2+3n};\ \frac{b}{2c}\right)\right.$$

$$\left. + f(\tilde{\nu})B\left(\frac{1}{2},\ \frac{3}{2+3n}\right)F\left(\frac{1}{2},\ \frac{1}{2};\ \frac{1}{2}+\frac{3}{2+3n};\ \frac{b}{2c}\right)\right] = 0$$

in which $B(p,\ q)$ and $F(\alpha,\ \beta;\ \gamma;\ z)$ are again the beta and hypergeometric functions as defined in *Equations* (105) and (106). Hence, the non-dimensionalized damage zone can be computed from,

$$\frac{c}{a} = 1 + \frac{\left(\pi\frac{\sigma_\infty}{\sigma_Y}\right)^2}{2\left[(1-f(\tilde{\nu}))H\left(\frac{1+2n}{2+3n},\ \frac{1}{2}-\frac{a}{2c}\right) + f(\tilde{\nu})H\left(\frac{3}{2+3n},\ \frac{1}{2}-\frac{a}{2c}\right)\right]^2 - \left(\pi\frac{\sigma_\infty}{\sigma_Y}\right)^2} \qquad (127)$$

where

$$H(\omega,\ \theta) = B\left(\frac{1}{2},\ \omega\right)F\left(\frac{1}{2},\ \frac{1}{2};\ \frac{1}{2}+\omega;\ \theta\right)$$

*Figure* 6.12 shows a comparison of the damage zones computed by *Equation* (127) with the FEM predictions for three strain hardening exponents, $n$ = 0.1, 0.2, 0.5 and for varying ratios of external loading $\sigma_\infty$ to yield stress $\sigma_Y$ where $\tilde{\nu} = 0.3$ is assumed. Observe that the agreement with the FEM analysis is very good. Note that in all three cases, the size of FEM results are larger than our CDM model when $\sigma_\infty = 0.8\sigma_Y$. This is because of finite domain of the FEM model which becomes more accentuated as the ratio $\sigma_\infty / \sigma_Y \rightarrow 1.0$. It would also be interesting to compare the Dugdale plastic zone in this plot. To do this, we formulate the plastic zone for strain hardening materials by extending the Dugdale model for elastic-perfectly plastic material. Instead of the constant stress distribution $\sigma_Y$ in the original Dugdale model for elastic-perfectly plastic material, the stress distribution in the plastic zone for straining hardening materials $\sigma(x)$ is assumed to be given by *Equation* (118). In fracture mechanics, the stress intensity factor (SIF) under Mode I loading can be obtained by means of a Green function [110]. Adopting this approach, the Green function for the center cracked plate is,

$$g(x,a) = 2\sqrt{\frac{a}{\pi(a^2 - x^2)}} \tag{128}$$

and the SIF is expressed by,

$$K_I(c) = \int_a^c g(x,c)\sigma(x)dx \tag{129}$$

Letting $x=a+b(1-\lambda)=c-b\lambda$, $K_I$ can be written as,

$$K_I(c) = \sqrt{\frac{2}{\pi}b}\int_0^1 \sigma(\lambda)\lambda^{-1/2}\left(1-\frac{b}{2c}\lambda\right)^{-1/2} d\lambda$$

In view of *Equation* (118), finally we have,

$$K_I(c) = \sigma_Y \sqrt{\frac{2}{\pi} b}\, H\left(\frac{2+n}{2+3n},\ \frac{b}{2c}\right)$$

Thus, the plastic zone at the front of the crack tip is given by,

$$b = \frac{\pi}{2} \frac{\left(\frac{K_I(c)}{\sigma_Y}\right)^2}{H^2\left(\frac{2+n}{2+3n},\ \frac{b}{2c}\right)} \tag{130}$$

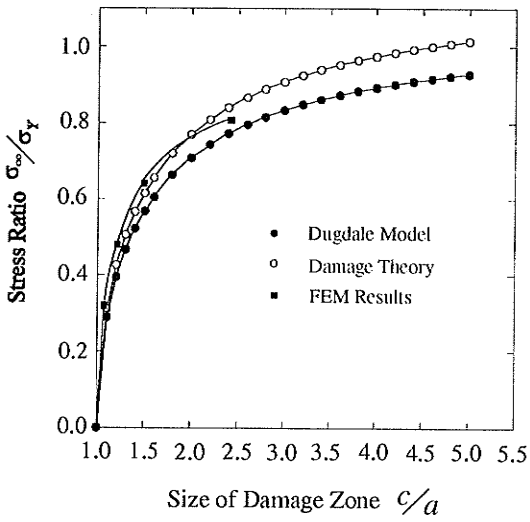
For the case of the external loading in the form of uniform tension, we have,

$$K_I(c) = \sigma_\infty \sqrt{\pi c}$$

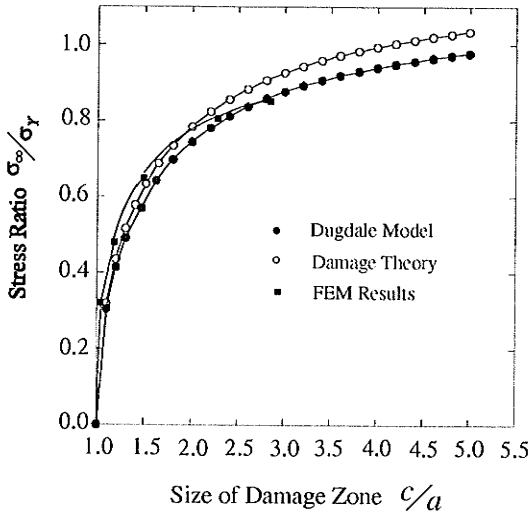
then, *Equation* (130) can be written as,

$$\frac{c}{a} = 1 + \frac{\left(\pi \frac{\sigma_\infty}{\sigma_Y}\right)^2}{2H\left(\frac{2+n}{2+3n},\ \frac{1}{2} - \frac{a}{2c}\right) - \left(\pi \frac{\sigma_\infty}{\sigma_Y}\right)^2} \tag{131}$$

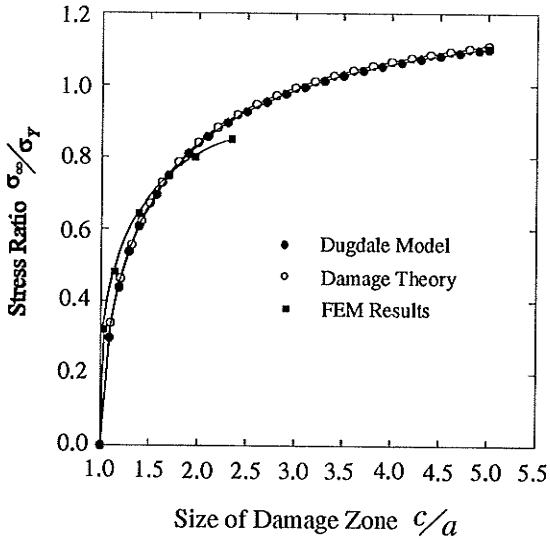
The results are plotted in *Figure* 6.12. Notice that the Dugdale plastic zone is comparatively larger than the damage zone predicted by the proposed model. However, as the strain hardening exponent $n$ is increased, the agreement between the two sizes becomes closer.




(*a*) $n$=0.1




(*b*) $n$=0.2




(*c*) $n$=0.5

*Figure* 6.12: Comparison of the Size of Damage Zones.

# CHAPTER SEVEN

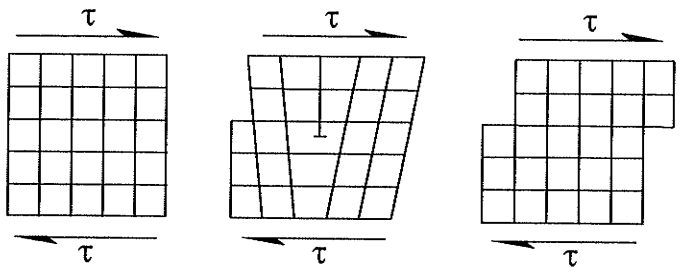
## DAMAGE PERFORMANCE IN THE VICINITY OF A MACROCRACK TIP

The influence of damage on macrocrack tip parameters is studied in this chapter. We have focus our work on the stress intensity factor only. Damage distributions and the size of the damage zone developed in the previous chapters are employed in the model developed here. The effects studied include local fracture path deflections, a reduction in the modulus of elasticity and a release of residual stresses during the microcracking process.

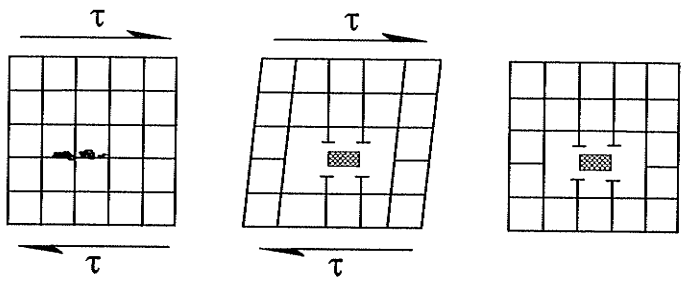
### 7.1 Solid State and Damage

At the microscale level, all materials are composed of atoms, with each atom held in place by bonds. Therefore, the deterioration of properties of a material is related to the debonding process between atoms. When a shear stress is applied, a dislocation may move gradually and may create a plastic strain without debonding as sketched in *Figure* 7.1(a). Due to the presence of the microdefects, it is possible that the dislocation may cease in these constrained zones as depicted in *Figure* 7.1(b)-(c). Also, during migration, the vacancies may aggregate to form di-vacancies or even higher vacancies [110]. Eventually, a void is created along the grain boundary [76, 111] as shown in *Figure* 7.2. Continued aggregation of vacancies causes the void to grow and coalesce to form a microcrack. In other words, damage has occurred. Microdefects usually run along grain boundaries but

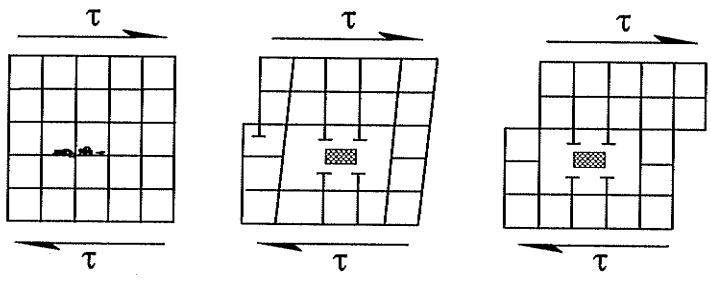
get arrested at boundary junctions. The grain boundary sliding stimulates the nucleation of grain boundary voids [113]. Note the unloading paths and the change of material behaviors corresponding to the three cases of *Figure* 7.1 are the same as presented in *Figure* 5.2.




(a) Elementary Deformation




(b) Elementary Damage




(c) Elementary Damage and Deformation

*Figure* 7.1: Elementary Deformation and Damage

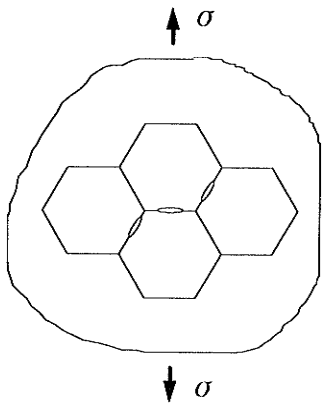



*Figure* 7.2: Voids or Microcracks along Grain Boundaries

## 7.2 Damage in the Vicinity of a Macrocrack

Damage distributions and damage zones just ahead of a macrocrack have been analyzed in previous chapters and reported in Mou and Han [61, 62]. They affect the crack propagation and the conventional fracture parameters such as the CTOD and SIF. This is because these parameters are dependent on the effective length and effective direction of the microcracks and their interactions, on the stability of the void growth, and on the coalescence process of the microcracks. Conceptually, the postulated macrocrack growth model in the classical theory implies a continuous separation of material along a plane ahead of the macrocrack. However, the experimental evidence of Anderson [49] showed that instead of continuous extensions, microcracks and voids are created and enlarged to join with the macrocrack. *Figure* 7.3 depicts the microcracks and voids distributed just ahead of a macrocrack under Mode I loading. A statistical distribution of these defects

sketched schematically in *Figure* 7.4 has been presented by Kachanov, Montagut and Laures [114].

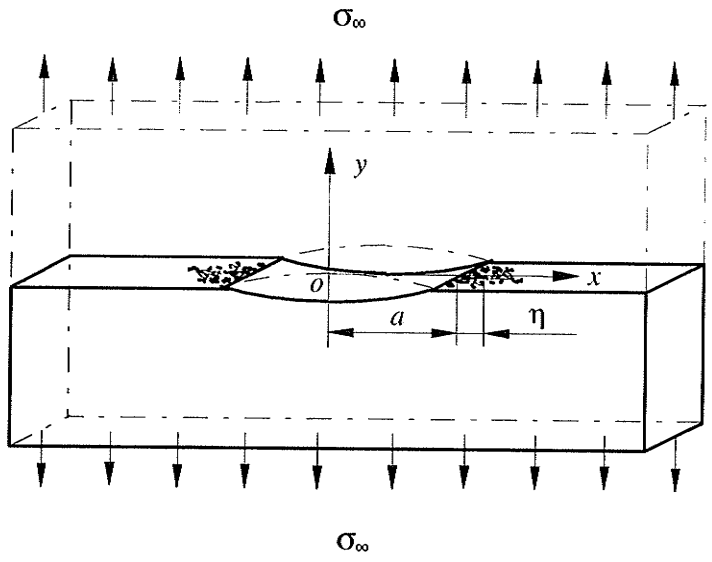



*Figure* 7.3: Microcracks and Voids in the Vicinity of a Macrocrack under Mode I Loading

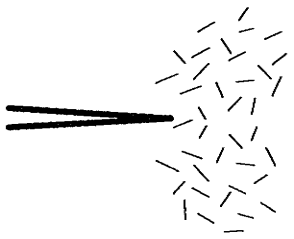


*Figure* 7.4: Statistical Distribution of Microcracks in the Vicinity of a Macrocrack

Under Mode I loading, a detailed observation around the macrocrack tip reveals that there is a small increment $\eta$ of the macrocrack length (see *Figure* 7.3) and a crack-tip opening angle (CTOA). In contrast to CTOD, this macrocrack length increment $\eta$ also called the *crack tip advance displacement* (CTAD) by Schwalbe [115], is a part of the damage zone. The second parameter, CTOA reflects the local slope of the macrocrack faces near the macrocrack tip. An experimental result showing the variation of CTAD as a function of the applied SIF for AlZnMgCu 0.5 material is depicted in *Figure* 7.5 [115]. When CTAD is considered, special attention must be exercised in the measurement of CTOD, since the clip gage values are usually converted to the point where the macrocrack tip was located, prior to the propagation of the macrocrack, i.e. at $x = a$. Therefore, CTOD has to be measured at some distance behind the tip, namely, at CTAD. Otherwise, the CTOD may vary with the development of microcracks as shown by the experimental result of Luo, Quarrington and Embury [116] in *Figure* 7.6. Also, in the process of void developments such as nucleation, growth and coalescence, voids coalesce to form microcracks in the vicinity of the tip of the macrocrack, i.e. in the damage zone. That is, the effective length and the effective direction of these microcracks are better reflected by CTAD and CTOA respectively. Thus, CTAD and CTOA used in conjunction with CTOD more accurately reflect the crack-tip behavior, but it should be mentioned that measurements of CTAD and CTOA are not trivial. At the microscale level, the macrocrack growth direction is most likely dictated by the instantaneous microstructure of the material, such as its grain size and grain boundary, the local orientation of crystallographic planes and the defects in the crystals.

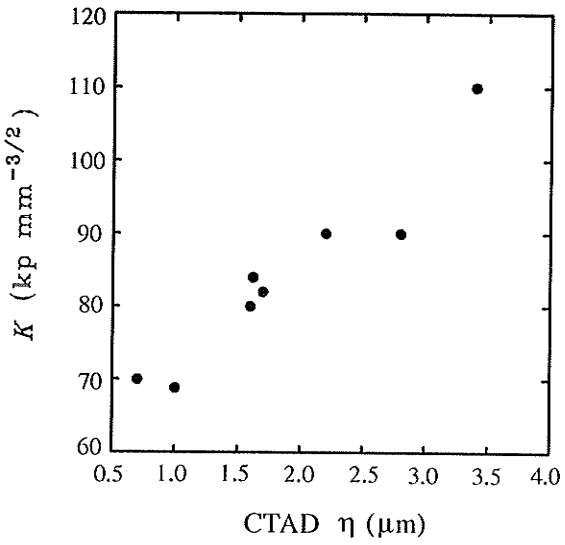



*Figure* 7.5: Crack Tip Advance Displacement and Applied SIF [115]

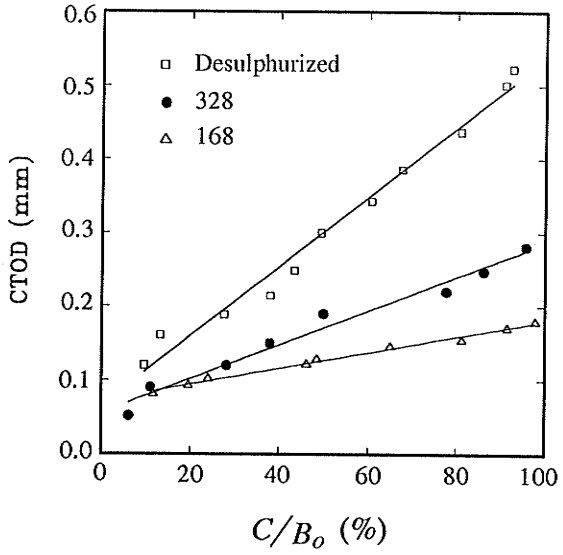



*Figure* 7.6: CTOD at Different Percentage of Microcrack Lengths [116]

($B_o$: the scanned length of macrocrack front, $C$: sum of the microcrack lengths measured in the direction of $B_o$)

## 7.3 The Effects of Fracture Path Deflections on the SIF

It is widely accepted that the direction of the crack extension can be predicted by one of the fracture mechanics parameters such as the SIF, the energy release rate or the strain energy density (S-criterion) [118]. Nuismer [119] established an energy release rate criterion for a microcrack propagating at an arbitrary angle from an existing macrocrack tip by assuming that the stress field at the macrocrack-microcrack junction is continuous. In the presence of a damage zone preceding the macrocrack, the crack extension becomes jagged as can be seen in *Figure* 7.7. For this situation, it is necessary to take into account the crack path deflections which is also consistent with the work of Rubinstein [120].



*Figure* 7.7: Local Fracture Path Deflections

To model this situation, we consider a single *effective* microcrack joined to the macrocrack, but at an unknown direction. This single effective microcrack is consistent with the concept advanced by Kachanov, Montagut and Laures [114] in their work on the

interactions of a macrocrack in a field of statistically distributed microcracks. They argued that the effects of the clusters of microcracks on the macrocrack tip can be simulated by a single *effective* collinear microcrack. We feel that it is more reasonable to assume an unknown direction for the single effective microcrack instead of the same direction as the macrocrack. Obviously, the length of this effective microcrack increases with the microcrack density inside the cluster, but still infinitesimal compared to the size of the macrocrack. It should also be mentioned that Kachanov et. al. found that the zone of "short range" interactions plays a more dominant role compared to the zone of "long range" interactions. The former is defined as the zone consisting of several microcracks closest to the main crack tip, while the latter is the zone relatively far away from the macrocrack. For a random field of microcracks, the effects of interactions may either be shielding or amplification of the SIF at the macrocrack tip. If the result is an amplification, the macrocrack will propagate until shielding is attained. Another important point to consider is that the presence of local peaks of SIFs at microcrack fronts can result in a local propagation of these fronts until they are stopped by local shielding. With these considerations, we can now examine a macrocrack with an infinitesimal path deflection at its tip. The stress field of a plane macrocrack is given by Williams [121] as,

$$\sigma_r = \frac{1}{4\sqrt{r}}\left\{a_1\left[5\cos\frac{\theta}{2}-\cos\frac{3\theta}{2}\right]+b_1\left[-5\sin\frac{\theta}{2}+3\sin\frac{3\theta}{2}\right]\right\} \\ -4a_2\cos^2\theta+o\left(\sqrt{r}\right)+\cdots \tag{132}$$

$$\sigma_\theta = \frac{1}{4\sqrt{r}}\left\{a_1\left[3\cos\frac{\theta}{2}+\cos\frac{3\theta}{2}\right]+b_1\left[-3\sin\frac{\theta}{2}-3\sin\frac{3\theta}{2}\right]\right\} \\ -4a_2\sin^2\theta+o\left(\sqrt{r}\right)+\cdots \tag{133}$$

$$\tau_{r\theta} = \frac{1}{4\sqrt{r}}\left\{a_1\left[\sin\frac{\theta}{2}+\sin\frac{3\theta}{2}\right]+b_1\left[\cos\frac{\theta}{2}+3\cos\frac{3\theta}{2}\right]\right\} \qquad (134)$$
$$+2a_2\sin^2\theta+o\left(\sqrt{r}\right)+\cdots$$

where a polar coordinate description is used as illustrated in *Figure* 7.8 and $a_1$, $a_2$, $b_1$ are constants determined by the boundary conditions.

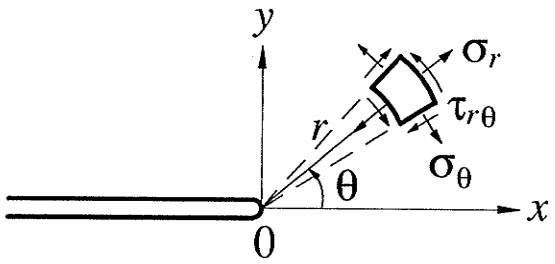



*Figure* 7.8: Stress Field of a Macrocrack

Due to the symmetry nature of $\cos\theta$ and the antisymmetry nature of $\sin\theta$, the stresses $\sigma_\theta$ and $\tau_{r\theta}$ in *Equations* (133) and (134) contain symmetrical and antisymmetrical components which correspond respectively to Mode I and Mode II cracks. Therefore, if we assume there is an infinitesimally small microcrack, then $\theta$ can be taken as the kink angle as shown in *Figure* 7.9(a). Neglecting higher order terms, *Equations* (133) and (134) can be written, for the case of a single kinked deflection, as follows,

$$\sigma_\theta = C_{11}^k\frac{K_I}{\sqrt{2\pi r}}+C_{12}^k\frac{K_{II}}{\sqrt{2\pi r}}=\frac{k_1}{\sqrt{2\pi r}} \qquad (135)$$

$$\tau_{r\theta} = C_{21}^{k}\frac{K_I}{\sqrt{2\pi r}} + C_{22}^{k}\frac{K_{II}}{\sqrt{2\pi r}} = \frac{k_2}{\sqrt{2\pi r}} \tag{136}$$

where $K_I$ and $K_{II}$ are SIFs for the macrocracks, and likewise, $k_1$, $k_2$ are SIFs for microcracks of the Mode I and Mode II respectively, as sketched in *Figure* 7.9(a). The coefficients $C_{ij}^{k}$ ($i = 1, 2; j = 1, 2$) are defined by,

$$C_{11}^{k} = \frac{1}{4}\left(3\cos\frac{\theta}{2} + \cos\frac{3\theta}{2}\right) = \cos^3\frac{\theta}{2}$$

$$C_{12}^{k} = -\frac{3}{4}\left(\sin\frac{\theta}{2} + \sin\frac{3\theta}{2}\right) = -3\sin\frac{\theta}{2}\cos^2\frac{\theta}{2}$$

$$C_{21}^{k} = \frac{1}{4}\left(\sin\frac{\theta}{2} + \sin\frac{3\theta}{2}\right) = \sin\frac{\theta}{2}\cos^2\frac{\theta}{2}$$

$$C_{22}^{k} = \frac{1}{4}\left(\cos\frac{\theta}{2} + 3\cos\frac{3\theta}{2}\right) = \cos\frac{\theta}{2}\left(1 - 3\sin^2\frac{\theta}{2}\right)$$

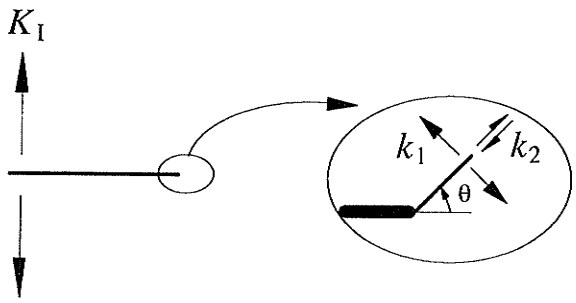
*Equations* (135) and (136) can be re-expressed as,

$$k_1 = C_{11}^{k}K_I + C_{12}^{k}K_{II}$$

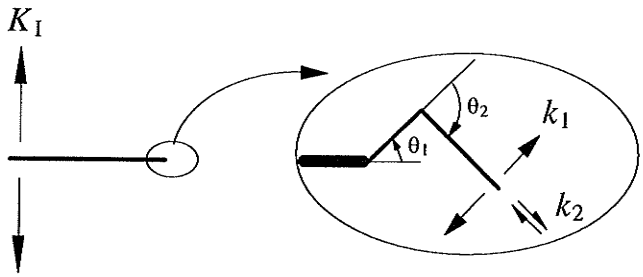
$$k_2 = C_{21}^{k}K_I + C_{22}^{k}K_{II}$$

or in matrix form,

$$\begin{Bmatrix} k_1 \\ k_2 \end{Bmatrix} = \begin{bmatrix} C_{11}^{k}(\theta) & C_{12}^{k}(\theta) \\ C_{21}^{k}(\theta) & C_{22}^{k}(\theta) \end{bmatrix} \begin{Bmatrix} K_I \\ K_{II} \end{Bmatrix} \tag{137}$$




(a) Single Kink




(b) Double Kink

*Figure* 7.9: Macrocrack with Microcrack Path Deflections

For a doubly kinked microcrack with kink angles $\theta_1$ and $\theta_2$ (see *Figure* 7.9(b)), the corresponding $k_1$ and $k_2$ are,

$$\begin{Bmatrix} k_1 \\ k_2 \end{Bmatrix} = \begin{bmatrix} C_{11}^k(\theta_1) & C_{12}^k(\theta_1) \\ C_{21}^k(\theta_1) & C_{22}^k(\theta_1) \end{bmatrix} \begin{bmatrix} C_{11}^k(\theta_2) & C_{12}^k(\theta_2) \\ C_{21}^k(\theta_2) & C_{22}^k(\theta_2) \end{bmatrix} \begin{Bmatrix} K_I \\ K_{II} \end{Bmatrix} \tag{138}$$

Thus, for a general case of a microcrack with $m$-number of infinitesimal kinked path deflections, we have,

$$\begin{Bmatrix} k_1 \\ k_2 \end{Bmatrix} = \begin{bmatrix} C_{11}^k(\theta_1) & C_{12}^k(\theta_1) \\ C_{21}^k(\theta_1) & C_{22}^k(\theta_1) \end{bmatrix} \cdots \begin{bmatrix} C_{11}^k(\theta_m) & C_{12}^k(\theta_m) \\ C_{21}^k(\theta_m) & C_{22}^k(\theta_m) \end{bmatrix} \begin{Bmatrix} K_I \\ K_{II} \end{Bmatrix} \tag{139}$$

Note that the overall size of a kinked microcrack should still be infinitesimal compared with the main crack, otherwise *Equation* (139) is invalid. For convenience, *Equations* (137) to (139) can be expressed by the following general expression,

$$\begin{Bmatrix} k_1 \\ k_2 \end{Bmatrix} = \begin{bmatrix} D_{11}^k(\theta) & D_{12}^k(\theta) \\ D_{21}^k(\theta) & D_{22}^k(\theta) \end{bmatrix} \begin{Bmatrix} K_I \\ K_{II} \end{Bmatrix} \tag{140}$$

Obviously, for the simple kinked case, $D_{ij}^k = C_{ij}^k$, $(i, j = 1, 2)$. The energy release rate argument can be used to combine $k_1$ and $k_2$ into an effective or a *deflected* SIF $K_D$. The result as given by Sih and Liebowitz [121] is,

$$K_D^2 = k_1^2 + k_2^2 \tag{141}$$

According to *Equations* (137) to (141), $K_D$ can be written in the following form under Mode I loading,

$$K_D = f(\theta) K_I \tag{142}$$

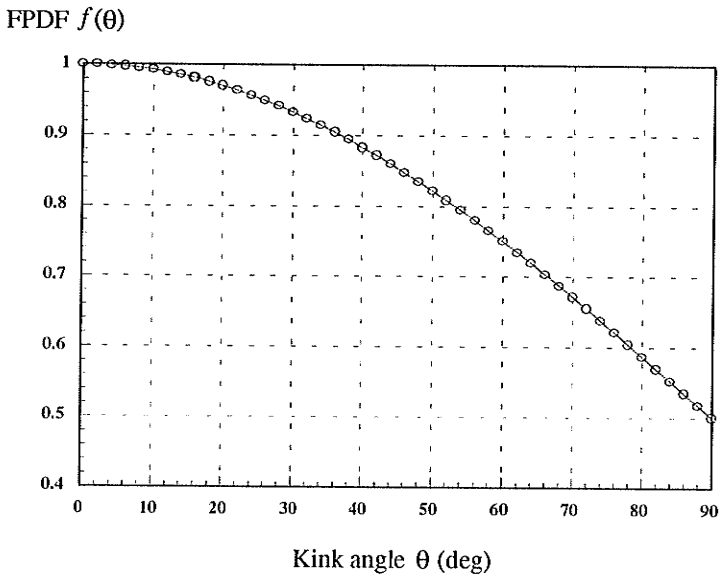
where we have termed $f(\theta)$ as the *fracture path deflection factor* (FPDF). For a pure Mode I case $(K_{II} = 0)$, the expression of $f(\theta)$ can be easily obtained as,

$$f(\theta) = \sqrt{\left(D_{11}^{k}\right)^2 + \left(D_{21}^{k}\right)^2}$$

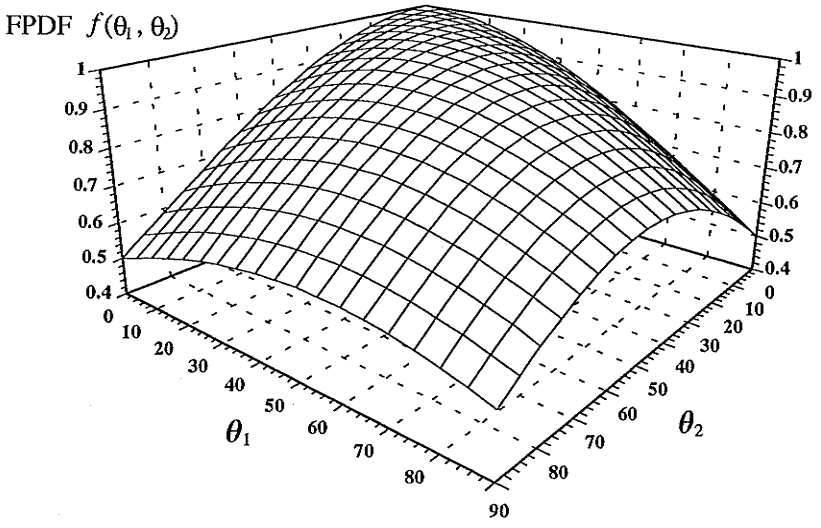
*Figure* 7.10 shows the variation of FPDF as a function of the deflection angles for single and double kink cases. For either situations, it can be seen that $f(\theta) \leq 1.0$ which implies that the infinitesimal fracture path deflection produces a shielding effect on the propagation of a macrocrack. This explains why path deflections (or CTOA) occur in stable crack propagations. For the single kinked case, the shielding effect increases with an increasing deflection angle, whereas for the double kinked case, the second deflection angle may amplify or shield the SIF computed from at the first deflection angle. However, the overall effect is still a shielding.

## 7.4 The Effect of Reduction in Moduli and Release of Residual Stress on the SIF

As mentioned, the damage near the tip of a macrocrack can cause a reduction in the modulus of elasticity of the material and thereby affects the SIF of the crack. Steif [68] studied this influence for a semi-infinite crack penetrating a circular inclusion. Budiansky, Hutchinson and Lambropoulos [66] and Hutchinson [67] considered the change of SIF resulting from strain changes due to the release of residual stresses when microcracks are formed in the near tip area of the macrocrack. However, in their model, effects such as damage distribution and damage size in the vicinity of the macrocrack tip were not considered. In Mou and Han [61, 62], a continuum damage mechanics-based model for the prediction of damage distribution and damage zone was proposed. This model will now be employed to investigate the effects of the damage on the SIF.




(a) Single Kink




(b) Double Kink

*Figure* 7.10: Influence of Fracture Path Deflections on the SIF

Assuming the damage near the macrocrack tip is isotropic, the damage distribution along the macrocrack for Mode I loading can be estimated from [46],

$$D = \frac{1-n}{2+3n} \ln\left(\frac{b}{x-a}\right)$$

where $n$ is the strain hardening exponent, $a$ is the half length of the macrocrack, $b$ is the size of the damage zone in the $x$-direction. In accordance to the incremental complementary energy equivalence proposed by Luo, Mou and Han [41], the reduced Young's modulus $\tilde{E}_D$ is given by,

$$\frac{E_o}{\tilde{E}_D} = \left(\frac{b}{x-a}\right)^{\frac{2(1-n)}{2+3n}}$$

Assuming this relationship is also valid in the entire area of the damage zone (see *Figure* 7.11), we have,

$$\frac{E_o}{\tilde{E}_D} = \left(\frac{R(\theta)}{r(\theta)}\right)^{\frac{2(1-n)}{2+3n}}$$

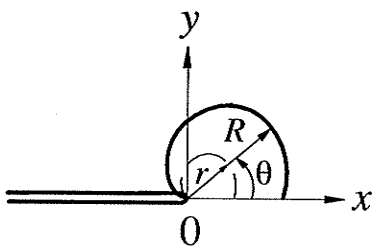



*Figure* 7.11: Damage Zone

Introducing a modulus reduction factor (MRF) $f(\tilde{E}_D)$ for the SIF as follows,

$$K_M = f(\tilde{E}_D)K_I \tag{143}$$

and noting that $K_M$ is the modified SIF due to a change of the modulus of elasticity, then $f(\tilde{E}_D)$ can be expressed as [67],

$$f(\tilde{E}_D) = 1 + (s_1 - \tfrac{5}{8})\delta_1 + (s_2 + \tfrac{3}{4})\delta_2 \tag{144}$$

where

$$s_1 = \frac{1}{32\pi}\int_0^{\pi}(11\cos\theta + 8\cos 2\theta - 3\cos 3\theta)\ln[R(\theta)]d\theta$$

$$s_2 = -\frac{1}{2\pi}\int_0^{\pi}(\cos\theta + \cos 2\theta)\ln[R(\theta)]d\theta$$

$$\delta_1 = \frac{1}{1-\nu}\left(\frac{G_o}{\tilde{G}_D} - 1\right)$$

$$\delta_2 = \frac{1}{1-\nu}\left(\tilde{\nu}\frac{G_o}{\tilde{G}_D} - \tilde{\nu}\right)$$

Note that $G_o, \nu_o$ and $\tilde{G}_D, \tilde{\nu}$ are the original and effective shear moduli, and Poisson's ratio respectively. Invoking the following relations,

$$G_o = \frac{E_o}{2(1+\nu)}, \qquad \tilde{G}_D = \frac{\tilde{E}_D}{2(1+\tilde{\nu})}$$

we have,

$$\frac{G_o}{\tilde{G}_D} = \frac{(1+\tilde{\nu})E_o}{(1+\nu)\tilde{E}_D}$$

Since $\tilde{E}_D$ is dependent on $r(\theta)$, the effective shear modulus $\tilde{G}_D$ and the effective Poisson's ratio $\tilde{\nu}$ (or alternatively, the parameters $\delta_1$, $\delta_2$) will also vary with $r(\theta)$. Introducing the averaging parameters $\overline{\delta}_1$ and $\overline{\delta}_2$ of the damage zone for the MRF as described by *Equation* (144), we have,

$$\overline{\delta}_1 = \frac{\iint_A \delta_1 dA}{\iint_A dA}, \qquad \overline{\delta}_2 = \frac{\iint_A \delta_2 dA}{\iint_A dA} \tag{145}$$

in which $A$ is the area of the damage zone. Strictly speaking, the stress field based on the HRR fields for a damaged material [36] should be used in establishing the shape of the damage zone. But if we assume the material to be undergoing elastic damage as depicted in *Figure* 5.2(a), then an approximation to the shape of the damage zone can be obtained via the elastic fields. The result is,

$$R(\theta) = \frac{c-a}{2}\left(1+\cos\theta+\tfrac{3}{2}\sin^2\theta\right) \tag{146}$$

where the size of the damage zone at $\theta$=0 is given by $R(0) = c - a$, and $c$ is determined from [62] as,

$$\frac{c}{a}=1+\frac{\left(\pi\frac{\sigma_\infty}{\sigma_Y}\right)^2}{2\left[(1-f(\tilde{\nu}))H\left(\frac{1+2n}{2+3n},\ \frac{1}{2}-\frac{a}{2c}\right)+f(\tilde{\nu})H\left(\frac{3}{2+3n},\ \frac{1}{2}-\frac{a}{2c}\right)\right]^2-\left(\pi\frac{\sigma_\infty}{\sigma_Y}\right)^2}$$

in which

$$f(\tilde{\nu})=\frac{45}{16(1+\tilde{\nu})(5-4\tilde{\nu})}$$

$$H(\omega,\ \theta)=B\left(\frac{1}{2},\ \omega\right)F\left(\frac{1}{2},\ \frac{1}{2};\ \frac{1}{2}+\omega;\ \theta\right)$$

Note that the functions $B(p,\ q)$, $F(\alpha,\ \beta;\ \gamma;\ z)$ are the beta and hypergeometric functions which are defined as follows,

$$B(p,\ q)=\frac{1}{q}\sum_{k=0}^{\infty}(-1)^k\frac{q(q-1)\cdots(q-k)}{k!(p+k)}$$

$$F(\alpha,\ \beta;\ \gamma;\ z)=\frac{\Gamma(\gamma)}{\Gamma(\alpha)\Gamma(\beta)}\sum_{n=0}^{\infty}\frac{\Gamma(\alpha+n)\Gamma(\beta+n)}{\Gamma(\gamma+n)}\frac{z^n}{n!}$$

*Figure* 7.12 shows the result of the modified SIF for $\tilde{\nu}=\nu_o=0.3$, taking into consideration the influence of a reduction in the modulus of elasticity. Observe that the result is always shielding. Also, the influence of a reduction in the modulus of elasticity parameter $E_0/\left(\tilde{E}_D\right)_{av}$ on the SIF is a linear variation whereas, with respect to the strain hardening exponent $n$, the variation is nonlinear. Note that the former curve agrees very closely with the first-order solution in Fig. 9 (isotropic damage) of Chow and Lu [73].

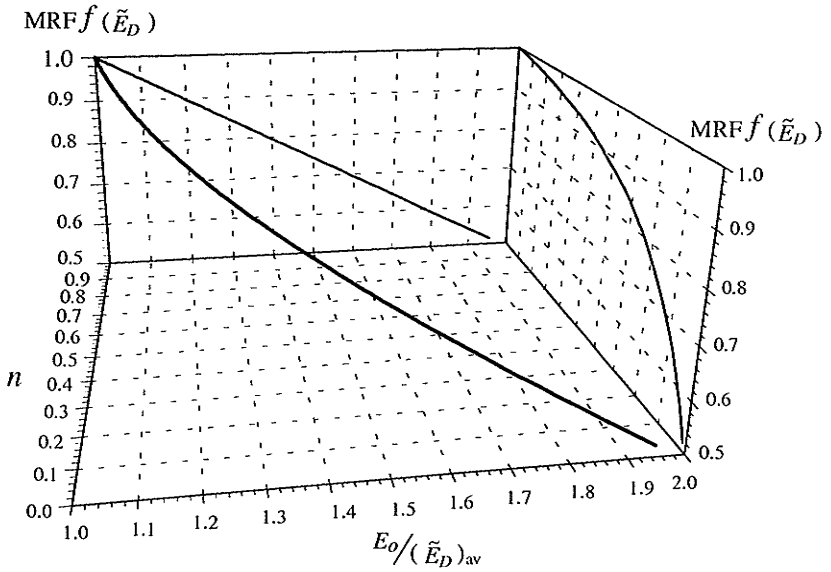



*Figure* 7.12: Influence of a Reduction in the Modulus on the SIF

## 7.5 The Effects of a Release of Residual Stresses on the SIF

In the process of microcracking, residual stresses are released. These residual stresses are originally developed during the formation of polycrystalline or multi-phase materials due to thermal mismatches between phases or thermal anisotropies of single crystals. Suppose that the microcracks are nucleated without any preferred orientations, then the release of the residual stresses can cause dilatational transformation. Thus, the strain within the region $r \leq R(\theta)$ is governed by,

$$\varepsilon_{ij} = \frac{1+\nu}{E_o}\sigma_{ij} - \frac{\nu}{E_o}\sigma_{kk}\delta_{ij} + \frac{1}{3}\omega\delta_{ij}$$

where $\delta_{ij}$ is the Kronecker delta and $\omega$ is the dilatational transformation strain. The induced SIF change is given by [66],

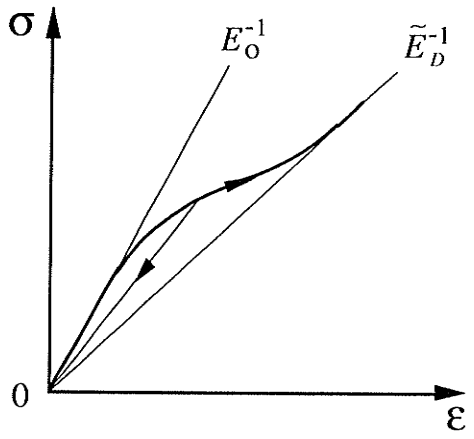
$$\Delta K = \frac{E}{3(1-\nu)\sqrt{2\pi}} \iint_A \omega[r(\theta)]^{-3/2} \cos\tfrac{3}{2}\theta dA \tag{147}$$

In general $\omega(r,\theta)$ is unknown apriori, but if we consider the critical condition when part of the damage zone has attained a fully uniform transformational dilatation with $\omega = \omega^T$, then *Equation* (147) becomes,

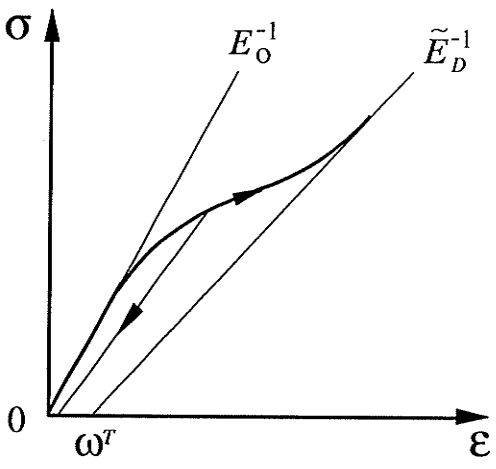
$$\Delta K = \frac{E\omega^T}{3(1-\nu)} \sqrt{\frac{2}{\pi}} \int_0^{\pi} \sqrt{r(\theta)} \cos\tfrac{3}{2}\theta d\theta \tag{148}$$

where $\omega^T$ is the value at a saturated state when microcracking ceases as depicted in *Figure* 7.13. Note that $r(\theta)$ in *Equation* (148) is valid only for the region where a fully transformational dilatation has occurred. Under this condition, the parameters $\delta_1$ and $\delta_2$ can be taken to have the same values as the averaged quantities $\bar{\delta}_1$ and $\bar{\delta}_2$ given by *Equation* (145). Thus, $r(\theta)$ can be evaluated from,

$$\frac{\iint_A \delta_1 dA}{\iint_A dA} - \frac{1}{1-\nu}\left[\frac{1+\bar{\nu}}{1+\nu}\left(\frac{R(\theta)}{r(\theta)}\right)^{\frac{2(1-n)}{2+3n}} - 1\right] = 0 \tag{149}$$




(a) without transformation strain




(b) with transformation strain $\omega^T$

*Figure* 7.13: Characteristic Tensile Stress-Strain Curves with a Saturation Stage

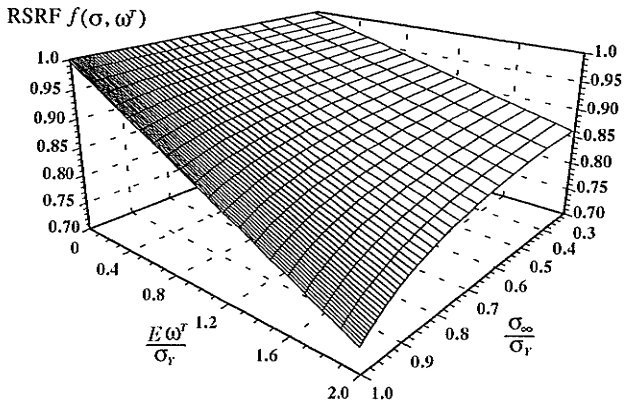
Similar to the MRF, we can introduce a residual stress release factor (RSRF) $f(\sigma,\omega^T)$ such that it modifies the original SIF as follows:

$$K_R = f(\sigma,\omega^T)K_I$$

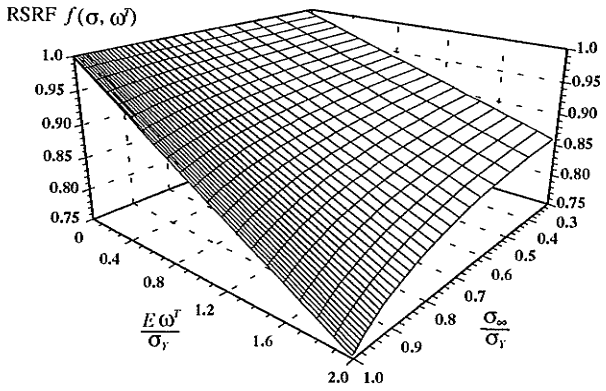
in which $K_R$ is the modified SIF due to a release of residual stresses. Comparing *Equations* (148), the RSRF can be computed from,

$$f(\alpha,\beta) = 1 + \frac{\alpha}{3\beta\pi(1-\nu)}\sqrt{\frac{2}{a}}\int_0^{\pi}\sqrt{r(\theta)}\cos\tfrac{3}{2}\theta d\theta \qquad (150)$$

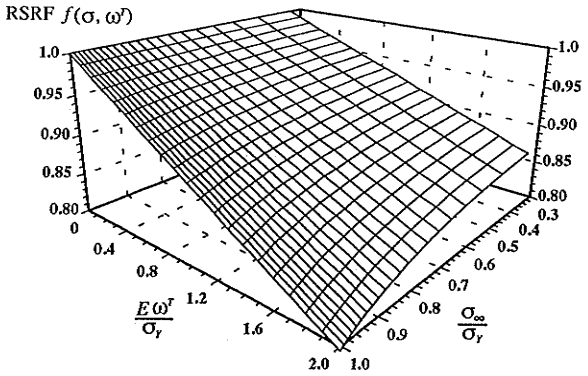
where $\alpha = E\omega^T/\sigma_Y$, $\beta = \sigma_\infty/\sigma_Y$ and, $r(\theta)$ can be determined from *Equation* (149). The results of RSRF as a function of the ratios $\alpha$ and $\beta$ are plotted in *Figure* 7.14 for the values of $n$ = 0.1, 0.2, 0.5, 0.7. Note that $\tilde{\nu} = \nu_o = 0.3$ is assumed in these plots. Clearly, $f(\alpha,\beta) \le 1$ in these graphs and once again, this implies that a shielding effect on the original SIF is produced by the transformational dilatation arising from a release of residual stresses. Observe from *Figures* 7.14 and 7.12 that for the selected range of loading $\sigma_\infty < 0.8\sigma_Y$ and $E\omega^T/\sigma_Y < 2$, the shielding effects are smaller for the case of a release of the residual stresses than a reduction in the modulus of elasticity.



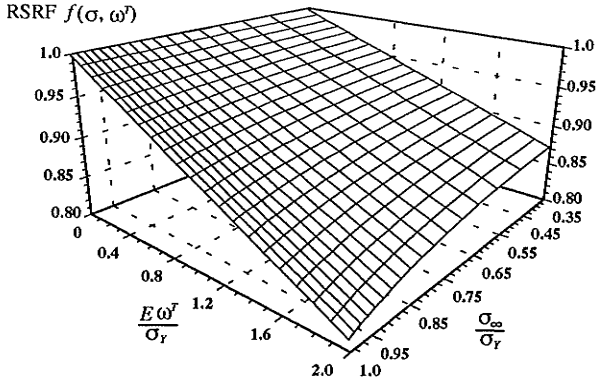

(a) $n = 0.1$




(b) $n = 0.2$




(c) $n = 0.5$




(d) $n = 0.7$

*Figure* 7.14: Influence of a Release of Residual Stresses on SIF

## 7.6 Toughening of Damaged Materials

In the proceeding sections, the shielding effects have been analyzed. In general, these effects can be represented by,

$$K_{\text{tip}} = K + \Delta K \tag{151}$$

where $K_{\text{tip}}$ denotes the stress intensity factor right at the macrocrack tip, $K$ is the applied stress intensity factor and $\Delta K$ represents the reduction of the stress intensity of the macrocrack in the original matrix material. To assess the toughening effect, it is natural to assume that the macrocrack starts to grow at,

$$K_{\text{tip}} = K_{\text{tip}}^{c} \tag{152}$$

where $K_{\text{tip}}^{c}$ is the critical fracture toughness of the macrocrack without considering damage. From *Equations* (151) and (152), we have,

$$\frac{K}{K_{\text{tip}}^{c}} = \frac{1}{1+\frac{\Delta K}{K}} \tag{153}$$

Note that the applied stress intensity factor $K$ represents the apparent fracture toughness measured from the standard fracture toughness test and attains the critical value $K_{\text{m}}$ when the macrocrack starts to grow. Correspondingly, $\Delta K$ becomes $\Delta K_{c}$. Therefore, *Equation* (153) can be rewritten as,

$$\frac{K_m}{K_{\text{tip}}^c} = \frac{1}{1+\frac{\Delta K_c}{K_m}} \tag{154}$$

It is obvious from *Equation* (154) that the crack tip shielding $(\Delta K_c < 0)$ would lead directly to the effect of microcrack toughening. However, it should be pointed out that *Equation* (154) is not sufficient to predict the toughening increment due to the damage in the vicinity of a macrocrack. This is because the microcracks adjacent to the macrocrack tip will cause a deterioration of the intrinsic resistance to fracture of the material, an effect which may partially or totally offset the toughness increment derived from the shielding which is also pointed out by Ortiz and co-workers [70, 71]. Therefore, one also needs to know the inherent toughness of the microcracked material compared to a similar material which does not undergo this same kind of stress induced microcracking or damage. One way or another, the toughness of a material with damage in the vicinity of a macrocrack must be determined or inferred from experiments.

# CHAPTER EIGHT

## SUMMARY, CONCLUSIONS AND FUTURE WORK

All the work described in Chapters 3-7 are now summarized, with the relevant conclusions are highlighted. This chapter then ends by presenting a section on suggested future work.

### 8.1 Summary

In this thesis, the hypothesis of incremental complementary energy equivalence is proposed to derive the constitutive equations under the damage state. Based on the proposed hypothesis, a large damage theory is formulated and an anisotropic damage model developed. Comparisons are made with the model developed by the total complementary energy equivalence via three applications: uniaxial tension, pure torsion and elastic-perfectly plastic behaved damage materials. Applying the new hypothesis to the isotropic damage case, a damage evolution model for ductile materials is obtained on the basis of the irreversible thermodynamics theory. The influence of the stress triaxiality and the strain hardening exponent on the evolution process are analyzed. Good agreements are found when the predictions are compared with experimental results.

Damage distributions and the size of damage zones in the vicinity of a macrocrack tip under Mode I loading are analyzed on the basis of the equations developed from the large damage theory but specialized for isotropic damage. The Dugdale's model for plastic zone is used here. The analytical results are compared with those from a finite element analysis. The results are also compared with the size of the plastic zones computed by extending Dugdale's model for elastic-perfectly plastic material to strain hardening materials. Having formulated the model for damage distribution and damage size analyses, the model is used to study the influence of damage on the stress intensity factor for Mode I loading. The effects considered include local fracture path deflections, a reduction in the modulus of elasticity and a release of residual stresses in the vicinity of a macrocrack tip. Shielding is produced in all these situations.

## 8.2 Conclusions

Some important conclusions can be obtained as a result of this doctoral research. They are now stated as follows:

1. A large damage theory developed via the new hypothesis of incremental complementary elastic energy equivalence is proposed in this thesis. This new hypothesis has the distinct advantage of being able to reflect damage by modeling the deterioration process incrementally. When the damage is small, namely, $D_i << 1$, this new theory reduces to the small damage model of Chow and Wang [34]. But as the damage gets larger, the theory of Chow and Wang becomes increasingly approximate. For example, the damage variables $D_1$ and $D_2$ predicted by these two theories for the case of uniaxial tension differ by at least 8.4% for

damage characterized by $\tilde{E}/E \leq 0.7$. Similarly, when the two theories are applied to analyze the experimentally obtained uniaxial tension results, the damage variable $D_1$ computed by the large damage model differs from that of the small damage model by at least 4% for $\varepsilon \geq 15\%$. In another example, the large damage theory is applied to model the cases of pure torsion and elastic perfectly-plastic material behavior. For the latter, the predictions of the two theories differ by 9.5% at $\varepsilon = 0.15$. Since the small damage model can be easily recovered from the proposed large damage theory, it can be concluded that this large damage theory is more general than the small damage theory.

2. It is assumed that in the large damage model the principal direction of the damage tensor is known apriori. This may pose a restriction if a general boundary-value problem is analyzed.
3. A ductile fracture in metals is the end result of a sequence of void nucleation, void growth and void coalescence. In CDM, this process can be interpreted as a sequence of damage generation, damage growth and damage instability. A continuum damage evolution model for ductile material is formulated based on the irreversible thermodynamics theory. According to this model, damage is dependent on the accumulated strain, stress triaxiality and strain hardening exponent of the material. Comparison with experiment results show that the model can predict the damage evolution very accurately. It is shown that the damage evolution of ductile materials is strongly affected by the stress triaxiality.
4. The hypothesis of incremental complementary energy equivalence for damage evaluation is also employed to formulate the equations for damage zone analysis in a material based on the Dugdale model. Damage distributions in the region of a macrocrack tip are calculated for an elastic perfectly-plastic response triggered by

damage. In deriving the size of the damage zone, the presence of voids is taken into account and this is carried out statistically via a weighting function. A finite element program is also developed for the purpose of comparison. Good agreement with the theoretical predictions is observed.

5. The study of the damage distribution and the size of the damage zone is extended to include strain hardening materials under elastic damage. As expected, the size of the damage zone becomes larger with a decrease of the strain hardening exponent and an increase of external loading. The size is also compared with the Dugdale plastic zone, which is obtained by extending Dugdale model for elastic-perfectly plastic materials to strain hardening materials. It is found that the Dugdale plastic zone is comparatively larger than the damage zone predicted by the model. However, as the strain hardening exponent $n$ is increased, the agreement between the sizes becomes closer.
6. Using the model developed for damage distribution and damage size, the damage performance in the vicinity of a macrocrack tip and its influence on the stress intensity factor are examined. This influence includes local fracture path deflections, a reduction in the modulus of elasticity resulted from damage in materials and a release of residual stresses during the microcracking process. It is found that all these factors produce a shielding effect on the stress intensity factor under Mode I loading. The influence of local fracture path deflections is found to be quite dependent on the deflection angles. For the single kinked case, the shielding effect increases with an increasing deflection angle, whereas for the double kinked case, the second deflection angle may amplify or shield the stress intensity factor computed from at the first deflection angle. However, the overall effect is still shielding. Finally, the shielding effect caused by a reduction in the

modulus of elasticity, decreases with an increase of the strain hardening exponent of materials. The influence of a release of residual stresses on SIF is dependent on the external loading and the material itself. Its shielding effect is also decreased when the strain hardening exponent of a material is increased. It has a relatively small effect on the stress intensity factor compared with the effect of a reduction in the modulus.

## 8.3 Recommendations for Future work

The following two recommendations are suggested for future work.

(1) Microcrack and void closure effect

Under the compressive stress state, damage of materials may be deactivated. For example, under a cyclically tensile and compressive loading condition, the developed damage in the tensile cycle may be rendered inactive during the compressive cycle, although damage still exists in the material. For this situation, it is necessary to develop a damage evolution model that is able to initiate damage deactivation

.

(2) Damage in anisotropic materials

This is a more general damage model in that not only the anisotropic damage is considered but also the anisotropic properties in material itself is taken into account. For example, damage in fiber reinforced materials.

# BIBLIOGRAPHY


[1] S. Murakami, "Progress of Continuum Damage Mechanics", *JSME International Journal*, **30**, 701-710, 1987.

[2] J. Lemaitre, *A Course on Damage Mechanics*, Springer-Verlag, 1992.

[3] L.M. Kachanov, "On Creep Rupture Time", *Izv. Acad. Nauk SSSR, Otd. Techn. Nauk* **8**, 26-31, 1958.

[4] F. Ghrib and R. Tinawi, "An Application of Damage Mechanics for Seismic Analysis of Concrete Gravity Dams", *Earthquake Engineering and Structural Dynamics*, **24**, 157-173, 1995.

[5] J.S. Jubran and W.F. Cofer, "Ultimate Strength Analysis of Structural Components Using the Continuum Damage Mechanics Approach", *Computer & Structures*, **39**, 741-752, 1991.

[6] C.L. Chow and J. Wang, "An Anisotropic Theory of Continuum Damage Mechanics for Ductile Fracture", *Engineering Fracture Mechanics*, **27**, 547-558, 1987.

[7] C.L. Chow and T.J. Lu, "A Damage Mechanics Approach to Ductile Failure in Notched Plates", *Recent Advances in Damage Mechanics and Plasticity*, AMD-Vol. 132, MD-Vol. 30, edited by J.W. Ju, 21-35, 1992.

[8] C.L. Chow and J. Wang, "On Crack Initiation Angle of Mixed Mode Ductile Fracture with Continuum Damage Mechanics", *Engineering Fracture Mechanics*, **32**, 601-612, 1989.

[9] C.L. Chow and T.J. Lu, "A Comparative Study of Continuum Damage Models for Crack Propagation under Gross Yielding", *International Journal of Fracture*, **53**, 43-75, 1992.

[10] J. Lemaitre and J. Chaboche, "A Non-Linear Model of Creep-Fatigue Damage Cumulation and Interaction", in *Mechanics of Visco-Elastic Media and Bodies*, edited by J. Hult, Springer-Verlag, Berlin, 1975, 291-300.

[11] S. Murakami and N. Ohno, "A Continuum theory of Creep and Creep Damage", *Proc. 3rd IUTAM Symp. on Creep in Structures*, edited by A.R.S. Ponter and D.R. Hayhurst, 442-444, Springer, Berlin, 1981.

[12] L.M. Kachanov, "Crack Growth under Conditions of Creep and Damage", in *Creep in Structures*, edited by A. Ponter and D. Hayhurst, Springer-Verlag, Berlin, 520-524, 1981.

[13] J. Lemaitre, "A Continuum Damage Mechanics Model for Ductile Fracture", *Journal of Engineering Materials and Technology*, **107**, 83-89, 1985.

[14] G. Le Roy, J.D. Embury, G. Edward and M.F. Ashby, "A Model of Ductile Fracture Based on the Nucleation and Growth of Voids", *Acta Metallurgica*, **40**, 1509-1522, 1981.

[15] M. Zheng, Z.J. Luo and X. Zheng, "A New Damage Model for Ductile Materials", *Engineering Fracture Mechanics*, **41**, 103-110,1992.

[16] R.P.S. Han and Y. Mou, "Void Induced Damage in Ductile Materials", *CANCAM'93*, Kingsdon, Canada, 1993.

[17] D. Krajcinovic and J. Lemaitre, *Continuum Damage Mechanics*, Springer New York, 1987.

[18] J.L Chaboche, "Continuum Damage Mechanics: Part I–General Concepts, Part II–Damage Growth, Crack Initiation, and Crack Growth", ASME *Journal of Applied Mechanics*, **55**, 59-72, 1988.

[19] T. Wang and Z. Lou, "A Continuum Damage Model for Weld Heat Affected Zone under Low Cycle Fatigue Loading", *Engineering Fracture Mechanics*, **37**, 825-829, 1990.

[20] J. Wang, "A Continuum Damage Mechanics Model for Low-Cycle Fatigue Failure of Metals", *Engineering Fracture Mechanics*, **41**, 437-441, 1992.

[21] J. Lubliner, J. Oliver, S. Oller and E. Onate, "A Plastic Damage Model for Concrete', *International Journal of Solids and Structures*, **25**, 299-326, 1989.

[22] C. Saouridis and G. Samake, "Caractéristion de l'endommagement et de la fissuration de plaques composites en béton armé", *Mémoire de DEA, Laboratorie de Mécanique et Technologie*, Cachan, France, 1985.

[23] Lee M. Taylor, E.P. Chen and Joel S. Kuszmaul, "Microcrack-Induced Damage Accumulation in Brittle Rock Under Dynamic Loading", *Computer Methods in Applied Mechanics and Engineering*, **55**, 301-320, 1986.

[24] B.M. Butcher, L.M. Barker, D.E. Munson and C.D. Lundergan, "Influence of Stress History on Time-Dependent Spall in Metals", *AIAA Journal*, **2**, 977-990, 1964.

[25] L., Seaman, R.C. Donald and A.S. Donald, "Computational Models for Ductile and Brittle Fracture", *Journal of Applied Physics*, **47**, 4814-4826, 1976.

[26] P. Perzyna, "Constitutive Modeling of Dissipative Solids for Postcritical Behavior and Fracture", ASME *Journal of Engineering Materials Technology*, **106**, 410-419, 1984.

[27] J.H. Schmitt and J.M. Jalinier, "Damage in Sheet Metal Forming — I, Physical Behavior", *Acta Metallurgica*, **30**, 1789-1798, 1982.

[28] J.M. Jalinier and J.H. Schmitt, "Damage in Sheet Metal Forming — II, Plastic Instability", *Acta Metallurgica*, **30**, 1799-1809, 1982.

[29] J.F. Knott, *Fundamentals of Fracture Mechanics*, Butterworths, 1973.

[30] P. Lukas and M. Klesnil, "Fatigue Damage and Resultant Dislocation Substructures", *Corrosion Fatigue: Chemistry, Mechanics and Microstructure,* edited by O. Devereux, A.J. McEvily and R.W. Staehle, NACE-2, 118-132, 1973.

[31] W. Schoch and H. Spahn, "On the Role of Stress Induced Corrosion and Corrosion Fatigue in the Formation of Cracks in Water Wetted Boiler Components", *Corrosion Fatigue: Chemistry, Mechanics and Microstructure,* edited by O. Devereux, A.J. McEvily and R.W. Staehle, NACE-2, 52-64, 1973.

[32] J.P. Cordebois and F. Sidoroff, "Damage Induced Elastic Anisotropy", *Mechanical Behavior of Anisotropic Solids, Proceedings of the Euromech Colloquium* 115, edited by J.P Boehler, 761-774, Martinus Nijhoff Publishers, 1979.

[33] F. Sidoroff, "Description of Anisotropic Damage Application to Elasticity", in IUTAM Colloquium, Physical Nonlinearities in Structural Analysis, 237-244, 1980.

[34] C.L. Chow and J. Wang, "An Anisotropic Theory of Elasticity for Continuum Damage Mechanics", *International Journal of Fracture*, **33**, 3-16, 1987.

[35] H. Lee, K. Peng and J. Wang, "An Anisotropic Damage Criterion for Deformation Instability and its Application to Forming Limit Analysis of Metal Plates", *Engineering Fracture Mechanics*, **21**, 1031-1054, 1985.

[36] J. Wang and C.L. Chow, "HRR Fields for Damaged Materials", *International Journal of Fracture*, **54**, 165-183, 1992.

[37] Y. Toi and J. Che, "Computational Damage Mechanics Models for Brittle Microcracking Solids Based on Mesoscopic Simulations", *Engineering Fracture Mechanics*, **48**, 483-498, 1994.

[38] Y. Toi and T. Kiyosue, "Damage Mechanics Models for Brittle Microcracking Solids Based on Three-Dimensional Mesoscopic Simulations", *Engineering Fracture Mechanics*, **50**, 11-27, 1995.

[39] B.M. Luccioni, S. Oller and R. Danesi, "Plastic Damaged model for Anisotropic Materials", *Applied Mechanics in the Americas*, **I**, 124-129, edited by L.A. Godoy, S.R. Idelsohn, P.A.A. Laura and D.T. Mook, *AAM and AMCA*, Santa Fe, Argentina, 1995.

[40] H. Broberg, "Damage Measures in Creep Deformation and Rupture", *Swedish Solid Mechanics Reports* **8**, 100-104, 1974.

[41] A. Luo, Y. Mou and R.P.S. Han, "A Large Anisotropic Damage Theory Based on an Incremental Complementary Energy Equivalence Model", *International Journal of Fracture*, in press, 1994.

[42] W.H. Tai and B.X. Yang, "A New Microvoid-Damage Model for Ductile Fracture", *Engineering Fracture Mechanics*, **25**, 337-384, 1986.

[43] G. Rousselier, "On 3-d Constitutive Equation and Ductile Rupture", *IUTAM Symposium*, Dourdam, 331-355, 1980.

[44] R.D. Thomson and J.W. Hancock, "Ductile Failure by Void Nucleation, Growth and Coalescence", *International Journal of Fracture*, **26**, 99-112, 1984.

[45] D.Z. Sun, D. Siegele, B. Voss and W. Schmitt, "Application of Local Damage Models to the numerical Analysis of Ductile Rupture", *Fatigue & Fracture in Engineering Materials & Structures*, **12**, 201-212, 1989.

[46] Y. Mou and R.P.S. Han, "Damage Evolution in Ductile Materials", *International Journal of Damage Mechanics*, in press, 1995.

[47] D.R. Hayhurst, P.R. Dimmer and C.J. Morrison, "Development of Continuum Damage in the Creep Rupture of Notched Bars", *Philosophical Transactions of the Royal Society of London*, **A 311**, 103-129, 1984.

[48] D.R. Hayhurst, P.R. Dimmer and C.J. Morrison, "The Role of Continuum Damage in Creep Crack Growth", *Philosophical Transactions of the Royal Society of London*, **A 311**, 131-158, 1984.

[49] T.L. Anderson, *Fracture Mechanics, Fundamentals and Applications*, CRC Press, 1991.

[50] J.H. Giovanola and I. Finnie, "The Crack-Opening Displacement (COD) as a Fracture Parameter and a Comparative Assessment of the COD and J-integral Concepts", *S. M. Archives* **9**, 227-257, 1984.

[51] C.C. Poe, "A Unifying Strain Criterion for Fracture of Fibrous Composite Laminates", *Engineering Fracture Mechanics*, **17**, 153-171, 1983.

[52] D.S. Dugdale, "Yielding of Steel Sheets Containing Slits", *Journal of Mechanics and Physics in Solids*, **8**, 100-104, 1960.

[53] J. Janson, "Dugdale-Crack in a Material with Continuous Damage Formation", *Engineering Fracture Mechanics*, **9**, 890-899, 1977.

[54] S. Wu, Y. Mai and B. Cotterell, "A Model of Fatigue Crack Growth Based on Dugdale Model and Damage Accumulation", *International Journal of Fracture*, **57**, 253-267, 1992.

[55] B. Budiansky and J.W. Hutchinson, "Analysis of Closure in Fatigue Crack Growth", ASME *Journal of Applied Mechanics*, **45**, 267-275, 1978.

[56] B. Budiansky and R.J. O'Connell, "Elastic Moduli of a Cracked Solid", *International Journal of Solids and Structures*, **12**, 81-97, 1976.

[57] E.P. Chen, "Continuum Damage Response of a Center-Cracked Plain Concrete Panel in Tension", *Engineering Fracture Mechanics*, **39**, 553-560, 1991.

[58] W.H. Tai, "Plastic Damage and Ductile Fracture in Mild Steels", *Engineering Fracture Mechanics*, **37**, 853-880, 1990.

[59] H. Chai, "Observation of Deformation and Damage at the Tip of Cracks in Adhesive Bonds Loaded in Shear and Assessment of a Criterion for Fracture", *International Journal of Fracture*, **60**, 311, 1993.

[60] W.F. Li and S.Y. Du, "Modeling of Anisotropic Damage at a Crack Tip in Composite Laminates", *Engineering Fracture Mechanics*, **45**, 381-385, 1993.

[61] Y. Mou and R.P.S. Han, "Damage Zones Based on Dugdale Model for Materials", *International Journal of Fracture*, **68**, 245-259, 1994.

[62] Y. Mou and R.P.S. Han, "Damage Zones in Strain Hardening Materials", Submitted to: *Mechanics of Materials*, 1994.

[63] Y. Fu and A.G. Evans, "Some Effects of Microcracks on the Mechanical Properties of Brittle Solids — I, Stress, Strain Relations", *Acta Metallurgica*, **33**, 1515-1523, 1985.

[64] A.G. Evans and Y. Fu, "Some Effects of Microcracks on the Mechanical Properties of Brittle Solids — II, Microcrack Toughening", *Acta Metallurgica*, **33**, 1525-1531, 1985.

[65] Y. Mou and R.P.S. Han, "Influence of Damage on Fracture Parameters at the Crack Tip", Accepted by: *Canada Congress of Applied Mechanics*, Victoria, BC., Canada, May 1995.

[66] B. Budiansky, J.W. Hutchinson and J.C. Lambropoulos, "Continuum Theory of Dilatational Transformation Toughening in Ceramics", *International Journal of Solids and Structures*, **19**, 337-355, 1983.

[67] J.W. Hutchinson, "Crack Tip Shielding by Micro-cracking in Brittle Solids", *Acta Metallurgica*, **35**, 1605-1619, 1987.

[68] P.S. Steif, "A Semi-Infinite Crack Partially Penetrating a Circular Inclusion", ASME *Journal of Applied Mechanics*, **54**, 87-92, 1987.

[69] M. Ortiz, "A Continuum Theory of Crack Shielding in Ceramics", ASME *Journal of Applied Mechanics*, **54**, 54-58, 1987.

[70] M. Ortiz, "Microcrack Coalescence and Macroscopic Crack Growth Initiation in Brittle Solids", *International Journal of Solids and Structures*, **24**, 231-250, 1988.

[71] M. Ortiz and A.E. Giannakopoulos, "Maximal Crack Tip Shielding by Microcracking", ASME *Journal of Applied Mechanics*, **56**, 279-283, 1989.

[72] S.X. Gong and S.A. Meguid, "Microdefect Interacting with a Main Crack: a General Treatment", *International Journal of Mechanics of Science*, **34**, 933-945 1992.

[73] C.L. Chow and T.J. Lu, "A Continuum Damage Mechanics Approach to Crack Tip Shielding in Brittle Solids", *International Journal of Fracture*, **50**, 79-114, 1991.

[74] Y. Mou and R.P.S. Han, "Crack Tip Shielding and Crack Tip Amplification in Materials", *International Conference on Failure Analysis and Prevention*, Beijing, P.R. China, June 1995.

[75] Y. Mou and R.P.S. Han, "Influence of Damage in the Vicinity of a Macrocrack Tip", Submitted to: *Engineering Fracture Mechanics*, 1995.

[76] G. Cordier and K. Dang Van, "Strain Hardening Effects and Damage in Plastic Fatigue", *IUTAM Symposium Senlis, Physical Non-Linearities in Structural Analysis*, edited by J. Hult and J. Lemaitre, France, 52-55, 1980.

[77] E. Krempl, "Inelastic Constitutive Equations and Phenomenological Laws of Damage Accumulation for Structural Metals", *IUTAM Symposium Senlis, Physical*

*Non-Linearities in Structural Analysis*, edited by J. Hult and J. Lemaitre, France, 115-129, 1980.

[78] J.W. Ju, "Isotropic and Anisotropic Damage Variables in Continuum Damage Mechanics", *Journal of Engineering Mechanics*, 2765-2770, 1990.

[79] P.I. Kattan and G.Z. Voyiadjis, "A Coupled Theory of Damage Mechanics and Finite Strain Elasto-Plasticity—I. Damage and Elastic Deformations", *International Journal of Engineering Science*, **28**, 421-435, 1990.

[80] L.M. Kachanov, *Foundations of Fracture Mechanics*, Nauka, 1974.

[81] L. Davison and A.L. Stevens, "Thermomechanical Constitution of Spalling Elastic Bodies" *Journal of Applied Physics*, **44**, 668-674, 1973.

[82] D. Krajcinovis and G.U. Fonseka, "The Continuous Damage Theory of Brittle Materials", ASME *Journal Applied Mechanics*, **48**, 809-815, 1981.

[83] D. Krajcinovic, "Continuous Damage Mechanics Revisited: Basic Concepts and Definitions", ASME *Journal of Applied Mechanics*, **52**, 829-834, 1985.

[84] C.L. Chow and T.J. Lu, "On Evolution Laws of Anisotropic Damage", *Engineering Fracture Mechanics*, **34**, 679-701, 1989.

[85] G.Z. Voyiadjis and P.I. Kattan, "A Coupled Theory of Damage Mechanics and Finite Strain Elasto-Plasticity—II. Damage and Finite Strain Plasticity", *International Journal of Engineering Science*, **28**, 505-524, 1990.

[86] S. Murakami, *Proceedings of 2nd International Conference on Constitutive Laws for Engineering Materials*, edited by C.S. Desai and E. Krempl, Elsevier, 1987.

[87] S.J. Kim and W.D. Kim, "A Progressive Damage Modeling Based on the Continuum Damage Mechanics and its Finite Element Analysis", ASME *Journal of Applied Mechanics*, **61**, 46-53, 1994.

[88] J.L. Chaboche, *Mechanical Behavior of Anisotropic Solids*, edited by J.P. Boehler, Martinus-Nijhoff, 737, 1982.

[89] L. Nobile, "Damage Mechanics of Concrete", *Engineering Fracture Mechanics*, **39**, 1011-1014, 1991.

[90] J. Betten, "Applications of Tensor Functions to the Formulation of Constitutive Equations Involving Damage and Initial Anisotropy", *Engineering Fracture Mechanics*, **25**, 573-584, 1986.

[91] S. Murakami, "Mechanical Model of Material Damage", ASME *Journal of Applied Mechanics*, **55**, 280-286, 1988.

[92] S.C. Hunter, *Mechanics of Continuous Media*, Ellis Horwood Limited, 1976.

[93] J. Lemaitre and J. Dufailly, "Damage Measurements", *Engineering Fracture Mechanics*, **28**, 643-661, 1987.

[94] J. Lemaitre and J.L. Chaboche, "A Nonlinear Model of Creep-Fatigue Damage Cumulation and Interaction", *IUTAM Symposium of Mechanics of Visco-Elasticity Media and Bodies*. Gotenbourg Sueden, Springer-Verlag, 1974.

[95] A. Needleman, "Void Growth in an Elastic-plastic Medium", ASME *Journal of Applied Mechanics*, **39**, 964-970, 1972.

[96] A.L. Gurson, "Continuum Theory of Ductile Rupture by Void Nucleation and Growth: Part I — Yield Criteria and Flow Rules for Porous Ductile Media", ASME *Journal of Engineering Materials and Technology*, **99**, 2-15, 1977.

[97] W.H. Hunt, J.R. Brockenbrough and P.E. Magnusen, "An Al-Si-Mg Composite Model System: Microstructural Effects on Deformation and Damage Evolution", *Scripta Metallurgica et Materialia*, **25**, 15-20, 1991.

[98] D. Krajcinovic, "Constitutive Equations for Damaging Materials", *Journal of Applied Mechanics*, **50**, 355-360, 1983.

[99] D. Krajcinovic and S. Selvaraj, "Creep Rupture of Metals — An Analytical Model", *Journal of Engineering Materials and Technology*, **106**, 405-409, 1984.

[100] J. Lemaitre and D. Marquis, "Modeling Complex Behavior of Metals by the 'State-Kinetic Coupling Theory'", *Journal of Engineering Materials and Technology*, **114**, 250-253, 1992.

[101] N.R. Hansen and H.L. Schreyer, "Deactivation of Damage Effects", *Recent Advances in Damage Mechanics and Plasticity*, AMD-Vol. 132, MD-Vol. 30, edited by J.W. Ju, 63-76, 1992.

[102] J.M. Jouin, "Comportement Sous Chargements Cycliques de Composites Bidirectionnels a Matrics SiC", *Materiaux Composites Pour Applications a Haute Temperature, Bordeaux, 169, (29-30 Mars)*, 1990.

[103] D.P. Rooke and F.J. Bradshaw, "A Study of Crack Tip Deformation and a Derivation of Fracture Energy", *Proceedings of 2nd International Conference of Fracture*, 46-57, Brighton, 1969.

[104] H.M. Westergaard, "Bearing Pressures and Cracks", ASME *Journal of Applied Mechanics*, **6**, A49-A53, 1939.

[105] G.R. Irwin, "Analysis of Stresses and Strains Near the End of a Crack Traversing a Plate", ASME *Journal of Applied Mechanics*, **24**, 361- 364, 1957.

[106] D.E. Grady and M.E. Kipp, "Continuum Modeling of Explosive Fracture in Oil Shale", *International Journal of Rock Mechanics and Mining Sciences & Geomechanics Abstracts*, **17**, 147-157, 1980.

[107] J.C. Jaeger and N.G.W. Cook, *Fundamentals of Rock Mechanics*, Chapman & Hall, New York, 1969.

[108] M. Abramowitz and I.A. Stegun, *Handbook of Mathematical Functions,* Dover Publications Inc., New York, 1972.

[109] J.W. Hutchinson, "Plastic Stress and Strain Fields at a Crack Tip", *Journal of the Mechanics and Physics of Solids*, **16**, 337-347, 1968.

[110] H. Liebowitz, *Fracture — An Advanced Treatise*, Volume I, *Microscopic and Macroscopic Fundamentals*, Academic Press, 1968.

[111] H. Liebowitz, *Fracture — An Advanced Treatise*, Volume III, *Engineering Fundamentals and Environmental Effects*, Academic Press, 1968.

[112] D.J. Cartwright and D.P. Rooke, "Green's Functions in Fracture Mechanics", *Fracture Mechanics, Current Status, Future Prospects*, Edited by R.A. Smith, Pergamon Press, 1979.

[113] M.F. Ashby, "Micromechanisms of Fracture in Static and Cyclic Failure", Fracture Mechanics: Current Status, Future Prospects, Edited by R.A. Smith, Peramon Press, 1979.

[114] M. Kachanov, E.L.E. Montagut and J.P. Laures, "Mechanics of Crack-microcrack Interactions", *Mechanics of Materials*, **10**, 59-71, 1990.

[115] K. Schwalbe, "Crack Propagation in AlZnMgCu 0.5 During Static Loading", *Engineering Fracture Mechanics*, **6**, 415-434, 1974.

[116] L.G. Luo, A.I. Quarrington and J.D. Embury, "On the Development of a Direct Method of Determining the Microcrack Resistance Curve", *Engineering Fracture Mechanics*, **21**, 465-472, 1985.

[117] G.C. Sih, "A Special Theory of Crack Propagation", in *Mechanics of Fracture 1, Methods of Analysis and Solutions of Crack Problems*, Edited by G.C. Sih, Noordhoff International Publishing, 1973.

[118] R.J. Nuismer, "An Energy Release Rate Criterion for Mixed Mode Fracture", *International Journal of Fracture*, **11**, 245-250, (1975).

[119] A.A. Rubinstein, "Mechanics of the Crack Path Formation", *International Journal of Fracture*, **47**, 291-305, 1991.

[120] M.L. Williams, "On the Stress Distribution at the Base of a Stationary Crack", ASME *Journal of Applied Mechanics*, **24**, 109-114, 1957.

[121] G.C. Sih and H. Liebowitz, *Mathematical Theories of Brittle Fracture, Fracture, An Advanced Treatise*, **2**, Academic Press, 1968.

# APPENDIX

## NOMENCLATURE

| | |
|---|---|
| $A$ | overall cross-sectional area of an element |
| $\tilde{A}$ | effective area of $A$ |
| $a$ | half length of the crack in Mode I |
| $B(p,q)$ | beta function |
| $b$ | size of the damage zone in Mode I |
| $c$ | length of $a+b$ |
| $\tilde{d}$ | effective void dimension |
| $D$ | damage variable |
| $D_o$ | initial damage |
| $D_1$, $D_2$, $D_3$ | damage in the principal coordinate |
| $\boldsymbol{D}$ | damage tensor |
| $D_{ij}$ | elements of $\boldsymbol{D}$ |
| $D_c$ | threshold damage at failure |
| $E$ | Young's modulus |
| $E_o$ | initial undamaged Young's modulus |
| $\boldsymbol{E}$ | elastic tensor |
| $\tilde{E}$ | effective Young's modulus |
| $\tilde{\boldsymbol{E}}$ | effective elastic tensor |

| | |
|---|---|
| $\tilde{\boldsymbol{E}}_{\boldsymbol{D}}$ | effective elastic tensor at the damage state $\boldsymbol{D}$ |
| $F(\alpha,\beta;\gamma;z)$ | hypergeometric function |
| $f(\theta)$ | fracture deflection factor |
| $f\left(\tilde{E}_D\right)$ | modulus reduction factor |
| $f\left(\sigma,\omega^T\right)$ | residual stress releases factor |
| $G$ | shear modulus |
| $G_o$ | initial undamaged shear modulus |
| $\tilde{G}$ | effective shear modulus |
| $\tilde{G}_D$ | effective shear modulus at damage state $D$ |
| $g_{ij}$ | direction cosines of the coordinate $(x_1', x_2', x_3')$ in $(x_1, x_2, x_3)$ |
| $\dot{\boldsymbol{J}}$ | thermodynamic conjugate flux vector |
| $K_I$ | stress intensity factor of Mode I |
| $K_{II}$ | stress intensity factor of Mode II |
| $K_D$ | stress intensity factor when the fracture deflection is considered |
| $K_M$ | stress intensity factor when a reduction in the modulus is considered |
| $K_R$ | stress intensity factor when the release of the residual stress is considered |
| $k_1$ | stress intensity factor of the microscopic Mode I |
| $k_2$ | stress intensity factor of the microscopic Mode II |
| $L_o$ | initial length of an element under loading |
| $\Delta L^l$ | increment in length of an element under loading |
| $\Delta L^u$ | increment in length of an element after unloading |
| $\Delta L_D^l$ | increment in length of an element under loading when damage happened |
| $\Delta L_D^u$ | increment in length of an element after unloading when damage happened |
| $\boldsymbol{M(D)}$ | damage effect tensor |
| $\left[\boldsymbol{M}_{ij}'(\boldsymbol{D})\right]$ | transformed damage effect tensor |

| | |
|---|---|
| $M_{ijkl}$ | elements of $\boldsymbol{M(D)}$ |
| $M'_{ij}$ | elements of the transformed damage effect tensor |
| $n$ | strain hardening exponent |
| $\vec{n}$ | loading orientation |
| $p$ | accumulated plastic strain |
| $p_c$ | threshold of the accumulated plastic strain at rupture |
| $Q$ | material dependent constant |
| $S$ | material dependent constituent |
| $r$ | internal variable of the isotropic hardening; |
| | radius of a point under consideration in the damage zone |
| $T$ | tension on an element; |
| | absolute temperature |
| $w(x)$ | weighting function |
| $(X_1, X_2, X_3)$ | principal coordinates |
| $(x_1,\ x_2,\ x_3)$ | Cartesian rectangular coordinate |
| $(x'_1,\ x'_2,\ x'_3)$ | Cartesian rectangular coordinate |
| $\boldsymbol{X}$ | thermodynamic conjugate force vector |
| $\boldsymbol{Y}$ | damage strain energy release rate |
| $z$ | complex variable |
| $\alpha$ | internal variable of the kinematic hardening |
| $\lambda$ | non-dimensional variable |
| $\eta$ | crack-tip advance displacement |
| $\rho$ | mass density of a material |
| $\omega$ | dilational transformation strain |
| $\omega^T$ | fully dilational transformation strain |

| | |
|---|---|
| $\xi$ | abscissa |
| $\delta_{ij}$ | Kronecker delta |
| $\varepsilon^e$ | elastic strain |
| $\varepsilon^e$ | elastic strain tensor |
| $\varepsilon^{e1}$ | strain deviator |
| $\varepsilon^e_{ij}$ | elements of the elastic strain tensor |
| $\varepsilon_H$ | hydrostatic strain |
| $\varepsilon^p$ | inelastic strain tensor |
| $\sigma$ | normal stress |
| $\sigma$ | stress tensor |
| $\sigma'$ | stress deviator |
| $\sigma_{eq}$ | von Mises equivalent stress |
| $\sigma_H$ | hydrostatic stress |
| $\sigma_{ij}$ | elements of $\sigma$ |
| $\sigma_D$ | stress tensor at the damage state $\boldsymbol{D}$ |
| $\sigma_Y$ | yielding stress |
| $\sigma_\infty$ | loading at infinite distance |
| $\tilde{\sigma}$ | effective normal stress |
| $\tilde{\sigma}$ | effective stress tensor |
| $\tilde{\sigma}_{ij}$ | elements of $\tilde{\sigma}$ |
| $\nu$ | Poisson's ratio |
| $\tilde{\nu}$ | effective Poisson's ratio |
| $\Psi$ | Westergaard stress function |
| $\Psi'$ | derivative of $\Psi$ with respect to $z$ |
| $\Psi_c$ | complementary energy |

| | |
|---|---|
| $\delta\Psi_c$ | incremental complementary energy |
| $\Re$ | real part of the Westergaard stress function |
| $\Im$ | imaginary part of the Westergaard stress function |
| $\psi^H$ | Helmholtz free energy |
| $\psi^e$ | elastic strain energy |
| $\psi^d$ | potential of dissipation |